Exotic Bose-Einstein Condensates: Binary mixtures and dipolar gases

Luis Ever Young Silva

IFT–T.001/2013

Esta tese contou com o apoio financeiro da CAPES e FAPESP (Brasil).

Exotic Bose-Einstein Condensates: Binary mixtures and dipolar gases

TESE

apresentada ao Instituto de Física Teórica
Universidade Estadual Paulista, Brasil

em cumprimento aos requisitos para a obteção do título de

Doutor

Fevereiro de 2013

Luis Ever Young Silva

nascido em Tunja, Boyacá, Colômbia.

Comissão Examinadora

Dr. Sadhan Kumar Adhikari
IFT-UNESP

Dr. Arnaldo Gammal
USP

Dr. Dionisio Bazeia Filho
UFPB

Dr. Roberto André Kraenkel
IFT-UNESP

Dr. Valery Shchesnovich
UFABC

Orientador: Dr. Sadhan Kumar Adhikari

Instituto de Física Teórica – UNESP
R. Dr. Bento Teobaldo Ferraz 271, bloco II
01140-070 São Paulo, Brasil

"La vida no es un sueño, es un viaje: un viaje a pie.
Y para viajar hay que estar despierto, ¿no? F. G."

Dedico este trabajo para mi mamita.
Olga: origen, resplandor y fuerza de todo lo que soy...

"E para se chegar, onde quer que seja, aprendi que não é preciso dominar a força, mas a razão. É preciso, antes de mais nada, querer. A. K."

Abstract

We described the basic ideas of Bose-Einstein condensation (BEC), and then we focused our study on extensions to more exotic condensates including mixtures of two components, where interesting characteristics are found due to the interspecies interaction, and magnetic dipolar gases, which with their anisotropic long-range dipolar interaction have opened up new avenues of research into cold atoms, in a quest for novel and fascinating features.

In this thesis, we present the mean-field model for the binary BEC interacting via inter- and intra-species contact and anisotropic long-range dipolar interactions for systems with different symmetric confinement where one or both of them could be dipolar. Specifically, we study the physical characteristics of interacting two-component mixtures of dipolar and nondipolar BECs, the formation and dynamics of bright solitons, the strong coupling domain for dipolar BECs, and the features of an untrapped bound dipolar droplet in a trapped nondipolar condensate.

Our numerical results are presented in density plots, stability phase plots, structure formation in densities, breathing oscillation, and more. However, these solutions, whenever possible, are associated with quantities widely handled in experimental techniques, through a specific types of atoms, number of particles, values of parameters of interaction or the anisotropy of trap, and others quantities related to experimental observables.

Key words: Bose-Einstein condensation; Gross-Pitaevskii equation; binary mixtures; dipolar atoms.

Subject: Atomic and molecular physics; ultra-cold trapped atoms.

Resumo

Nesta tese estudamos conceitos básicos de um condensado de Bose-Einstein (BEC) e sua extensão para sistemas com propriedades mais "exóticas", incluindo misturas de dois componentes, com algumas características interessantes encontradas devido à interação entre espécies, e condensados de átomos com forte momento (magnético) dipolar, nos quais a interação dipolo-dipolo (anisotrópica e de longo-alcance), abre novas possibilidades de pesquisa na procura por desconhecidas e fascinantes características para gases atômicos ultra-frios. Mostramos o modelo de campo-médio para misturas de dois BECs interagindo através do potencial de contato e da interação dipolar de longo-alcance empregando termos não lineares de inter e intra-espécies. Aplicamos este modelo em sistemas binários com diferentes armadilhas em que um deles ou ambos podem ser dipolares. Especificamente, estudamos as características físicas de uma mistura de dois BECs - com e sem interação dipolar -, a formação (e dinâmica) de bright solitons para um BEC dipolar, algumas propriedades interessantes para um BEC dipolar no limite de interação forte, e as características de um BEC dipolar quase-livre vinculado à um outro BEC não dipolar confinado numa armadilha magnética.

Apresentamos nossos resultados numéricos usando gráficos de densidade, diagramas de fase, de formação de estruturas nas densidades ou a dinâmica dos sistemas, entre outros. Sempre que possível, nossos resultados serão associados com quantidades usadas em técnicas experimentais através de um tipo específico de átomo, o número de partículas, os valores dos parâmetros de interação, a anisotropia da armadilha ou outras quantidades relacionadas com observáveis experimentais.

Palavras chaves: Condensado de Bose-Einstein; equação Gross-Pitaevskii; misturas interagentes; átomos dipolares.

Áreas do conhecimento: Física atômica e molecular, átomos ultra-frios.

Contents

Agradecimentos

Esta tese de doutorado é mais do que o resultado de intenso trabalho durante esses três anos, é ele a prova de um projeto de vida no qual meus familiares, amigos e companheiros têm jogado, sem dúvida, um papel transcendente. Para eles um imenso sentimento de gratidão e tudo o melhor que esteja por vir.

Acredito no fato de que, acima da distância, ao meu lado sempre estiveram os sorrisos dos meus sobrinhos, a força da minha avó, o coração da minha irmãzinha *Yudy*, *Maye* "*echada pa'lante*", *Ariano* quem sempre será meu modelo a seguir, a coragem de meu irmão *Elver* e a tenacidade da minha *mãe*. Juntos, todos eles são meu maior orgulho e, sem dúvida, formaram cada uma das linhas deste projeto, sendo então, coautores inquestionáveis deste trabalho.

Até agora, importantes amigos escreveram ao meu lado muitas histórias cheias de passagens interessantes, injusto é não indicar aqui todas aquelas aventuras.. mas as lembranças sempre ficarão ligadas ao sopro vital da dança.. logo companheiros neste caminho: *Andre, Marce, Jey, Karina, Lili, Flavinha, Ale, Yaky, Daniel, Fercho, Iro, Chamo, Jehann, Jhon, Mario, Marcos, Rodo, Ooomar, Roni, Danny, Raúl, Oscar*.. Obrigado pela grande amizade que compartilhamos...

Sou muito afortunado por ter percorrido meu processo de formação com a orientação do professor *Sadhan Adhikari*, quem deixa comigo inúmeros exemplos de dedicação, paciência, determinação e confiança - sinais de sempre atingir a flecha no olho do peixe - neste caminho para desvendar a forma real do mundo. Professor, por seu direcionamento e conselhos, por suas histórias de vida, por sua participação direta e ativa na realização desta tese e nossas publicações: toda minha gratidão. Também desejo agradecer aos professores *Luca Salasnich* e *Antun Balaž*, por tomarem parte de seu tempo em nossos projetos e toda a amabilidade durante minha permanência na Itália e Sérvia. Do mesmo modo, agradeço à toda equipe de professores e trabalhadores do IFT em São Paulo.

Finalmente, agradeço à CAPES e FAPESP pelo apoio financeiro que fez possível a realização deste projeto.

List of Figures

List of Tables

1

Introduction to Bose-Einstein Condensate (BEC)

One of the appeals of research on quantum systems is the possibility of exploring quantum phenomena on a macroscopic scale. Regardless of whether constructed using electrons (as in superconductors) or neutral atoms (as in ultracold gases), these systems permit the establishment of a wonderful application of quantum physics. In 1924 A. Einstein predicted the phenomenon that is now known as Bose-Einstein condensation [1]. Following the work of S. N. Bose [1] on the statistics of photons, Einstein extended this treatment to a gas of non-interacting massive particles (bosons), and concluded that, below a certain temperature, a finite fraction of the total number of particles would occupy the lowest-energy single-particle state.

At first, the physics community remained skeptical to the idea that the Bose-Einstein condensation could be realized experimentally for interacting particles, or that it could be any more than a theoretical phenomenon in non-interacting gas. However, in 1938 the lamda transition for superfluidity in the liquid ^{4}He below a characteristic temperature ($\sim$2.17 K) was discovered, establishing this system as a prototype Bose–Einstein condensate, and allowing the development of many physical concepts, such as the model of two fluids [2]. The hunt for Bose-Einstein condensation finally ended in 1995 with an experiment on dilute atomic gases of rubidium [3] and sodium [4], in which the atoms were confined in magnetic

[1] Satyendra Nath Bose was a talented Indian physicist best known for his work on quantum mechanics, in the early 1920s, and the groundwork for Bose–Einstein statistics.

traps and cooled down to extremely low temperatures, of the order of fractions of microkelvins. This Bose-Einstein condensed atomic cloud is dilute because its density is typically 10^{13}-10^{15} particles cm^{-3}, and from a theoretical point of view they are dilute in the sense that the strength of the interactions is much less than the interparticle spacing. In addition to sodium and rubidium, other cases such as lithium [5], hydrogen [1], potassium [6], cesium [7], and some elements off the first column of the periodic table, the rare-earth ytterbium [8], and alkaline earth metals such as calcium [9] and strontium [10] have been condensed.

More recently, Bose-Einstein condensate (BEC) of ^{52}Cr [11], ^{164}Dy [12], and ^{168}Er [13] atoms with larger (magnetic) dipole moments have become available for experimental studies, and even polar molecules with much larger (electric) dipole moments are being considered [14] for BEC experiments. After the experimental realization of a dipolar BEC of atoms with magnetic moments, there has been renewed interest in the study of the static and dynamic properties of such a condensate in the pursuit of novel and interesting properties and features emerging as a consequence of anisotropic long-range dipolar interaction. In order to describe the Bose-Einstein condensate, formed by N interacting bosons, of massa m, confined by an external potential U_{ext}, in the picture of second quantization we can take the following many-body Hamiltonian:

$$\begin{aligned} \hat{H} &= \int d\mathbf{r}\ \hat{\psi}^{\dagger}(\mathbf{r}) \left[-\frac{\hbar^2}{2m}\nabla^2 + U_{ext}(\mathbf{r}) \right] \hat{\psi}(\mathbf{r}) \\ &+ \frac{1}{2}\int d\mathbf{r}\ d\mathbf{r}'\ \hat{\psi}^{\dagger}(\mathbf{r})\hat{\psi}^{\dagger}(\mathbf{r}')U(\mathbf{r}-\mathbf{r}')\hat{\psi}(\mathbf{r}')\hat{\psi}(\mathbf{r}), \end{aligned} \tag{1.1}$$

where $\hat{\psi}(\mathbf{r})$ and $\hat{\psi}^{\dagger}(\mathbf{r})$ are the boson field operators that annihilate and create a particle at the position $\mathbf{r}$, respectively, and $U(\mathbf{r}-\mathbf{r}')$ is the two-body interatomic potential. For this general Hamiltonian exactly solving the full many-body equation can be computationally expensive or even intractable for systems with very large values of N.

On the other hand, the Bose-Einstein condensates produced in labs to date have mostly been described very well by mean-field theory which, at zero temperature and when the interaction is not too strong, allows Bose gases to be considered as being governed by a single wave function (the latter plays the role of an order parameter). In addition to the convenience of avoiding heavy numerical work, mean-field theories allow one to understand the properties of a system in terms of a set of parameters which have a clear physical meaning. The key point for a mean-field description of a dilute Bose gas was formulated in 1947 by Bogoliubov [15]. The basic idea is that the one-body ground state plays a special role and, at very low temperatures, carries most of the physical information about the Bose condensed cloud.

This idea led Bogoliubov to suggest that one could describe a weakly interacting Bose gas at low temperatures, separating out the condensate contribution to the bosonic field operator through the following substitution:

$$\hat{\psi}(\mathbf{r}) = \psi(\mathbf{r}) + \delta\hat{\varphi}(\mathbf{r}), \tag{1.2}$$

where $\psi(\mathbf{r})$ is a classical field, a complex function that does not possess any operator character and is often called the wave function for the condensate. Above the critical temperature it vanishes, while it becomes nonzero if the temperature is lower than its critical value. For this reason, $\psi(\mathbf{r})$ is also called the order parameter of the phase transition from an ordinary Bose gas to a condensate.
In Eq. (1.2) $\delta\hat{\varphi}(\mathbf{r})$ represents the contribution to the bosonic field of quantum or thermal fluctuations. Bogoliubov developed the first-order theory for the excitations of interacting Bose gases by treating this operator $\delta\hat{\varphi}(\mathbf{r})$ as a small perturbation [15].

We write the time evolution of the field operator, in order to derive the equation for the condensate wave function, for the generalization of the Bogoliubov prescription to the case of time dependent configurations:

$$i\hbar\frac{\partial}{\partial t}\hat{\psi}(\mathbf{r},t) = \Big[\hat{\psi}(\mathbf{r},t), \hat{H}\Big]. \tag{1.3}$$

For the many-body Hamiltonian Eq. (1.1), the previous Heisenberg equation is given by:

$$i\hbar\frac{\partial}{\partial t}\hat{\psi}(\mathbf{r},t) = \Big[-\frac{\hbar^2}{2m}\nabla^2 + U_{ext}(\mathbf{r}) + \int d\mathbf{r}'\ \hat{\psi}^\dagger(\mathbf{r}',t)U(\mathbf{r}-\mathbf{r}')\hat{\psi}(\mathbf{r}',t)\Big]\hat{\psi}(\mathbf{r},t). \tag{1.4}$$

For Bose-Einstein condensates, interactions typically have a short range much less than the interparticle spacing, and, at low temperatures, only s-wave scattering is important. In this form we can introduce a simple model, approximating the interatomic potential with an effective interaction as

$$U(\mathbf{r}-\mathbf{r}') = g\delta(\mathbf{r}-\mathbf{r}'), \tag{1.5}$$

where g is a coupling constant. At very low energies it is sufficient to consider s-wave scattering and the standard scattering theory for two particles with identical masses m yields [1]

$$g = \frac{4\pi\hbar^2 a}{m}, \tag{1.6}$$

where the constant a is called the scattering length. For the commonly used bosonic alkali-metal atoms (^{87}Rb, ^{23}Na), the scattering length is positive and is of the order of $100a_0$, with a_0 the Bohr radius. At this point we return to the Bogoliubov prescription Eq. (1.2) and retain only the leading term in that

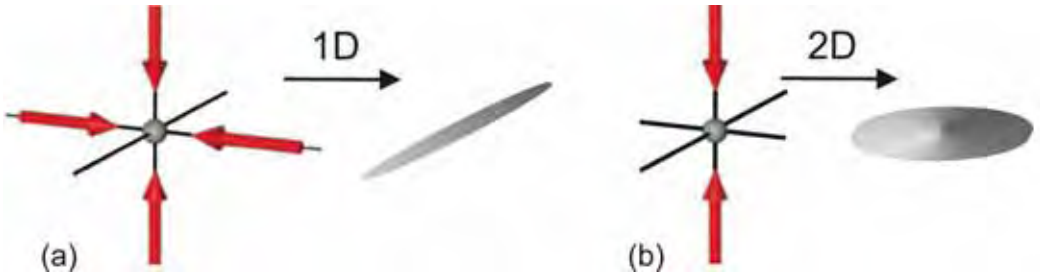

Figure 1.1: Intuitive picture for the (a) one-dimensional (1D) cigar-shape and (b) two-dimensional (2D) disk-shape in a trapped gas. Both configurations achieved with a strong harmonic trap in the transverse radial for 1D and axial directions for 2D.

expression. Furthermore, using the effective interaction Eq. (1.5) in Eq. (1.4) we found the following closed equation for the condensate wave function:

$$i\hbar\frac{\partial}{\partial t}\psi(\mathbf{r},t) = \Big[-\frac{\hbar^2}{2m}\nabla^2 + U_{ext}(\mathbf{r}) + g|\psi(\mathbf{r},t)|^2\Big]\psi(\mathbf{r},t). \tag{1.7}$$

This equation is known as the Gross-Pitaevskii (GP) equation, and it is now well established that, at ultralow temperatures, dilute Bose-Einstein condensates can be accurately described by this three-dimensional (3D) GP equation [2, 15, 16]. The normalization of the order parameter chosen here is

$$\int d\mathbf{r}\ |\psi(\mathbf{r},t)|^2 = N. \tag{1.8}$$

The shape of the external potentials (U_{ext}) for ultracold atoms can be created by applied magnetic fields, laser light or other external fields. To control the parameters in quantum systems is very important, so to modify the cloud of atoms changing the external potential is a wonderful tool in ultra cold atoms. Generally, the external potential for BECs is a harmonic potential with the form [1, 15]:

$$U_{ext}(\mathbf{r}) = \frac{1}{2}m\left(\omega_x^2x^2 + \omega_y^2y^2 + \omega_z^2z^2\right), \tag{1.9}$$

where ω_i ($i = x, y$, and z) represents the angular frequency of the trap along the each direction. The external potential can be designed to be highly asymmetric so that certain degrees of freedom are frozen out [17]. The trap is spherically-symmetric for $\omega_x = \omega_y = \omega_z$. A strong confinement in two directions, $\omega_x \simeq \omega_y \gg \omega_z$, creates a elongated tube of atoms along the z axis and such one-dimensional (1D) systems has the cigar shape Fig. 1.1 (a). On the other hand, when $\omega_x \simeq \omega_y \ll \omega_z$, a pancake shaped trap is formed and we have a two-dimentional (2D) system where the cloud of atoms has a disk-shape Fig. 1.1 (b).

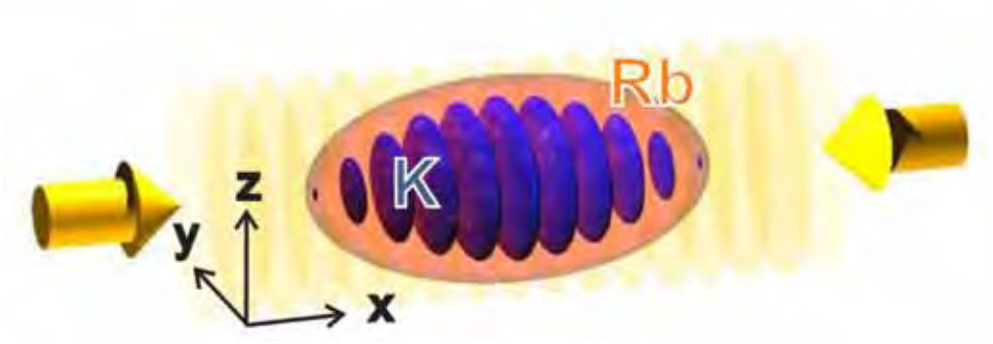

Figure 1.2: Illustrative picture of the experimental configuration produced by G. Lamporesi *et. al.* [19] for study a system in mixed dimensions with ultracold gases. Two-dimensional strong confinement by optical lattice resulting in disk shapes for trapped gas of ^{41}K atoms (blue) with a negligible effect on trapped cloud of ^{87}Rb atoms (pink) that remains in a three-dimensional configuration.

These possibilities of manipulation and control the magnetic and optical external potentials for different confinements allowed the theoretical study and experimental realization of fascinating systems with ultra-cold atoms. For example, recently we show that self-localized ground states can be created in the spin-balanced gas of fermions with repulsion between the spin components, merging the spatial growth of the s-wave scattering length (which accounts for the repulsion between the components) in one or two directions, and the external harmonic confining potential, acting in the other directions [18]. As another example, systems composed of interacting parts where distinct types of particles live in different spatial dimensions have been studied. In 2010 the Bose-Einstein condensation in trapped atoms for a mix-dimensional system composed of two species (^{41}K and ^{87}Rb) has been realized for G. Lamporesi *et. al.* [19]. In this experiment the dimensionality of space can be changed by means of strong potential confining for one specie (^{41}K acquiring a disk-shape symmetry) while having a negligible effect on the other specie (^{87}Rb) that remains with 3D configuration, such as in Fig. 1.2. The Fig. 1.2 was produced by G. Lamporesi *et. al.* [19] [2] in order to illustrate the experimental configuration for scattering in mixed dimensions with ultracold gases BEC.

The present thesis deals with the physical properties of some *exotic* [20] condensates including mixtures of two components, where interesting characteristics are found due to the interspecies interaction, and magnetic dipolar gases, which with their anisotropic long-range dipolar interaction have opened up new avenues of research into cold atoms, in a quest for novel and fascinating features.

[2] The picture 1.2 was obtained from the figure 1 in the reference [19].

We focused our study on quantum gases, using coupled mean-field equations to describe binary mixtures and dipolar BECs in different cases of concrete scientific interest, some of which include some beyond mean-field corrections. Broadly speaking, we perform numerical simulation of the 3D GP equation (1.7) using the split-step Crank-Nicolson method [21–23] and variational solutions [24], if possible. Our numerical results are presented in density plots, stability phase plots, structure formation in densities, breathing oscillation, numerical values for chemical potential, root mean square (rms) for the sizes, and more. However, these numerical solutions, are not only numbers, whenever possible, are associated with quantities widely handled in experimental techniques, using a specific type of atoms, number of particles, value of parameters of interaction or the anisotropy of trap, and other quantities related to experimental observables.

In chapter 2 we study a binary BEC, where the confining potentials of the two BEC components have distinct asymmetry, so that the components belong to different space dimensions, as in the experiment by G. Lamporesi *et al.* [19]. Using a Lagrangian approach we derive a binary 3D GP equation and we show that this binary equation can be used to perform numerical simulations and analytical calculations for the investigation of the static and dynamic properties of a binary BEC in mixed dimensions. A brief introduction to the physical properties of dipolar Bose-Einstein condensates is given in chapter 3. Then, using numerical and variational analyses of the 3D GP equation, in chapter 4 we study the formation and dynamics of bright solitons in a cigar-shaped dipolar Bose-Einstein condensate for large *repulsive* atomic interactions. A phase diagram showing the region of stability of the solitons is obtained. We also study the dynamics of the breathing oscillation of the solitons initiated by a sudden change of the scattering length, as well as the collision dynamics of two solitons at large velocities.

Another interesting physical phenomenon we know of, is in the strong coupling regime (also called unitarity limit), where the atomic scattering length goes to infinity ($a \to \infty$) and all of the properties of a uniform dilute Bose atomic quantum gas are determined by density $\bar{n}$. So a uniform dilute Bose gas of known density has a universal behavior as a tends to infinity at unitarity, while most of its properties are determined by a universal parameter ξ. The usual mean-field equation is not valid at this limit and beyond mean-field corrections become important. In chapter 5 we use a dynamical model (BEC-unitarity crossover model) including such corrections to investigate a trapped disk-shaped dipolar Bose-Einstein condensate of large scattering length and we suggest a scheme for determining the universal parameter ξ from the study of this dipolar BEC in the strong-coupling domain. In this geometry, the strongly repulsive dipolar interaction should drastically reduce three-body loss by molecule formation common in nondipolar condensates. This will facilitate an experiment on a disk-shaped dipolar BEC close to strong coupling. Here we study the sensitivity of our re-

sults on the parameter ξ and discuss the possibility of extracting the value of this parameter from experimental observables.

In chapter 6 we study the static properties of disk-shaped binary dipolar Bose-Einstein condensates of ^{168}Er-^{164}Dy and ^{52}Cr-^{164}Dy mixtures under the action of inter- and intra-species contact and dipolar interactions and demonstrate the effect of dipolar interaction using the mean-field approach. Throughout this study we use realistic values of inter- and intra-species dipolar interactions and intra-species scattering lengths and consider the inter-species scattering length as a parameter. The stability of the binary mixture is illustrated with phase plots involving the number of atoms of the species. The binary system always becomes unstable as the number of atoms increases beyond a certain limit. As the inter-species scattering length increases corresponding to more repulsion, an overlapping mixed state of the two species changes to a separated demixed configuration. During transition from a mixed to a demixed configuration as the inter-species scattering length is increased for parameters to just below the stability line, the binary condensate shows special structures in its density in the form of red-blood-cell-like biconcave and Saturn-ring-like shapes, which are direct manifestations of dipolar interaction.

In chapter 7 we study the statics and dynamics of an untrapped dipolar droplet bound by inter-species contact interaction in a trapped nondipolar Bose-Einstein condensate. Our findings are demonstrated in terms of stability phase plots of a binary mixture of a bound droplet of dipolar ^{164}Dy in a trapped nondipolar ^{87}Rb BEC with a variable number of ^{164}Dy atoms and a variable inter-species scattering length. The shape and size (statics) as well as the small breathing oscillation (dynamics) of the dipolar droplet are studied using the numerical and variational solutions of a mean-field model. We also suggest an experimental procedure for achieving such a ^{164}Dy droplet by relaxing the trap on the ^{164}Dy BEC in a trapped binary ^{87}Rb-^{164}Dy mixture.

Finally, the thesis is concluded in chapter 8, where a summary of the discussed topics is presented, which includes a detailed review of our findings. This work was based on references [25–29].

2

Binary BEC in Mixed Dimensions

In 2010 an experiment by Lamporesi *et al.* [19] investigated the mixed dimensional scattering occurring when the collisional atoms of two species of a binary Bose-Einstein condensate (BEC) live in different space dimensions. This achievement opened the way to the experimental and theoretical studies of a binary BEC with the components belonging to mixed dimensions. In this chapter we use a Lagrangian approach to derive a binary three−dimensional (3D) Gross−Pitaevskii (GP) equation and we study numerically the static and dynamic properties of a binary BEC where the trap anisotropy of the two components are distinct. When component 2 has a fully asymmetric trap, component 1, due to its specific trap symmetry, will be assumed to have a quasi one-dimensional(1D) or quasi two-dimensional(2D) configuration. The quasi-1D shape emerges when the traps in the two transverse directions are much stronger than that in the linear direction. The quasi-2D shape emerges when the trap in the direction perpendicular to the 2D plane is much stronger than those in the 2D plane. In this fashion one could have an effective 1D-3D, and 2D-3D mixed configuration for the traps acting on the binary BEC [1].

Previously, there have been studies of binary boson-boson, mixtures, and for this system is possible to have either a mixed or demixed phase [30, 31]. Now we shall consider one case where one of the components have a quasi-1D shape and the other component a quasi-2D shape due to specific trap symmetry of

[1] In reference [19] G. Lamporesi *et. al.* reported the first experimental realization of a mix-dimensional system composed of two species (^{41}K and ^{87}Rb), confining one specie with disk-shape symmetry while having a negligible effect on the other that remains with 3D configuration, materializing the possibility to form a binary mixture of ultracold atoms.

the two components. In that case the binary mixture is described by a 1D-2D configuration where the first quasi-1D component lies along the z axis and the quasi-2D component in the (x, y) plane. Also we studied small oscillations of this binary BEC initiated by a sudden change of the radial angular frequency of the quasi-2D component.

2.1 Theoretical Formulation

The action of a system of two BECs is given by [32]

$$A = \int (\mathcal{L}_1 + \mathcal{L}_2 + \mathcal{L}_{12})\, d^3\mathbf{r}\, dt\,, \tag{2.1}$$

here the interspecies Lagrangian density has the form:

$$\mathcal{L}_{12} = g_{12}|\psi_1|^2|\psi_2|^2, \tag{2.2}$$

where g_{12} is the interspecies nonlinearity

$$g_{12} = \frac{2\pi\hbar^2 a_{12}}{m_R}, \tag{2.3}$$

with a_{12} the interspecies scattering length, and $m_R \equiv m_1 m_2/(m_1 + m_2)$ the reduced mass. The intraspecies Lagrangian density is :

$$\mathcal{L}_j = i\frac{\hbar}{2}(\psi_j \partial_t \psi_j^\star - \psi_j^\star \partial_t \psi_j) + \frac{\hbar^2}{2m_j}|\nabla_{\mathbf{r}}\psi_j|^2 + U_j(\mathbf{r})|\psi_j|^2 + \frac{g_j}{2}|\psi_j|^4, \tag{2.4}$$

with $i = \sqrt{-1}$ and $U_j(\mathbf{r})$ the external potential acting on the j-th BEC component $(j = 1, 2)$, which is described by the macroscopic wave function $\psi_j(\mathbf{r}, t)$, here ∂_t denotes time derivative, and the intraspecies nonlinearity g_j is

$$g_j = \frac{4\pi\hbar^2 a_j}{m_j}, \tag{2.5}$$

where a_j is the intraspecies scattering length for species j, m_j is the mass of species j, and

$$\int |\psi_j(\mathbf{r}, t)|^2 = N_j, \tag{2.6}$$

is the normalization chosen here. By extremizing the action A with respect to $\psi_1^\star(\mathbf{r}, t)$ and $\psi_2^\star(\mathbf{r}, t)$ we obtain the following binary GP equation [32]

$$i\hbar\partial_t\psi_1 = \Big[-\frac{\hbar^2}{2m_1}\nabla^2 + U_1(\mathbf{r}) + g_1|\psi_1|^2 + g_{12}|\psi_2|^2\Big]\psi_1\,, \tag{2.7}$$

$$i\hbar\partial_t\psi_2 = \Big[-\frac{\hbar^2}{2m_2}\nabla^2 + U_2(\mathbf{r}) + g_2|\psi_2|^2 + g_{12}|\psi_1|^2\Big]\psi_2\,. \tag{2.8}$$

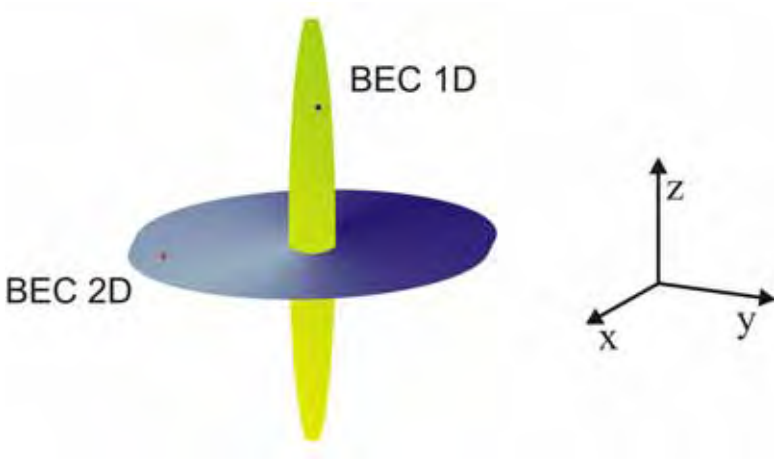

Figure 2.1: Illustrative picture for binary BEC with the components belonging to mixed dimensions. The cigar-shape (BEC 1D) and disk-shape (BEC 2D) configurations achieved in an axially-symmetric setting with a strong harmonic trap in the transverse radial and axial directions, respectively.

These two coupled partial differential equations are both in 3+1 (space-time) dimensions. In the general case, these can be solved numerically using a split-step Crank-Nicolson discretization method [21–23].

An interesting possibility is a binary system where one cigar-shaped BEC is perpendicular to the plane of other two-dimensional BEC Fig. 2.1. This kind of configuration can be obtained by considering the following trapping potential acting on the first component:

$$U_1(\mathbf{r}) = \frac{1}{2}m_1(\omega_{1x}^2 x^2 + \omega_{1y}^2 y^2) + W_1(z), \tag{2.9}$$

where $W_1(z)$ is a generic potential in z direction, and ω_{1x} and ω_{1y} are the angular frequencies of the harmonic trap along transverse x and y directions. The transverse harmonic potentials are assumed to be so strong that the first BEC is quasi-1D, i.e. in an elongated cigar-shaped configuration. For the second BEC we use the following confining potential

$$U_2(\mathbf{r}) = W_2(x, y) + \frac{1}{2}m_2\omega_{2z}^2 z^2 \ , \tag{2.10}$$

where $W_2(x, y)$ is a generic potential in (x, y) plane, while the harmonic potential of angular frequency ω_{2z} along the z axis is so strong that the second BEC is a quasi-2D in the (x, y) plane. This case can be simplified if we impose cylindrical symmetry in the harmonic potential acting on the first BEC ($\omega_{1x} = \omega_{1y} = \omega_{1\rho}$) and also in the generic potential acting on the second BEC, i.e. $W_2(x, y) = W_2(\rho)$ with $\rho = (x^2 + y^2)^{1/2}$.

In this form, the 1D-2D binary BEC will be described for the following coupled 3D Gross-Pitaevskii equations

$$i\hbar\partial_t\psi_1(\rho,z;t) = \Big[-\frac{\hbar^2}{2m_1}\Big(\frac{\partial^2}{\partial\rho^2}+\frac{1}{\rho}\frac{\partial}{\partial\rho}+\frac{\partial^2}{\partial z^2}\Big)+\frac{1}{2}m_1\omega_{1\rho}^2\rho^2+ \frac{1}{2}m_1\omega_{1z}^2z^2+g_1|\psi_1|^2+g_{12}|\psi_2|^2\Big]\psi_1(\rho,z;t)\,, \tag{2.11}$$

$$i\hbar\partial_t\psi_2(\rho,z;t) = \Big[-\frac{\hbar^2}{2m_2}\Big(\frac{\partial^2}{\partial\rho^2}+\frac{1}{\rho}\frac{\partial}{\partial\rho}+\frac{\partial^2}{\partial z^2}\Big)+\frac{1}{2}m_2\omega_{2\rho}^2\rho^2+ \frac{1}{2}m_2\omega_{2z}^2z^2+g_2|\psi_2|^2+g_{12}|\psi_1|^2\Big]\psi_2(\rho,z;t)\,, \tag{2.12}$$

where the trapping potentials $W_1(z)$ and $W_2(\rho)$ was taken as

$$W_1(z)=\frac{1}{2}m_1\omega_{1z}^2z^2;\quad W_2(\rho)=\frac{1}{2}m_2\omega_{2\rho}^2\rho^2, \tag{2.13}$$

in Eq. (2.9) and (2.10) respectly.

2.2 Numerical Results

We shall present results for the coupled 1D-2D case when the cigar-shaped BEC is perpendicular to the disk-shaped BEC. The cigar-shaped BEC, labeled 1, lies along the z axis and has angular frequencies satisfying $\omega_{1\rho}/\omega_{1z}=10$. The disk-shaped BEC, labeled 2, lies in the (x,y) plane and has trapping angular frequencies satisfying $\omega_{2z}/\omega_{2\rho}=10$. For simplicity, we work in dimensionless units $m_1=m_2=\hbar=1$, set $N_1=N_2=N$ and in this chapter we shape the strength of nonlinearities intra and inter-species using a simpler number, for example: $Ng_{12}=4\pi$. For the cigar-shaped BEC we take $\omega_{1z}=1$ and for the disk-shaped BEC we take $\omega_{2\rho}=1$.

It is easier to study the behavior of this system by looking at the linear and radial densities, which are calculated from the solution of Eq. (2.11) and (2.12) via

$$|f_1(z;t)|^2=2\pi\int_0^\infty \rho\; d\rho|\psi_1(\rho,z;t)|^2, \tag{2.14}$$

$$|h_2(\rho;t)|^2=\int_{-\infty}^\infty dz|\psi_2(\rho,z;t)|^2. \tag{2.15}$$

To solve the coupled GP equation Eq. (2.11 and 2.12) we employ the split-step Crank-Nicolson discretization technique [21–23] with real and imaginary time propagation. We essentially use the Fortran programs provided in reference [21]. The convergence of the numerical result was tested by varying the space (typically ~ 0.05) and time (typically ~ 0.001) steps and the total number of spatial and temporal discretization points.

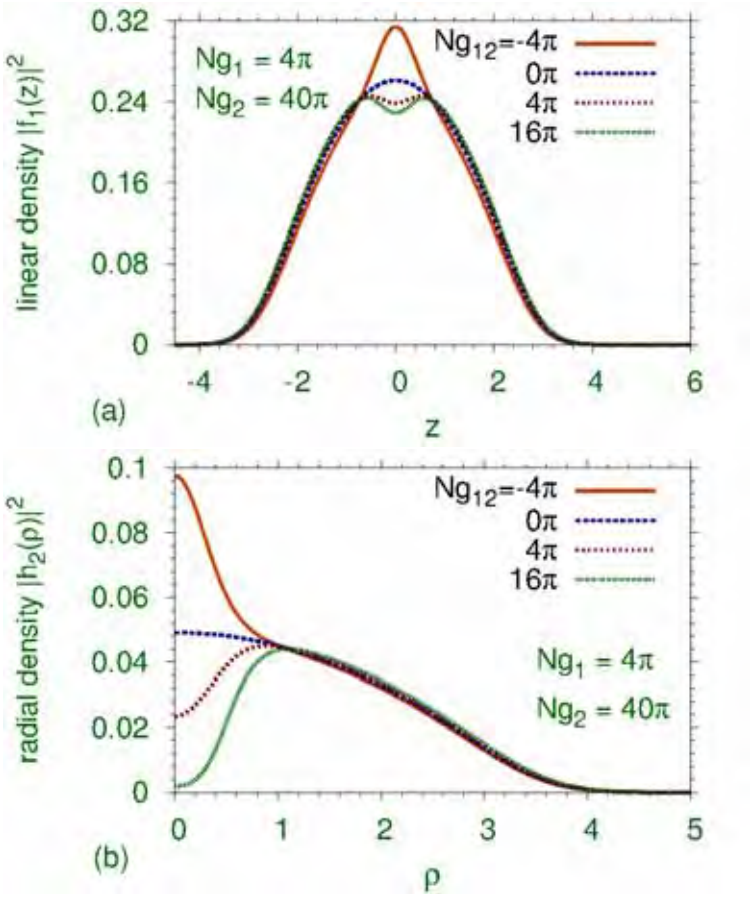

Figure 2.2: Plot of (a) linear $|f_1(z;t)|^2 = 2\pi \int_0^\infty \rho \; d\rho |\psi_1(\rho, z; t)|^2$ and (b) radial $|h_2(\rho; t)|^2 = \int_{-\infty}^{\infty} dz |\psi_2(\rho, z; t)|^2$ densities of a binary perpendicular cigar-disk mixture as obtained from the three-dimensional(3D) Gross-Pitaevskii (GP) equations (2.11) and (2.12) in dimensionless units for the nonlinearities $Ng_1 = 4\pi$, $Ng_2 = 40\pi$ and different values of Ng_{12}. Both densities are normalized to unity.

2.2.1 Mixing - Demixing States

In Figs. 2.2 (a) and (b) we plot the linear $|f_1(z)|^2$ and radial densities $|h_2(\rho)|^2$ respectively, obtained from the 3D equations (2.11) and (2.12) for $Ng_1 = 4\pi$, $Ng_2 = 40\pi$ and for different values of Ng_{12}. The case for $g_{12} = 0$ corresponds with the absence of coupling. We have an attractive interspecies interaction ($g_{12} < 0$) corresponding to the mixing state (overlapping phases of two components). In the same form, for a repulsive interspecies interaction ($g_{12} > 0$) we observe that the highest value of density is not located in the center point of the traps, corresponding to the demixing state (separated phases of two components).

.

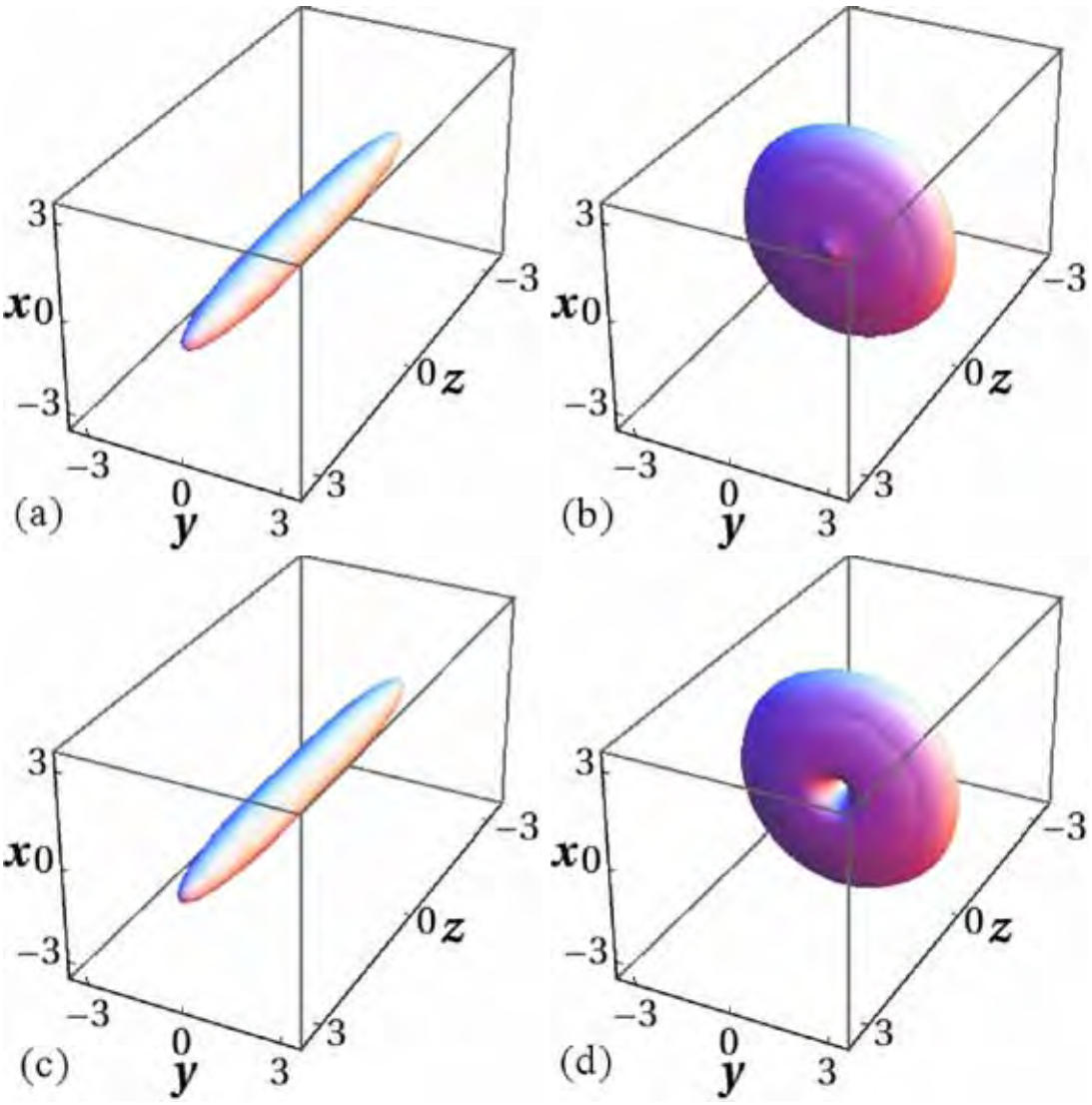

Figure 2.3: Three-dimensional contour plot of the (a) cigar and (b) disk densities $|\psi_j(\rho, z; t)|^2$ of the binary BEC of Fig. 2.2 for attractive interspecies interaction $Ng_{12} = -4\pi$. The same for the (c) cigar and (d) disk densities of the binary BEC for repulsive interspecies interaction $Ng_{12} = 16\pi$. Density on contour = 0.01, and $Ng_1 = 4\pi$, $Ng_2 = 40\pi$.

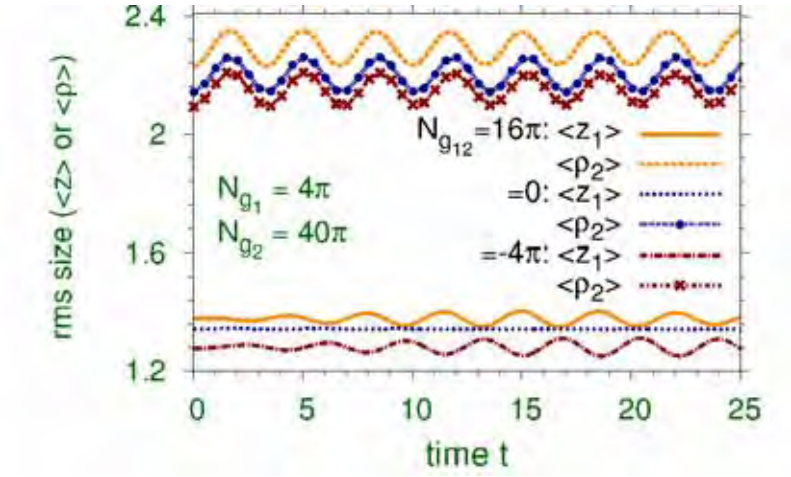

Figure 2.4: Evolution of axial $\langle z \rangle$ and radial $\langle \rho \rangle$ rms sizes of the cigar- and disk-shaped components of the binary Bose-Einstein condensate (BEC) after a sudden reduction of the radial angular frequency of the disk shaped component by 5%, for the nonlinearities $Ng_1 = 4\pi, Ng_2 = 40\pi$, and different values of Ng_{12}.

To study these configurations, we consider the 3D profile of the density $|\psi_j(\rho, z; t)|^2$ of the two species for the cases depicted in Figs. 2.2 (a) and (b) with $Ng_{12} = -4\pi$ and $Ng_{12} = 16\pi$. For this purpose, in Fig 2.3 (a) and (b) we plot the contours of cigar and disk-shape profiles for attractive interaction interspecies ($Ng_{12} = -4\pi$). The same plots for repulsive interspecies interaction ($Ng_{12} = 16\pi$) are illustrated in Figs. 2.3 (c) and (d). The density $|\psi_j(\rho, z; t)|^2$ on the surface of these plots is 0.01. In Figs. 2.3 (a) and (b) it is possible to see that the two components have the highest value of density in the center of system conforming the mixing state and in Figs. 2.3 (c) and (d) we observe that both BECs are moving away from each other in agreement with the demixing state.

2.2.2 Dynamics

We investigated the dynamics of the 1D-2D system. For this purpose we consider the coupled system presented in Figs. 2.2 (a) and (b) with $Ng_1 = 4\pi, Ng_2 = 40\pi$, and different values of Ng_{12}. After the stationary condensate is created during time evolution of the numerical routine using real-time propagation, we reduce the radial angular frequency of the disk-shaped quasi-2D BEC suddenly by 5% (the new angular frequencies being $\omega_{1\rho} = \omega_{2z} = 10, \omega_{1z} = 1, \omega_{2\rho} = 0.95,$) and study the subsequent dynamical evolution of the system.

The relevant dynamics are best illustrated by plotting the evolution of the rms axial size of the cigar-shaped (quasi-1D) BEC and the rms radial size of the disk-shaped (quasi-2D) BEC, in Fig. 2.4 for the sets of nonlinearities exhibited in Figs.

2.2. These results are calculated with the 3D GP equations (2.11) and (2.12). For the sets of nonlinearities illustrated in Fig. 2.4 ($Ng_1 = 4\pi, Ng_2 = 40\pi$, with different values of $Ng_{12} = 0, 4\pi$ and 16π) the angular frequency of the quasi-2D disk-shaped BEC was modified and exhibited sinusoidal oscillation for the axial size of the disk-shaped BEC right from $t = 0$.

It took some five units of time for similar sinusoidal oscillation to initiate in the unperturbed cigar-shaped component due to the non-zero coupling term g_{12}. We can see that this effect on the unperturbed BEC disappears without the presence of coupling interspecies (for $g_{12} = 0$ in Fig. 2.4). This is an important opportunity to see changes on global features (macroscopic properties) in a quantum system.

In summary, we realize the description of a binary BEC where the components are subject to distinct trap symmetries belonging to two different spatial dimensions. In particular, we considered the possibility that the first component is in 1D (cigar shape) and the second in 2D (disk shape). The 1D and 2D configurations were achieved in an axially-symmetric setting with a strong harmonic trap in the transverse radial and axial directions, respectively. We found the numerical solutions for this 3D binary GP equation, in the coupled 1D-2D case where the cigar-shaped component is in the z direction and the disk-shaped component remains in the (x, y) plane, by calculating the density profiles and dynamics for small oscillation of the binary 1D-2D BEC, initiated by a sudden change of the radial angular frequency of the 2D component, for different values of nonlinearities. Now we have an important background to study more complex coupled systems.

This same approach could be used in many situations of interest when one or both of the BEC components have extreme distinct cigar and disk shapes and when we are interested in density and dynamics in axial and radial directions, respectively, is possible starting from these binary three-dimensional Gross-Pitaevskii equations (2.7) and (2.8) and using a Lagrangian variational approach to derive a binary effective nonlinear Schrödinger equation [2] with components in different reduced dimensions, the first component in one dimension and the second in two dimensions as appropriate to represent a cigar-shaped BEC coupled to a disk-shaped BEC.

[2] In Appendix A and more widely in reference [25], we present effective reduced equations for the study of a binary Bose-Einstein condensate, where the confining potentials of the two BEC components have distinct asymmetry so that the components belong to different space dimensions.

3

BEC with Dipolar Interaction

The experimental observation of a dipolar Bose-Einstein condensation (BEC) of ^{52}Cr [11], ^{164}Dy [12] and ^{168}Er [13] atoms with large magnetic moments has opened up new avenues of research into cold atoms, in a quest for novel and interesting features related to anisotropic long-range dipolar interaction. Polar molecules, with much larger (electric) dipole moments, are also being considered [14] for BEC experiments. The experimental realization of these BECs with a long-range dipolar interaction allows the study of new atomic systems with variable short-range interaction and many distinct features [33–37]. Among the interesting features of a dipolar trapped BEC, one can mention its peculiar shape [38–41], anisotropic soliton, vortex soliton [26, 42, 43] vortex lattice [44], as well as super-fluid soliton [45] states. The atomic interaction in a dilute BEC of alkali-metal and other types of atoms (with negligible dipole moments) is represented by an S-wave (short-range) contact (delta-function) potential. However, the non-local anisotropic long-range dipolar interaction acts in all partial waves and is attractive in certain directions and repulsive in others. The energy V_{dd} due to the dipole-dipole interaction, of two dipoles oriented with an extra applied electric field along the z direction, has the following form [20, 46]:

$$V_{dd}(\mathbf{R}) = \frac{C_{dd}}{4\pi}\frac{1-3\cos^2\theta}{R^3}, \quad \mathbf{R} = \mathbf{r} - \mathbf{r}', \tag{3.1}$$

where $\mathbf{R}$ is the vector joining the two dipoles, the coupling constant is $C_{dd} = \mu_0\bar{\mu}^2$, for particles having a permanent magnetic dipole moment $\bar{\mu}$, μ_0 is the permeability of vacuum, and θ is the angle made by the vector $\mathbf{R}$ with the polarization z direction (Fig. 3.1).

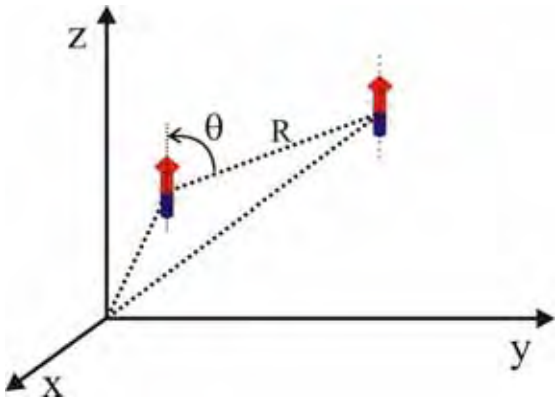

Figure 3.1: Intuitive picture for two particles interacting via the dipole-dipole interaction in a external applied field along the z direction. Here $\mathbf{R}$ corresponds to vector joining the two dipoles and θ is the angle made by the vector $\mathbf{R}$ with the polarization z direction.

This dipolar potential has two notable features: first is the rather complicated angular dependence, to exhibit the anisotropic character. The second characteristic is the inverse-cube dependence on the separation showing the long-range of this interaction, in contrast to the usual short-range interaction for nondipolar BEC. This anisotropic nature is described in Figs. 3.2 (a) and (b). The Fig. 3.2 (a) was produced[1] in order to illustrate the experimental results in dipolar BEC [11], where the contact interaction is reduced with respect to the long-range dipole-dipole interaction, and the anisotropy of the dipolar interaction manifests itself in an elongation of the condensate along the magnetization direction giving in a change for the condensate aspect ratio [11]. In the same form, biconcave profile density could arise in disk shaped dipolar gases because to dipole-dipole repulsion along the radial direction drives the atoms to a peripheral region. These red-blood-cell-like biconcave profiles, such as Fig 3.2 (b), have been found in a previous paper related with the single-component case [35]. These characteristics are a manifestation of the dipolar interaction, and here we emphasize that this type of features have been found in our results. The biconcave profile density was found in our study of binary dipolar BEC near the stability (chapter 6), and also evidence for the change in the condensate aspect ratio was found in chapter 7 studying an untrapped dipolar droplet bound in a trapped nondipolar BEC.

To include these effects of dipole-dipole interaction, it is convenient to introduce an additional dipolar nonlinearity

$$F_{dd}(\mathbf{r},t) = \int V_{dd}(\mathbf{R})|\psi(\mathbf{r}',t)|^2 d\mathbf{r}'. \tag{3.2}$$

[1] The picture 3.2 (a) was obtained from the homepage of research group of Tilman Pfau *et. al.*: News From The Lab: A quantum ferrofluid, 2007. http://www.pi5.uni-stuttgart.de/en/

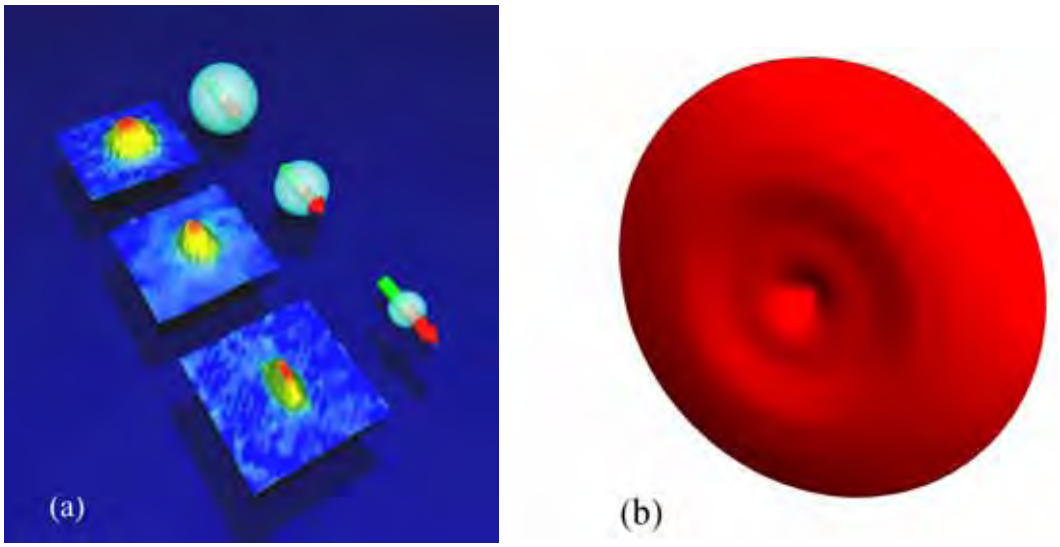

Figure 3.2: Illustrative picture of the dipolar effects. (a) From top to bottom: the (isotropic) contact interaction (symbolized by the grey "sphere") is reduced with respect to the long-range dipole-dipole interaction. The anisotropy of the dipolar interaction manifests itself in an elongation of the condensate along the magnetization direction giving in a change for the condensate aspect ratio (color experimental images on the left)[11]. (b) The red-blood-cell like biconcave profile as a manifestation of the dipolar interaction in disk-shaped condensate. Most of the atoms leave the central region of the disk because of dipolar repulsion in the plane [35].

Now one just needs to introduce this dipolar contribution to the mean-field potential in the Gross-Pitaevskii (GP) equation:

$$i\hbar\frac{\partial}{\partial t}\psi(\mathbf{r},t) = \Big[-\frac{\hbar^2}{2m}\nabla^2 + U_{ext}(\mathbf{r}) + \frac{4\pi\hbar^2}{m}aN|\psi(\mathbf{r},t)|^2 + F_{dd}(\mathbf{r},t)\Big]\psi(\mathbf{r},t), \quad (3.3)$$

with m, a and N the mass, scattering length, and number of atoms, respectively and normalization $\int|\psi(\mathbf{r},t)|^2 d\mathbf{r} = 1$. The external potential $U_{ext}(\mathbf{r})$ is:

$$U_{ext}(\mathbf{r}) = \frac{1}{2}m\omega\left(x^2 + y^2 + \lambda^2 z^2\right), \quad (3.4)$$

where $\lambda = \omega_z/\omega$, the angular frequencies of trap are $\omega_x = \omega_y = \omega$ and ω_z corresponding to axial symmetry. In some circumstances, it is convenient to define a measure to quantify the strength of dipolar interaction, using the dipole moment and the mass m of the atom, we can define the following length:

$$a_{dd} = \frac{\mu_0\bar{\mu}^2 m}{12\pi\hbar^2}, \quad (3.5)$$

Table 3.1: Dipolar quantities for some atoms and molecules. For the molecular species, the values are taken from [46]. The parameter ε_{dd} determines if the contribution of dipolar interaction can be negligible or is necessary to include the dipolar effects.

Species	Dipole moment	a_{dd}	ε_{dd}
^{87}Rb	1.0 μ_B	0.7 a_0	0.007
^{52}Cr	6.0 μ_B	15 a_0	0.15
^{168}Er	7.0 μ_B	66 a_0	0.66
^{164}Dy	10.0 μ_B	131 a_0	1.31
ND_3	1.5 D	3.6 $\times 10^3 a_0$	36
HCN	3.0 D	2.4 $\times 10^4 a_0$	240

this length measures the strength of the dipole-dipole interaction and its experimental value in case of atoms of ^{52}Cr is $a_{dd}(\mathrm{Cr}) = 15a_0$ [11, 33, 34, 47], where a_0 is the Bohr radius [2]. Using this value is possible to calculate the strength of dipolar interaction for other elements. We have, for example, that in case of ^{168}Er:

$$a_{dd}(\mathrm{Er}) = \frac{\mu_0\ \bar{\mu}_{Er}^2\ m_{Er}}{12\pi\hbar^2} = 15a_0 \times \left(\frac{\bar{\mu}_{Er}}{\bar{\mu}_{Cr}}\right)^2 \frac{m_{Er}}{m_{Cr}} = 66a_0, \tag{3.6}$$

in same form, we used $a_{dd}(\mathrm{Dy}) = 131a_0$ as value for the strength of dipolar interaction of ^{164}Dy. To compare the dipolar and contact interactions, the ration of the strength of the dipolar interaction to the s-wave scattering length is expressed by

$$\varepsilon_{dd} = \frac{a_{dd}}{a}, \tag{3.7}$$

associating the relative strength of the dipolar and contact interactions. This parameter ε_{dd} determines the physical properties of the system establishing if the contribution of dipolar interaction can be negligible or if is necessary to include the dipolar effects. In Table 3.1 we have some typical values of the dipolar quantities for different types of atoms and molecules [46], showing that both atoms with larger magnetic dipole moments ($\bar{\mu} \simeq 10\mu_B$) and polar molecules, with much larger electric dipole moments ($1\mathrm{D} \simeq 3.3 \times 10^{-30}\ C \cdot m$), have an important contribution of dipolar interaction and any theory needs a way to include this interaction in order to describe suitably its physical characteristics.

On other hand, we can defined the oscillator length l_0 by

$$l_0 = \sqrt{\frac{\hbar}{m\omega}}, \tag{3.8}$$

[2] From experimental measures for ^{52}Cr we have that its magnetic dipole moment is $\bar{\mu} = 6\mu_B$, where μ_B is the Bohr magneton [11, 33].

where ω is an angular frequency generally associated with the trap frequencies. The length scale a_{dd}, and l_0 could be used to transform Eq. (3.3) into the following dimensionless form:

$$i\frac{\partial}{\partial t}\psi(\mathbf{r},t) = \Big[-\frac{1}{2}\nabla^2 + U_{ext}(\mathbf{r}) + g|\psi(\mathbf{r},t)|^2 + g_{dd}\int U_{dd}(\mathbf{R})|\psi(\mathbf{r}',t)|^2 d\mathbf{r}'\Big]\psi(\mathbf{r},t), \tag{3.9}$$

where $g = 4\pi a N$, $g_{dd} = 3Na_{dd}$, and

$$U_{dd}(\mathbf{R}) = \frac{1-3\cos^2\theta}{R^3}, \tag{3.10}$$

is the simpler form of the dipolar interaction. In Eq. (3.9) we use an oscillator unit, this means: length is expressed in units of the oscillator length l_0, energy in units of the oscillator energy $\hbar\omega$, density $|\psi|^2$ in units of l_0^{-3}, and time in units of $t_0 = \omega^{-1}$. Here the dimensionless trapping potential $U_{ext}(\mathbf{r})$, for axial symmetry, has the form:

$$U_{ext}(\mathbf{r}) = \frac{1}{2}\left(x^2 + y^2 + \lambda^2 z^2\right), \tag{3.11}$$

here the parameter λ determines the anisotropy of trap, i.e, $\lambda \ll 1$ for cigar-shaped and $\lambda \gg 1$ for systems with disk-shape symmetry. This GP equation (3.9) is an integro-differential equation, which usually complicates the numerical solution procedure. The evaluation of the dipolar integral term in this equation in coordinate space is not straightforward due to the divergence at short distances. However, this has been tackled by evaluating the dipolar term in the momentum ($\mathbf{k}$) space. The integral can be simplified in Fourier space by means of the following convolution theorem [3]:

$$\int U_{dd}(\mathbf{r}-\mathbf{r}')|\psi(\mathbf{r}',t)|^2 d\mathbf{r}' = \mathcal{F}^{-1}\{\mathcal{F}[U_{dd}](\mathbf{k})\mathcal{F}[|\psi|^2](\mathbf{k})\}(\mathbf{r}), \tag{3.12}$$

where $\mathcal{F}[\,]$ and $\mathcal{F}^{-1}\{\}$ are the Fourier transform (FT) and inverse FT, respectively. The FT of the dipole potential is known analytically, and has the form [46]:

$$U_{dd}(\mathbf{k}) = \frac{4\pi}{3}\left(\frac{3k_z^2}{\mathbf{k}^2} - 1\right). \tag{3.13}$$

In this form, the divergence of the dipolar term at short distances has been handled by treating this term in momentum ($\mathbf{k}$) space. The FT of density $|\psi|^2$ is evaluated numerically by means of a standard fast FT (FFT) algorithm. A simpler form for the dipolar integral in (Fourier) momentum space Eq. (3.12) arises from the following convolution integral:

$$\int d\mathbf{r}' U_{dd}(\mathbf{R})n(\mathbf{r}') = \int \frac{d\mathbf{k}}{(2\pi)^3} e^{-i\mathbf{k}\cdot\mathbf{r}} U_{dd}(\mathbf{k})n(\mathbf{k}), \tag{3.14}$$

[3] In Appendix B we present the procedure to include the dipolar term in our numerical solutions using the convolution theorem as in reference [46].

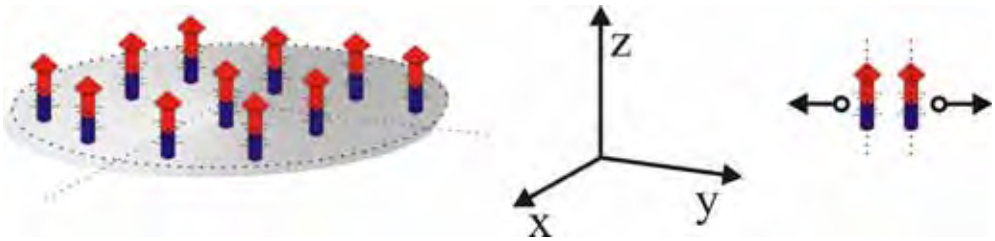

Figure 3.3: Intuitive picture for the stability of a disk-shaped dipolar BEC in an axially-symmetric setting with a strong harmonic trap in the axial directions. With the dipoles oriented along the strong confinement axis, the main effect of the dipole-dipole interaction is repulsive and as a peculiarity, in dipolar BEC, it is only stable for the number of atoms below a critical value.

with $n(\mathbf{r},t) = |\psi(\mathbf{r},t)|^2$, where the FT is defined by

$$A(\mathbf{k}) = \int d\mathbf{r} B(\mathbf{r}) e^{i\mathbf{k}\cdot\mathbf{r}}, \quad B(\mathbf{r}) = \frac{1}{(2\pi)^3} \int d\mathbf{k} A(\mathbf{k}) e^{-i\mathbf{k}\cdot\mathbf{r}}. \tag{3.15}$$

Previously, there have been studies of stability for nondipolar Bose gas [48–52], however the stability of a dipolar BEC depends not only on its scattering length or number of particles, but also on the trap geometry [11, 46, 47, 53, 54] more strongly that the nondipolar case. The dipolar interaction can shift from repulsive to attractive for different configurations of traps, a disk-shaped trap gives a repulsive dipolar interaction and the dipolar BEC is more stable, whereas a cigar-shaped trap yields an attractive dipolar interaction and hence favors a collapse instability. In the disk configuration, the dipolar interaction is highly repulsive, as parallel dipoles arranged in a plane with the dipole moment perpendicular to the plane repel each other (Fig. 3.3). In contrast, a cigar-shaped trap yields an attractive dipolar interaction, as the dipoles lie along the same line, corresponding with the direction of magnetization (z axis). The dipoles attract each other, which may favor a collapse (Fig. 3.4).

In this thesis we perform numerical simulation of the 3D GP equation (3.9) using the split-step Crank-Nicolson method [21–23]. The dipolar integral Eq. (3.12), involving the FT of density multiplied by the FT of dipolar interaction, is evaluated using the convolution theorem (3.12). The inverse FT is evaluated by means of a standard FFT algorithm. The FFT algorithm is carried out in Cartesian coordinates and hence the GP equation is solved in three dimensions irrespective of the symmetry of the trapping potential. Using the GP Eq. (3.3) in chapter 4 we study the properties of the statics and dynamics of the cigar-shaped bright solitons for *repulsive* short-range interaction in a dipolar BEC.

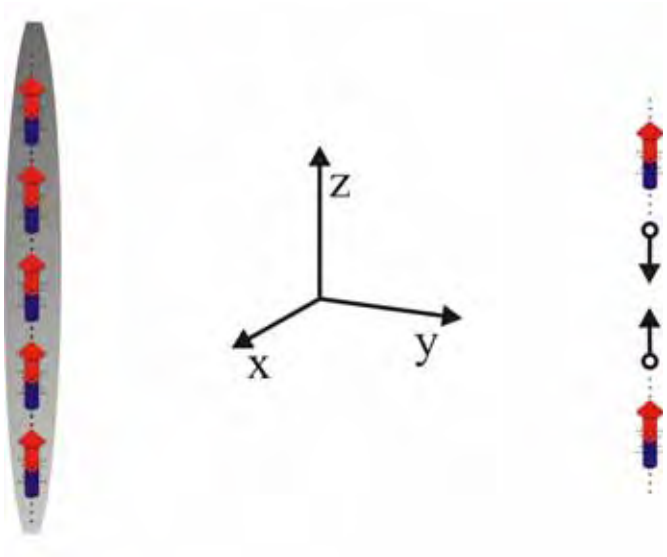

Figure 3.4: Illustrative picture for the stability of a cigar-shaped dipolar BEC in an axially-symmetric setting with a strong harmonic trap in the transverse radial direction. With the dipoles oriented along the weak confinement axis, the dipole-dipole interaction is essentially attractive, which leads to an instability of the dipolar BEC.

We show a system that is formed under very general conditions and could be of greater experimental interest. In chapter 5 we study the static and dynamic properties of a disk-shaped dipolar BEC for large scattering length using a beyond-mean-field model [45, 55], to show the sensitivity of the result to the universal behavior of the dipolar condensate under a strong-coupling regime. In chapter 6, we numerically solve two coupled Gross-Pitaevskii equations for the binary dipolar BEC [28]. Finally, in chapter 7 we study some properties which are of great interest, such as how all the features and properties of a trapped dipolar BEC would manifest in a 3D quasi-free untrapped dipolar BEC bound to a trapped nondipolar BEC by attractive inter-species contact interaction [29].

4

Bright Soliton on Dipolar BEC

A bright soliton is a self-reinforcing solitary wave that maintains its shape, while traveling at constant speed, due to a cancellation of nonlinearity and dispersive effects. Previously, there have been theoretical studies of solitons in nondipolar Bose-Einstein condensate (BEC) [56–62] and more recently we have demonstrated the creation of bright solitons in Fermi gases[1] with two-components spin-balanced by means of the self-repulsive nonlinearity in combination with the harmonic trapping potential acting in one or two transverse directions [18]. Experimentally, bright solitons and soliton trains were created in a BEC of ^{7}Li [32, 63] and ^{85}Rb atoms [64] by turning the atomic attractive interaction from repulsive using a Feshbach resonance [65] and releasing the BEC to be axially free. The controllable short-range interaction with the exotic dipolar interaction makes the dipolar BEC an interesting system for soliton generation in the cigar configuration due to added *dipolar attraction* and a challenging system for theoretical investigation [66] to study the interplay between the dipolar and short-range interactions.

We study cigar−shaped (one−dimensional) bright solitons for *repulsive* short range interaction in a dipolar BEC free to move along the axial direction and trapped in the radial direction, using the three-dimensional (3D) Gross-Pitaevskii (GP) equation, and study their statics and dynamics. The present one-dimensional (1D) solitons can be formed under very general conditions and hence, are of

[1] In Fermi gases, with balanced spin-up and spin-down components, self-localized ground states (i. e., bright solitons) may be achieved by making the repulsion between the spin components accordingly modulated in one or two directions, and the application of the ordinary external trapping potential in the other direction(s), see reference [18].

greater experimental interest. For a conventional BEC without dipole moment, bright solitons appear only for attractive atomic interaction [57, 64]. Here phase plots showing the stability of the solitons for different dipolar and short-range interactions are obtained. Also we study breathing oscillation and collision of two bright solitons as well as the statics and dynamics of the bright solitons using a Gaussian variational approach.

4.1 Analytical Consideration

There have been prior studies of solitons in cigar-shaped dipolar BEC using a reduced quasi-1D simple model [67, 68]. As there is no collapse in 1D (models with cubic nonlinearity as in this case), such studies predict solitons for attractive interaction for an arbitrarily large number of atoms. But nondipolar BEC bright solitons [61] in 3D are stable up to a critical number of atoms, beyond which the system collapses. The same is found to be true for a dipolar BEC. We reported these critical numbers for dipolar BEC solitons in figure 4.1. We study the bright solitons in a dipolar BEC [11, 33, 34, 47] of N atoms, using the following dimensionless GP equation, similar with Eq. (3.9) in chapter 3, with an potential trap equal zero along the z direction

$$i\frac{\partial\phi(\mathbf{r},t)}{\partial t} = \Bigg[-\frac{1}{2}\nabla^2 + \frac{\rho^2}{2} + 4\pi aN|\phi(\mathbf{r},t)|^2 + 3a_{dd}N\int U_{dd}(\mathbf{r}-\mathbf{r}')|\phi(\mathbf{r}',t)|^2 d\mathbf{r}'\Bigg]\phi(\mathbf{r},t), \tag{4.1}$$

where $i=\sqrt{-1}$, the normalization is

$$\int |\phi(\mathbf{r},t)|^2 d\mathbf{r} = 1, \tag{4.2}$$

and a is the atomic scattering length. Here the length a_{dd} and $U_{dd}(\mathbf{r}-\mathbf{r}')$ are measures of the dipolar interaction defined in Eqs. (3.5) and (3.10) of chapter 3 respectly. The trap $\rho^2/2$ acts in the radial $\rho\equiv(x,y)$ direction only. In Eq.(4.1) we use oscillator units, where a unit of length is the oscillator length, defined in Eq. (3.8), taken as $l_0 = 1\mu$m and a unit of time is taken as t_0 =1 ms. Lagrangian density of Eq. (4.1) for bright solitons is [69]

$$\mathcal{L} = \frac{i}{2}\left(\phi\,\partial_t\phi^\star - \phi^\star\,\partial_t\phi\right) + \frac{1}{2}|\nabla\phi|^2 + \frac{\rho^2}{2}|\phi|^2 + 2\pi aN|\phi|^4 + \frac{3}{2}a_{dd}N|\phi|^2\int U_{dd}(\mathbf{r}-\mathbf{r}')|\phi(\mathbf{r}',t)|^2 d\mathbf{r}'. \tag{4.3}$$

where ∂_t denotes time derivative and $\phi^\star$ correspond with the complex conjugate to the wave function ϕ. It is straightforward to verify that Eq. 4.1 is the Euler-Lagrange equations for the Lagrangian density 4.3, we can find this equation by

deriving for $\phi^\star$

$$\frac{d}{dt}\left(\frac{\partial \mathcal{L}}{\partial \dot{\phi}^\star}\right) - \frac{\partial \mathcal{L}}{\partial \phi^\star} = 0, \tag{4.4}$$

using Eq. (4.3) in Eq. (4.4), we have the following expression for the dynamics of a bright soliton in dipolar BEC

$$\begin{aligned}\frac{i}{2}\partial_t\phi(\mathbf{r},t) &- \Big\{ -\frac{i}{2}\partial_t\phi(\mathbf{r},t) + \frac{1}{2}\frac{\partial}{\partial\phi^\star}[(\nabla\phi^\star)(\nabla\phi)] + \frac{\rho^2}{2}\phi(\mathbf{r},t) + 4\pi aN|\phi|^2\phi(\mathbf{r},t) \\ &+ 3a_{dd}N\phi(\mathbf{r},t)\int U_{dd}(\mathbf{r}-\mathbf{r}')|\phi(\mathbf{r}',t)|^2 d\mathbf{r}'\Big\} = 0,\end{aligned} \tag{4.5}$$

using $|\nabla\phi|^2 = (\nabla\phi^\star)(\nabla\phi) = \nabla(\phi^\star\nabla\phi) - \phi^\star\nabla^2\phi$ we have

$$\begin{aligned}i\partial_t\phi(\mathbf{r},t) = \Big[-\frac{1}{2}\nabla^2 &+ \frac{\rho^2}{2} + 4\pi aN|\phi(\mathbf{r},t)|^2 \\ &+ 3a_{dd}N\int U_{dd}(\mathbf{r}-\mathbf{r}')|\phi(\mathbf{r}',t)|^2 d\mathbf{r}'\Big]\phi(\mathbf{r},t),\end{aligned} \tag{4.6}$$

where the last mathematical expression corresponds with the dynamics equation for a bright soliton in dipolar BEC: Eq. (4.1).

4.1.1 Variational Approximation

For a variational study we use the following Gaussian ansatz [70]:

$$\phi(\mathbf{r},t) = \frac{\pi^{-3/4}}{w_\rho\sqrt{w_z}}\exp\left(-\frac{\rho^2}{2w_\rho^2} - \frac{z^2}{2w_z^2} + i\alpha\rho^2 + i\beta z^2\right), \tag{4.7}$$

where w_ρ and w_z are time-dependent widths and α and β are time-dependent phases. Using the last ansatz of Eq. (4.7) into the Lagrangian density Eq. (4.3), we can obtain the effective Lagrangian $L \equiv \int \mathcal{L}\, d\mathbf{r}$ (per particle):

$$\begin{aligned}L = \int \Big[\frac{i}{2}(\phi\ \partial_t\phi^\star &- \phi^\star\ \partial_t\phi) + \frac{1}{2}|\nabla\phi|^2 + \frac{\rho^2}{2}|\phi|^2 + 2\pi aN|\phi|^4 \\ &+ \frac{3}{2}a_{dd}N|\phi|^2\int U_{dd}(\mathbf{r}-\mathbf{r}')|\phi(\mathbf{r}',t)|^2 d\mathbf{r}'\Big]\, d\mathbf{r},\end{aligned} \tag{4.8}$$

that we choose to divide into five integrals

$$L = L_1 + L_2 + L_3 + L_4 + L_5 \tag{4.9}$$

where each integral can be solved independently to obtain

$$\begin{aligned}L_1 &= \frac{i}{2}\int(\phi\ \partial_t\phi^\star - \phi^\star\ \partial_t\phi)\, d\mathbf{r}, \\ L_1 &= \frac{2\pi^{-1/2}}{\omega_\rho^2\omega_z}\left[\dot{\alpha}\frac{\omega_\rho^4}{2}(\sqrt{\pi}\omega_z) + \dot{\beta}\frac{\omega_\rho^2}{2}\left(\frac{\sqrt{\pi}}{2}\omega_z^3\right)\right] = \omega_\rho^2\dot{\alpha} + \frac{1}{2}\omega_z^2\dot{\beta},\end{aligned} \tag{4.10}$$

$$
\begin{aligned}
L_2 &= \frac{1}{2}\int |\nabla\phi(\mathbf{r},t)|^2 d\mathbf{r}, \\
L_2 &= \frac{1}{2}\int (\nabla\phi^\star)(\nabla\phi)\; d\mathbf{r} = 2\alpha^2\omega_\rho^2 + \frac{1}{2\omega_\rho^2} + \beta^2 w_z^2 + \frac{1}{4\omega_z^2},
\end{aligned} \tag{4.11}
$$

$$
\begin{aligned}
L_3 &= \frac{1}{2}\int \rho^2 |\phi(\mathbf{r},t)|^2\; d\mathbf{r}, \\
L_3 &= \frac{\pi^{-3/2}}{2w_\rho^2 w_z}\int \rho^2 \exp\left(-\frac{\rho^2}{w_\rho^2} - \frac{z^2}{w_z^2}\right)\; d\mathbf{r} = \frac{1}{2}w_\rho^2,
\end{aligned} \tag{4.12}
$$

$$
\begin{aligned}
L_4 &= 2\pi a N \int |\phi(\mathbf{r},t)|^4\; d\mathbf{r}, \\
L_4 &= \frac{2\pi^{-2} a N}{w_\rho^4 w_z^2}\int \exp\left(-\frac{2\rho^2}{w_\rho^2} - \frac{2z^2}{w_z^2}\right)\; d\mathbf{r} = \frac{aN}{\sqrt{2\pi} w_\rho^2 w_z},
\end{aligned} \tag{4.13}
$$

and finally the fifth integral can be simplified in Fourier space by means of convolution theorem, as is showing in Appendix B, to obtain

$$
\begin{aligned}
L_5 &= \frac{3}{2} a_{dd} N \int \left[\int U_{dd}(\mathbf{r}-\mathbf{r}')|\phi(\mathbf{r}',t)|^2 d\mathbf{r}'\right] |\phi(\mathbf{r},t)|^2 d\mathbf{r}, \\
L_5 &= \frac{a_{dd} N}{\sqrt{2\pi}} \frac{(-1)}{w_\rho^2 w_z} f(\kappa),
\end{aligned} \tag{4.14}
$$

where

$$
f(\kappa) = \frac{1 + 2\kappa^2 - 3\kappa^2 d(\kappa)}{1-\kappa^2}, \quad d(\kappa) = \frac{\operatorname{atanh}(\sqrt{1-\kappa^2})}{\sqrt{1-\kappa^2}}, \quad \kappa \equiv \frac{w_\rho}{w_z}, \tag{4.15}
$$

at once the effective Lagrangian Eq. (4.8) has the form

$$
L = w_\rho^2 \dot{\alpha} + \frac{1}{2} w_z^2 \dot{\beta} + 2w_\rho^2 \alpha^2 + w_z^2 \beta^2 + \frac{1}{2}\left(\frac{1}{w_\rho^2} + \frac{1}{2w_z^2} + w_\rho^2\right) + \mathcal{E}_{\text{dip}}, \tag{4.16}
$$

with

$$
\mathcal{E}_{\text{dip}} = \frac{N a_{dd}}{\sqrt{2\pi}} \frac{1}{w_\rho^2 w_z}\left[\frac{a}{a_{dd}} - f(\kappa)\right], \tag{4.17}
$$

In the cigar shape, the dipolar interaction becomes attractive and contributes negatively in $\mathcal{E}_{\text{dip}}$. We used the Euler-Lagrange equations for parameters w_ρ, w_z, α, and β to obtain the following equations for each one

$$
\frac{d}{dt}\left(\frac{\partial L}{\partial \dot{q}_j}\right) - \frac{\partial L}{\partial q_j} = 0, \quad q_j = [w_\rho, w_z, \alpha, \beta], \tag{4.18}
$$

this means, using the Eq. (4.16) into Eq. (4.18) we obtain the following expressions for the widths

$$\frac{\partial L}{\partial w_\rho} = 2w_\rho\dot{\alpha} + 4w_\rho\alpha^2 - \frac{1}{w_\rho^3} + w_\rho - \frac{1}{\sqrt{2\pi}}\frac{N}{w_\rho^3 w_z}\left[2a - a_{dd}\; g(\kappa)\right] = 0, \tag{4.19}$$

where

$$g(\kappa) = \frac{2 - 7\kappa^2 - 4\kappa^4 + 9\kappa^4 d(\kappa)}{(1-\kappa^2)^2}, \tag{4.20}$$

now for w_z we found

$$\frac{\partial L}{\partial w_z} = w_z\dot{\beta} + 2w_z\beta^2 - \frac{1}{2w_z^3} - \frac{N}{\sqrt{2\pi}w_\rho^2 w_z^2}\left[a - a_{dd}\; h(\kappa)\right] = 0, \tag{4.21}$$

with

$$h(\kappa) = \frac{1 + 10\kappa^2 - 2\kappa^4 - 9\kappa^2 d(\kappa)}{(1-\kappa^2)^2}, \tag{4.22}$$

and for parameters α and β we have

$$\frac{d}{dt}\left(\frac{\partial L}{\partial \dot{\alpha}}\right) - \frac{\partial L}{\partial \alpha} = \dot{\omega}_\rho - 2\omega_\rho\alpha = 0, \tag{4.23}$$

$$\frac{d}{dt}\left(\frac{\partial L}{\partial \dot{\beta}}\right) - \frac{\partial L}{\partial \beta} = \dot{\omega}_z - 2\omega_z\beta = 0, \tag{4.24}$$

from equations 4.23 and 4.24 we can write

$$\alpha = \frac{\dot{\omega}_\rho}{2\omega_\rho} \rightarrow \dot{\alpha} = \frac{1}{2\omega_\rho}\left(\ddot{\omega}_\rho - \frac{\dot{\omega}_\rho^2}{\omega_\rho}\right), \tag{4.25}$$

and

$$\beta = \frac{\dot{\omega}_z}{2\omega_z} \rightarrow \dot{\beta} = \frac{1}{2\omega_z}\left(\ddot{\omega}_z - \frac{\dot{\omega}_z^2}{\omega_z}\right), \tag{4.26}$$

now with the substitution of α and β in Eqs. (4.19) and (4.21) we obtained a new form by the equations of the widths

$$\ddot{w}_\rho + w_\rho = \frac{1}{w_\rho^3} + \frac{N}{\sqrt{2\pi}w_\rho^3 w_z}\left[2a - a_{dd}\; g(\kappa)\right], \tag{4.27}$$

$$\ddot{w}_z = \frac{1}{w_z^3} + \frac{2N}{\sqrt{2\pi}w_\rho^2 w_z^2}\left[a - a_{dd}\; h(\kappa)\right], \tag{4.28}$$

Equations (4.27) and (4.28) determine the dynamics of bright solitons. The stationary widths are obtained from these equations by setting $\ddot{w}_\rho = \ddot{w}_z = 0$. If μ is the chemical potential with which the stationary wave function $\phi(\mathbf{r}, t)$ propagates in time, it means

$$\phi(\mathbf{r}, t) \sim \exp(-i\mu t)\phi(\mathbf{r}), \tag{4.29}$$

then from equation of a bright soliton in dipolar BEC Eq. (4.1) multiplying by $\phi^\star(\mathbf{r})$ and integrating we found the following expression to chemical potential

$$\mu = \int \left[\frac{1}{2}|\nabla\phi(\mathbf{r})|^2 + \frac{\rho^2}{2}|\phi(\mathbf{r})|^2 + 4\pi a N|\phi(\mathbf{r})|^4 + 3a_{dd}N \int U_{dd}(\mathbf{r}-\mathbf{r}')|\phi(\mathbf{r}')|^2|\phi(\mathbf{r})|^2 d\mathbf{r}' \right] d\mathbf{r}, \tag{4.30}$$

where the variation of the kinetic energy term was carried out by performing an interaction by parts. In this form the variational estimate for the stationary chemical potential μ is given by

$$\mu = \frac{1}{2w_\rho^2} + \frac{1}{4w_z^2} + \frac{w_\rho^2}{2} + 2\,\mathcal{E}_{\text{dip}}, \tag{4.31}$$

in similar form, the energy for this system can be written as [1]:

$$E = N \int \left[\frac{1}{2}|\nabla\phi(\mathbf{r})|^2 + \frac{\rho^2}{2}|\phi(\mathbf{r})|^2 + 2\pi a N|\phi(\mathbf{r})|^4 + \frac{3}{2}a_{dd}N \int U_{dd}(\mathbf{r}-\mathbf{r}')|\phi(\mathbf{r}')|^2|\phi(\mathbf{r})|^2 d\mathbf{r}' \right] d\mathbf{r}, \tag{4.32}$$

using the ansatz of Eq. (4.7) and (4.29) we get the following equation

$$\frac{E}{N} = \frac{1}{2w_\rho^2} + \frac{1}{4w_z^2} + \frac{w_\rho^2}{2} + \mathcal{E}_{\text{dip}}, \tag{4.33}$$

corresponding with the expression for energy per particle in the stationary state with the variational approximation. From Eqs. (4.30) and (4.32) is straightforward to verify the thermodynamic relation $\mu = \partial E/\partial N$ to calculate the chemical potential from the energy of the stationary state.

4.2 Numerical Results

We perform a 3D numerical simulation in Cartesian (x, y and z) variables employing imaginary and real-time propagation with the Crank-Nicolson method using Fortran programs provided in reference [21]. The dipolar interaction is evaluated by the usual fast Fourier transformation [46]. The accuracy of the

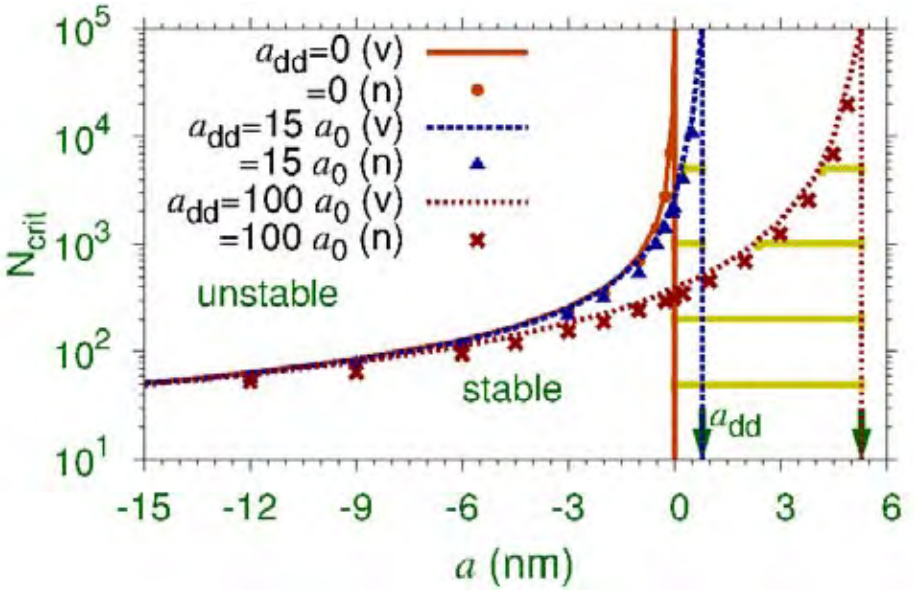

Figure 4.1: Stability phase plot for variational (v) and numerical (n) results showing the critical number (N_{crit}) of atoms versus scattering length (a) for BEC with different strengths of dipolar interaction (a_{dd}). The two arrows at $a = a_{dd}$ show the limit of the region in which a soliton can appear. In dipolar BEC, bright solitons can appear for repulsive contact interaction, the yellow horizontal lines (right side) denote this region of stability inaccessible for nondipolar BECs.

numerical simulation was tested by varying the size of space and time steps and the total number of space and time steps. For bright solitons the system must be attractive. In the absence of dipole moment ($a_{dd} = 0$), attraction corresponds to $a < 0$. For $a_{dd} > 0$, the dipolar interaction in Eq. (4.1) contributes attractively in the cigar shape, which can compensate for the atomic short-range repulsion, thus forming bright solitons for $a > 0$. From a variational study Eq. (4.28), we choose $[a - a_{dd}h(\kappa)] = 0$ while one must have $N \to \infty$. Then from Eq. (4.27), as $N \to \infty$, one must have $[2a - a_{dd}g(\kappa)] = 0$. These two conditions can be simultaneously satisfied as $\kappa \to 0$ for a weakly bound soliton of infinite extension along the axial direction while $h(\kappa = 0) = g(\kappa = 0)/2 = 1$. Consequently, bright solitons are allowed for $-\infty < a < a_{dd}$ and for N below a critical number (N_{crit}) of atoms, as Eq. (4.27) and Eq. (4.28) only permit solutions for $N < N_{\text{crit}}$.

4.2.1 Stable State

As discussed previously, this system collapses for $N > N_{\text{crit}}$. These results are illustrated in Fig. 4.1 , where we show N_{crit} versus a for $a_{dd} = 15a_0$ (^{52}Cr atom), and $100a_0$, for bright solitons from numerical and variational calculation.

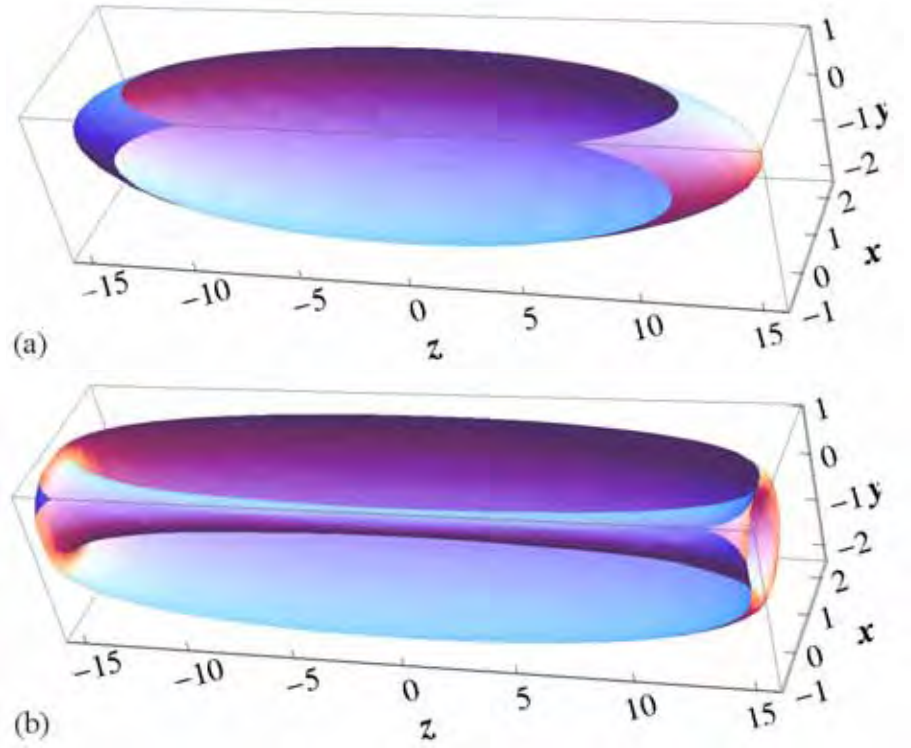

Figure 4.2: A sectional view of the three-dimensional (3D) contour plot of density for a (a) bright ($a_{dd} = 15a_0$ and $a = 0.5$ nm) and (b) vortex ($a_{dd} = 100a_0$, $a = 4$ nm, $l = 1$) solitons of $N = 1000$ atoms. The lengths x, y and z are in units of $l_0(= 1\mu\text{m})$ and the density on the contour is 0.001. Both of these solitons correspond to a repulsive region ($a > 0$) inaccessible to nondipolar BEC.

The value $a_{dd} = 100a_0$ is considered to simulate a possible dipolar BEC of dipolar atoms (or molecules) of larger dipole moment, such as ^{164}Dy [12, 71], or ^{168}Er [13], which can be considered for BEC experiment. The unstable, attractive region of collapse ($N > N_{\text{crit}}, a < a_{dd}$), stable soliton formation ($N < N_{\text{crit}}, a < a_{dd}$) and the repulsive region of expansion ($a > a_{dd}$) are clearly shown in figure 4.1 where we found a new region of stability for $a > 0$ (yellow horizontal lines right side of Fig. 4.1) inaccessible for the nondipolar BECs.

In our numerical simulation we shall consider dipolar BEC with $a_{dd} > a > 0$, domain of soliton controlled by dipolar interaction and unreachable for a normal BEC with $a_{dd} = 0$. To illustrate the shape of the quasi-1D soliton, in figure 4.2 (a) we show a section of the 3D contour plot of density of a bright soliton of 1000 atoms for $a = 0.5$ nm, and $a_{dd} = 15a_0 = 0.7938$ nm. In similar form, we suggest a cigar-shaped vortex soliton for repulsive short-range interaction, this means a bright soliton of (quantized) unit angular momentum in a dipolar BEC

Table 4.1: Numerical (n) and variational (v) chemical potential μ, root-mean-square sizes $\langle z\rangle$, $\langle\rho\rangle$, and number of atoms N for a soliton before collision at $t = 0$ that is equivalent to Fig. 4.2 (a), and a soliton after the dynamic simulation at t =11.22 ms corresponding to Fig. 4.4. These results are showing the quasi-elastic nature of collision.

	bright (v)	bright (n)	bright (n)
t	0	0	11.22 ms
μ	0.9815	0.9822	0.9877
$\langle z\rangle$	6.0973	6.0958	6.0805
$\langle\rho\rangle$	0.9935	0.9924	0.9625
N	1000	1000	1000

with $a > 0$ inaccessible to nondipolar BEC. Without dipolar interaction, for usual BEC, solitons with intrinsic vorticity trapped in the cigar-shaped potential were considered by Salasnich et. al. [72]. Vortex states of higher angular momentum ($l > 1$) are unstable and decay into multiple vortices of angular momentum $\hbar$. To obtain a quantized vortex of angular momentum $l\hbar, l = 1$, around axial z axis, one has to introduce a phase (equal to the azimuthal angle) in the wave function [73]. This procedure introduces a centrifugal term $l^2/2\rho^2$ in the GP equation for a vortex and we adopt this method to find a vortex soliton. In Fig. 4.2 (b) we show a section of the 3D contour plot of the density of a vortex soliton for $N = 1000, a = 4$ nm, and $a_{dd} = 100a_0 = 5.2917$ nm, which clearly exhibits the vortex core along the z axis.

4.2.2 Collision dynamics

Beginning with the initial soliton created by imaginary-time propagation we can obtain a subsequent dynamic generated by real-time propagation. In this form we now investigate the collision between two bright solitons of figure 4.2 (a). Two such solitons, prepared by imaginary-time propagation, are placed at $z = \pm 25.6$ μm at $t = 0$ and are then advanced by real-time propagation of Eq. (4.1) with $N = 2000$. Each soliton is attributed a velocity of about 10 mm/s towards center $z = 0$ by including a phase factor $\exp(ivz)$ with v a constant in the initial wave function. The real-time simulation is terminated when the solitons reach $z = \mp 25.6$ μm at $t = 11.22$ ms. There is no exchange of atoms between solitons during collision. To quantitatively compare the solitons before ($t = 0$) and after ($t = 11.22$ ms) collision, we show in Table 4.1 the numerical and variational results of chemical potential, rms sizes, and number of atoms of the initial and final solitons, to be in good agreement with each other.

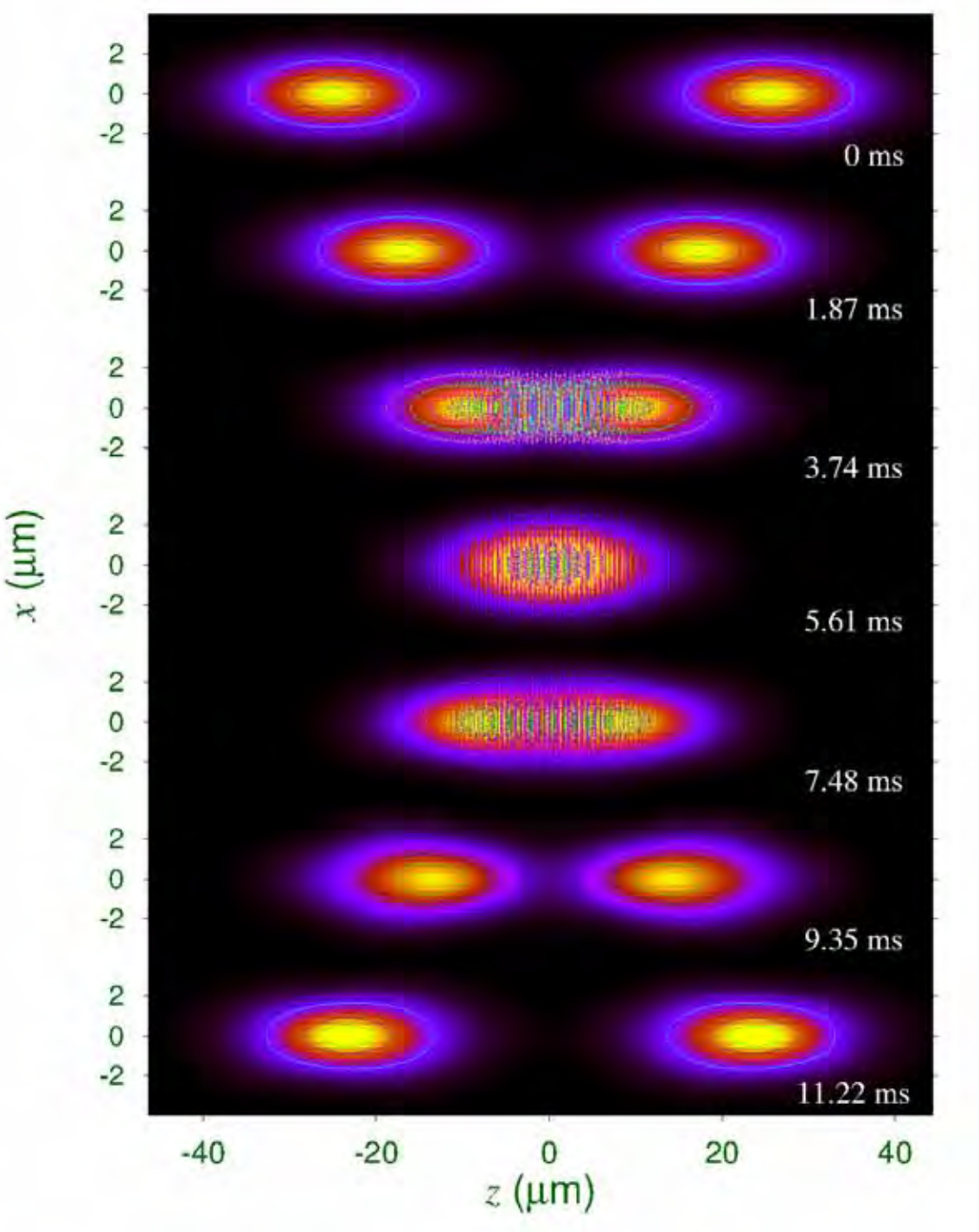

Figure 4.3: Contour plot of density $|\phi(x, 0, z, t)|^2$ of two colliding bright solitons of figure 4.2 (a) each one with $N = 1000$ atoms, $a_{dd} = 15a_0$ and $a = 0.5$ nm, and with relative velocity 1 cm/s, before (0, 1.87 and 3.74 ms), during (5.61 ms) and after (7.48, 9.35 and 11.22 ms) collision.

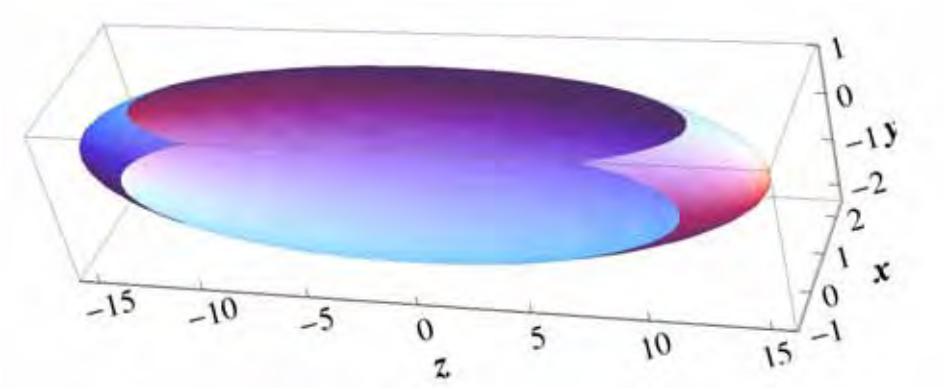

Figure 4.4: A sectional view of the 3D contour plot of density for a bright soliton at time $t = 11.22$ ms after the collision considered in figure 4.3. The lengths x, y and z are in units of $l_0 (= 1\mu\text{m})$ and the density on the contour is 0.001. The result agrees with the figure 4.2 (a) before the collision. The similarity of plots for the initial state with the final state after collision demonstrates the elastic nature of the collision.

The collision dynamics are illustrated in figure 4.3 for bright solitons, where we show snapshots of contour plots of density $|\phi(x, 0, z, t)|^2$ at different times before (0, 1.87 ms, 3.74 ms), during (5.61 ms) and after (7.48 ms, 9.35 ms, 11.22 ms) collision. The solitons come towards each other, interact at $z = 0$ and then separate and come out practically unchanged.

The quasi-elastic collision at such a large relative velocity of 1 cm/s demonstrates the solitonic nature and robustness of the bright soliton [2]. To illustrate the quasi-elastic nature of collision, we show in figure 4.4 the 3D contour density plot of the final states at time $t = 11.22$ ms after the collision illustrated in figure 4.3 for bright solitons. The similarity of plots in figures 4.4, for the final states after collision, with the initial states in figures 4.2 (a) demonstrates the elastic nature of the collision.

The quasi-elastic collision at high velocity is insensitive to the initial phase of the solitons. At low velocity ($\sim$0), the interaction is sensitive to the initial phase. Two solitons placed side-by-side at rest along the z direction of opposite phase repel, whereas two of the same phase attract and form a stable bound soliton molecule [57]. The dynamics of the formation of the soliton molecule from two equal-phase solitons of Fig. 4.2 (a) is shown in Fig. 4.5, where we plot the contour plot of 1D density $d(z, t) \equiv 2\pi \int \rho \, d\rho |\phi(\mathbf{r}, t)|^2$ versus time t and z.

[2] Video clips of the collision dynamics for bright solitons of figure 4.3 are also prepared and contained at http://www.youtube.com/watch?v=ds2CzZqN9M4

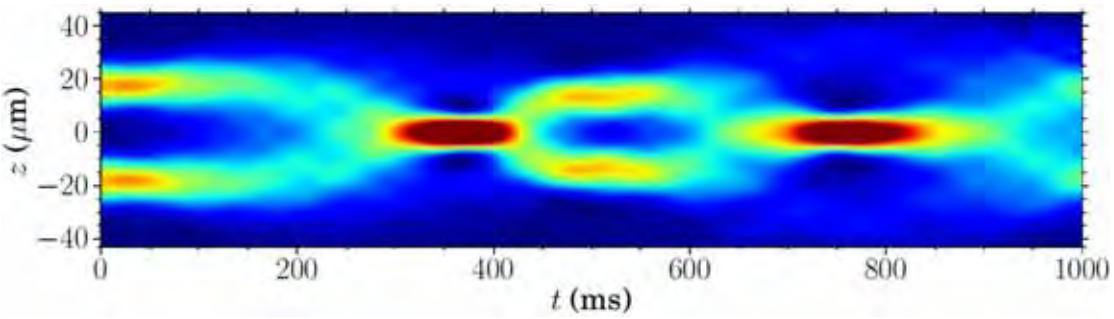

Figure 4.5: Dynamics of soliton pair formation from the contour plot of 1D density $d(z,t) \equiv 2\pi \int \rho \, d\rho |\phi(\mathbf{r},t)|^2$ versus time of two bright solitons of Fig. 4.2 (a) each one with $N = 1000$ atoms, $a_{dd} = 15a_0$, $a = 0.5$ nm and the same phase. Both solitons are placed side by side at rest ($t = 0$) with low velocity (~ 0), due to dipolar attraction some time afterwards, the solitons come close, coalesce and oscillate forming a stable bound soliton molecule.

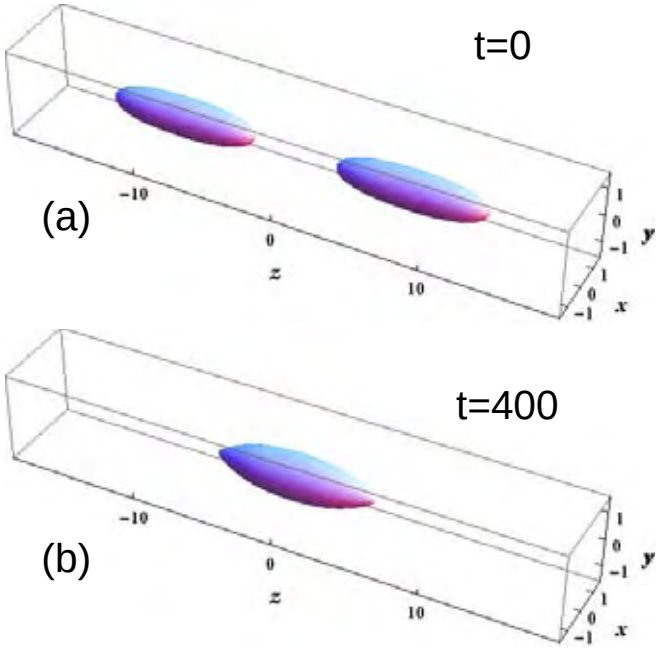

Figure 4.6: Three-dimensional contour plots of densities $|\phi(\mathbf{r},t)|^2$ for (a) two initial bright solitons placed side by side at rest at $t = 0$ and (b) a soliton molecule formed from these two equal-phase bright solitons at $t = 400$ ms during collision. Both solitons with $N = 1000$ atoms, $a_{dd} = 15a_0$, $a = 0.5$ nm and the same phase such as in Fig. 4.5 at low velocity.

The initial positions of the bright solitons are ± 17.6 μm. Due to dipolar attraction the solitons come close, coalesce and oscillate forming a stable bound soliton molecule [57] [3]. In this case the two bright solitons in Fig. 4.5, after formation, the soliton molecule breaks into two solitons, and then forms a molecule, thus oscillating between a molecule and two-soliton phases. This is illustrated in Figs. 4.6 (a) and (b) where we exhibit the 3D contour plots of the two interacting bright solitons of Fig. 4.5 at $t = 0$ and 400 ms, before and during collision at low velocity respectively.

In summary, all of our variational results for bright solitons are in good agreement with the numerical results, and a very important point is that for this system, distinguished by the dipolar interaction, we found new results which are inaccessible for a normal BEC with $a_{dd} = 0$ and could be created realized in a laboratory with current technology.

[3] Video clips of the molecule formation dynamics of figure 4.5 are also prepared for bright solitons and contained at http://www.youtube.com/watch?v=tnnF0nbi1gs

5

Universality of a Dipolar Condensate at Unitarity

The properties of a uniform dilute interacting (Bose or Fermi) atomic quantum gas interacting by an S-wave contact interaction at zero temperature is determined by two scales: the atomic scattering length a and density n. As $a \to \infty$ at unitarity (strong-coupling regime), the first scale is not of concern; the observables of the gas are solely determined by density and the gas exhibits a universal behavior. Bulk chemical potential $\tilde{\mu}$ of the unitary gas is proportional to the *only* available energy scale, Fermi energy (or the chemical potential of the noninteracting gas)

$$E_F = \frac{\hbar^2}{2m}(6\pi^2 n)^{2/3} \tag{5.1}$$

so that

$$\tilde{\mu} = \xi E_F \ , \tag{5.2}$$

where ξ is a universal parameter and m is the mass of an atom [45, 74–79]. Similarly, the energy per particle $\tilde{E}$ of the unitary gas is proportional to the energy per particle $E(\equiv 3E_F/5)$ of the noninteracting gas.[76, 77]. The Fermi energy is a physically meaningful quantity for the Fermi gas, but the same can also be used as an energy scale for the Bose gas [75, 79]. The Bose and Fermi gases should behave similarly at unitarity. Consequently, ξ should be the same for the Bose and Fermi gases. The parameter ξ relating the energy of the noninteracting and unitary gases, has been "measured" experimentally from a study at or near unitarity of the density [74, 80], or of ground-state energy, of a trapped Fermi

gas. But a similar experiment is more difficult for a Bose-Einstein condensate (BEC) due to a large probability of three-body loss by molecule formation at or near unitarity, which is the threshold for molecule formation [79].

In the weak-coupling limit $an^{1/3} < 1$ ($an^{1/3}$ is a dimensionless quantity), the mean-field Gross-Pitaevskii (GP) equation gives a good description of a trapped BEC. In the strong-coupling regime ($an^{1/3} > 1$) the GP equation highly overestimates the atomic contact interaction and leads to unphysical results. Experimental activities to access the strong-coupling regime of a BEC, to test the beyond mean-field corrections [81], and to extract the parameter ξ from these studies have just begun [79]. Although unitarity is also the threshold for molecule formation in a two-component (spin up and down) Fermi gas, the probability of formation of diatomic molecules is highly suppressed in this case due to Pauli repulsion among spin-parallel fermions in the three-fermion system and hence is not of concern [74].

Lately, BECs of ^{52}Cr [11, 33], ^{164}Dy [12, 71] and ^{168}Er [13] with large dipolar interaction have been observed and studied. The inter-atomic interaction now has two components: an S-wave contact interaction and an anisotropic long-range dipolar interaction. This allows one to study the dipolar BEC with a variable contact interaction [12, 33] using a Feshbach resonance [65]. The intrinsically anisotropic dipolar BEC [34, 82] has many distinct features [11, 26, 33]. The stability of a dipolar BEC depends not only on the scattering length, but also on the trap geometry [33]. A disk-shaped trap leads to a repulsive dipolar interaction and the dipolar BEC is more stable, whereas a cigar-shaped trap yields an attractive dipolar interaction and hence favors instability towards collapse [33, 40].

In this chapter we study the static and dynamic properties of a disk-shaped dipolar BEC for large scattering length using a beyond-mean-field model [45, 55] for the BEC-unitarity crossover. We consider the strong-coupling limit of the contact interaction only and *not* the same limit of dipolar interaction. In the weak-coupling limit, this crossover model reduces to the GP equation and the Lee-Huang-Yang (LHY) correction [83], so away from the strong-coupling regime our results will not be sensitive to ξ, whereas in the strong-coupling regime of large scattering length it reduces to the universal result at unitarity, where the LHY correction will yield an unphysical divergent result. We use the fact that in the disk configuration, the dipolar interaction is highly repulsive, as parallel dipoles arranged in a plane with the dipole moment perpendicular to the plane repel each other [11, 33]. The strongly repulsive dipolar interaction should reduce three-body loss by molecule formation in the strong-coupling regime, as the rate of the reaction $3A \to A_2 + A$ should be suppressed in this setting with A representing a dipolar atom and A_2 a molecule. Also, as both the contact and long-range dipolar interactions contribute to molecule formation, the threshold for molecule

formation will be displaced from unitarity, especially in strongly dipolar BECs, thus creating a new scenario of experiment with a dipolar BEC in the strong-coupling regime to determine the parameter ξ. As unitarity will not be the threshold for molecule formation and three-body loss will be reduced in a disk-shaped dipolar BEC, experiments close to the strong-coupling regime will be easier to perform in this set up.

5.1 Analytical Formulation

5.1.1 General Dipolar Gross-Pitaevskii Equation

We consider a dipolar BEC of N atoms, using the next dimensionless GP equation, similar with Eq. (3.9) in chapter 3, where a bulk chemical potential $\tilde{\mu}$ is the nonlinear term [33]:

$$i\frac{\partial\phi(\mathbf{r},t)}{\partial t} = \left[-\frac{\nabla^2}{2} + U_{ext}(\mathbf{r}) + \tilde{\mu}(a,N) + F_{dd}(a_{dd},N)\right]\phi(\mathbf{r},t), \tag{5.3}$$

with $i=\sqrt{-1}$, density $n=N|\phi|^2$, normalization $\int|\phi(\mathbf{r})|^2d\mathbf{r}=1$, atomic scattering length a and the dipolar nonlinearity given by

$$F_{dd}(a_{dd},N) = 3a_{dd}N\int U_{dd}(\mathbf{R})|\phi(\mathbf{r}',t)|^2d\mathbf{r}', \tag{5.4}$$

where the length a_{dd} measures the strength of dipolar interaction, $\mathbf{r}\equiv\{x,y,z\}$, and $\mathbf{R}=\mathbf{r}-\mathbf{r}'$. Here $U_{dd}(\mathbf{R})$ represents the dipole-dipole interaccion defined in Eq. (3.10) of chapter 3. Moreover, for a disk-shaped dipolar BEC

$$U_{ext}(\mathbf{r}) = \frac{1}{2}(x^2+y^2+\lambda^2z^2), \tag{5.5}$$

is the harmonic trap with $\lambda\gg1$ the trap anisotropy.

In Eq. (5.3) the $\mathbf{r}$ and t dependence of $\tilde{\mu}$ and F_{dd} are not explicitly shown. The length is measured in units of $l_0\equiv\sqrt{\hbar/m\omega}$, where ω is the harmonic angular frequency in x or y directions, and time t in units of $t_0=\omega^{-1}$. For weak coupling the bulk chemical potential $\tilde{\mu}$ has the normal form to GP equation:

$$\tilde{\mu}(a,n) = 4\pi an, \tag{5.6}$$

at unitarity, the bulk chemical potential of Eq. (5.3) is independent of a and is [75]:

$$\tilde{\mu}(n) = \frac{1}{2}\xi(6\pi^2n)^{2/3}, \tag{5.7}$$

proportional to the Fermi energy.

5.1.2 BEC-Unitarity Crossover

Lee, Huang, and Yang (LHY) [83] obtained the leading terms of the beyond-mean-field expression for energy of a uniform Bose gas from which the following expression for the bulk chemical potential can be obtained [84]:

$$\tilde{\mu}(a,N) = 4\pi an\left[1+\alpha a^{3/2}\sqrt{n}\right], \tag{5.8}$$

where $\alpha = 32/(3\sqrt{\pi})$. The lowest order term in this expansion is the GP result Eq.(5.6). However, the expression of Eq.(5.8), although giving the leading correction for larger $an^{1/3}$, diverges in the strong-coupling regime, and hence has only limited validity along the BEC-unitarity crossover. In addition to studying the system in the weak-coupling limit Eq.(5.6) and unitarity Eq.(5.7), we also consider the system along the full BEC-unitarity crossover from weak to strong coupling, as the parameter $an^{1/3}$ is increased. For this purpose we consider the following minimal crossover model for the bulk chemical potential consistent with weak and strong couplings [27]

$$\tilde{\mu}(a,n) = 4\pi n^{2/3} f(\chi), \tag{5.9}$$

$$f(\chi) = \frac{\chi + (1+\nu)\alpha\chi^{5/2}}{1+\nu\alpha\chi^{3/2}+(1+\nu)\gamma\chi^{5/2}}, \tag{5.10}$$

where

$$\chi = an^{1/3},\ \alpha = \frac{32}{3\sqrt{\pi}},\ \frac{\alpha}{\gamma} = \frac{\xi}{8\pi}(6\pi^2)^{2/3}\ , \tag{5.11}$$

and ν is the only free parameter in this expression. The parameters α and γ are determined by the constraints that expression Eq.(5.9) be consistent with the LHY correction Eq.(5.8) as well as the unitarity limit Eq.(5.7). The expression of Eq. (5.9) is weakly sensitive to ν and a smooth interpolation between the weak and strong-coupling regimes is obtained for any small ν. In this study we use $\nu = 1$. This value of ν was used [85] successfully in a study of $^6Li_2$ BEC in the BEC-unitarity crossover.

The crossover model Eq.(5.9) yields the hydrodynamic equations of the dipolar BEC at zero temperature, which enables one to study collective dynamical properties of the system in the full crossover from weak-coupling to unitarity [45, 55]. Equations (5.3) and (5.9) should be considered as a generalization of the GP equation with beyond mean-field corrections to properly include the effect of interaction for large positive scattering length. The saturation of the interaction at unitarity is properly taken care of in the crossover model Eq.(5.9). As an application we shall study here the properties of a disk-shaped dipolar BEC in the strong-coupling regime to show the sensitivity of the result to the universal parameter ξ.

5.1.3 Variational Approximation at Unitarity

At unitarity, the dipolar mean-field equations (5.3), (5.5), and (5.7) can be conveniently solved by a time-dependent Lagrangian variational approach. This can be used to study physical properties of the dipolar BEC at unitarity such as the size and chemical potential. This is done by reducing Eq. (5.3) to a system of second order nonlinear ordinary differential equations involving the variational parameters. The Lagrangian density of Eq. (5.3) is given by [26]

$$\begin{aligned}\mathcal{L} &= \frac{i}{2}\left(\phi\,\partial_t\phi^\star - \phi^\star\,\partial_t\phi\right) + \frac{1}{2}|\nabla\phi|^2 + \frac{1}{2}(\rho^2+\lambda^2 z^2)|\phi|^2 \\ &+ \frac{3\xi}{10}(6\pi^2 N)^{2/3}|\phi|^{10/3} + \frac{3}{2}a_{dd}N|\phi|^2\int U_{dd}(\mathbf{r}-\mathbf{r}')|\phi(\mathbf{r}')|^2 d\mathbf{r}', \end{aligned} \tag{5.12}$$

where ∂_t denotes time derivative. Recalling that $n = N|\phi|^2$, it can be straightforwardly verified that Eqs. (5.3) and (5.7) are the Euler-Lagrange [24]. To develop the variational approximation, we consider the following Gaussian ansatz for the wave function [26]

$$\phi(\mathbf{r},t) = \sqrt{\frac{\pi^{-\frac{3}{2}}}{w_\rho^2 w_z}}\,\exp\left[-\frac{\rho^2}{2w_\rho^2} - \frac{z^2}{2w_z^2} + i\delta\rho^2 + i\beta z^2\right], \tag{5.13}$$

where the time-dependent variational parameters w_ρ and w_z are the radial and axial widths and δ and β are the chirps. The Lagrangian density can be calculated by substituting the wave function Eq.(5.13) in Eq. (5.12). Then the effective Lagrangian ($L \equiv \int \mathcal{L}\,d\mathbf{r}$) becomes

$$\begin{aligned} L &= \frac{1}{2}\left(2w_\rho^2\dot{\delta} + w_z^2\dot{\beta}\right) + \frac{1}{2}\left(\frac{1}{w_\rho^2} + \frac{1}{2w_z^2} + 4w_\rho^2\delta^2 + 2w_z^2\beta^2\right) \\ &+ \frac{1}{4}\left(2w_\rho^2 + \lambda^2 w_z^2\right) - \frac{Na_{dd}}{\sqrt{2\pi}}\frac{f(\kappa)}{w_\rho^2 w_z} + \frac{9\mathcal{C}}{w_z^{2/3}w_\rho^{4/3}}, \end{aligned} \tag{5.14}$$

where

$$\mathcal{C} = \frac{\sqrt{3/5}}{50\pi}\xi(6\pi^2 N)^{2/3}, \tag{5.15}$$

$$f(\kappa) = \frac{1+2\kappa^2}{1-\kappa^2} - \frac{3\kappa^2\,\tanh^{-1}(\sqrt{1-\kappa^2})}{(1-\kappa^2)^{\frac{3}{2}}}, \tag{5.16}$$

and $\kappa = w_\rho/w_z$ is the ratio of the radial to axial widths of the BEC. The corresponding Euler-Lagrange equations

$$\frac{d}{dt}\left(\frac{\partial L}{\partial \dot{q}_j}\right) - \frac{\partial L}{\partial q_j} = 0, \quad q_j = [w_\rho, w_z, \delta, \beta]. \tag{5.17}$$

governing the evolution of the widths w_ρ and w_z yield

$$\ddot{w}_\rho + w_\rho = \frac{1}{w_\rho^3} - \frac{a_{dd}}{\sqrt{2\pi}} \frac{Ng(\kappa)}{w_\rho^3 w_z} + \frac{12\mathcal{C}}{w_z^{2/3} w_\rho^{7/3}}, \tag{5.18a}$$

$$\ddot{w}_z + \lambda^2 w_z = \frac{1}{w_z^3} - \frac{a_{dd}}{\sqrt{2\pi}} \frac{2N}{w_\rho^2 w_z^2} h(\kappa) + \frac{12\mathcal{C}}{w_z^{5/3} w_\rho^{4/3}}, \tag{5.18b}$$

where

$$g(\kappa) = \frac{2 - 7\kappa^2 - 4\kappa^4}{(1-\kappa^2)^2} + \frac{9\kappa^4 \tanh^{-1}(\sqrt{1-\kappa^2})}{(1-\kappa^2)^{\frac{5}{2}}}, \tag{5.19a}$$

$$h(\kappa) = \frac{1 + 10\kappa^2 - 2\kappa^4}{(1-\kappa^2)^2} - \frac{9\kappa^2 \tanh^{-1}(\sqrt{1-\kappa^2})}{(1-\kappa^2)^{\frac{5}{2}}}. \tag{5.19b}$$

Equations (5.18a) and (5.18b) provide the dynamics of the evolution of radial and axial widths, respectively. The widths for a stationary state can be obtained by setting $\ddot{w}_\rho = 0$ and $\ddot{w}_z = 0$ in Eqs. (5.18a) and (5.18b). The chemical potential μ with which the stationary wave function propagates in time, e.g. $\phi(\mathbf{r}, t) \sim \exp(-i\mu t)\phi(\mathbf{r})$, is given by

$$\mu = \frac{1}{2}\left(\frac{1}{w_\rho^2} + \frac{1}{2w_z^2}\right) + \frac{1}{4}\left(2w_\rho^2 + \lambda^2 w_z^2\right) - \frac{2Na_{dd}}{\sqrt{2\pi}} \frac{f(\kappa)}{w_\rho^2 w_z} + \frac{5}{3} \frac{9\mathcal{C}}{w_z^{2/3} w_\rho^{4/3}}, \tag{5.20}$$

in this variational approximation.

5.2 Numerical Calculation

We perform numerical simulation of the 3D GP equation (5.3) using the split-step Crank-Nicolson method described in reference [21]. In this algorithm we used space step 0.1, time step 0.002 and employed upto 512 space discretization points in each Cartesian direction. We performed an error analysis of the results for chemical potential and rms sizes and found that the maximum numerical error of the results reported here is less than 0.5 %.

5.2.1 Experimental Considerations

From experimental realization of dipolar BECs with ^{52}Cr , ^{164}Dy and ^{168}Er, effects of stronger dipolar interaction can be studied. In the actual experiment on ^{164}Dy a dipolar BEC of 15000 atoms in a fully anisotropic trap with frequencies $\{f_x, f_y, f_z\} = \{380, 500, 1570\}$ Hz was obtained [12]. For ^{164}Dy, an estimate for the scattering length is $a \approx 100a_0$, and for the magnetic moment an estimate is $\bar{\mu} = 10\mu_B$ where μ_B is the Bohr magneton, consequently, $a_{dd} \simeq 131a_0$ with a_0 the Bohr radius [12].

Table 5.1: Theoretical result and experimental evaluation of the parameter $\beta \equiv (\xi - 1)$ for the Bose and Fermi gases. Most accurate theoretical and experimental estimates converge to a value of β very close to -0.6 corresponding to $\xi \sim 0.4$.

		$\beta \equiv (\xi - 1)$
Fermi, Theory	Astrakharchik *et al.*[76]	-0.58
	Carlson *et al.* [77]	-0.58
	Perali *et al.* [86]	-0.545
Fermi, Expt (^{6}Li)	Bartenstein *et al.* [80]	$-0.73^{+0.12}_{-0.09}$
	Navon *et al.* [87]	$-0.59(1)$
	Luo and Thomas [88]	≈ -0.6
Fermi, Expt (^{40}K)	Stewart *et al.* [78]	$-0.54^{+0.05}_{-0.12}$
Bose, Theory	Diederix *et al.* [75]	-0.54
	Lee *et al.* [49]	-0.34
Analysis, Expt ($^6Li_2$) [80]	Adhikari [85]	< 0.6
Bose, Expt (^{7}Li)	Navon *et al.* [79]	$> -0.56(8)$

In this chapter, to simulate an experiment with ^{164}Dy, we use the frequencies $\{f_x, f_y, f_z\} = \{436, 436, 1570\}$ Hz, so that $\lambda = 3.601$, where we take a geometrical mean of the frequencies in x and y directions to generate an axially-symmetric BEC. The length scale employed here, for angular frequency $\omega = 2\pi \times 436$ Hz, is $l_0 = 0.376$ μm.

Next we summarize the different theoretical and experimental estimates of ξ obtained so far for bosons and fermions. Often the parameter ξ is written as $\xi \equiv (1+\beta)$ and different estimates of β are given in Table 5.1, where the variational calculations of reference [49] for bosons is upper bound and the experimental result of reference [79] for ^{7}Li is a lower bound. Yet another estimate of ξ can be obtained from a consideration of Fermi superfluid in the BEC side of the Bardeen-Cooper-Schrieffer-BEC (BCS-BEC) crossover.

Here we reconsider an analysis [85] of the experiment [80] on ^{6}Li in the BEC side of BEC-unitarity crossover. The molecular BEC of $^6Li_2$ was then studied with Eqs. (5.3), (5.9), and (5.10) but using the constant $\xi_{\rm mol}(6\pi^2)^{2/3}/(2\pi)$, where $\xi_{\rm mol}$ is the universal parameter of reference [85], in place of $\xi(6\pi^2)^{2/3}/(8\pi)$ considered here. This implies that for a comparison of the two studies we should take $\xi = 4\xi_{\rm mol}$. The analysis of reference [85] yielded $\xi_{\rm mol} \approx 0.4$, so that $\xi \approx 1.6$ corresponding to $\beta \approx 0.6$. In that analysis [85] it was assumed that $a_m = 0.6a_f$, with a_m the molecular scattering length, which implies that the bosonic molecular unitarity of $^6Li_2$ was achieved for the same strength of atomic interaction as the fermionic unitarity of ^{6}Li. Actually, the bosonic molecular unitarity should be achieved at a different value of interaction and into the BEC side of the BCS-BEC crossover, where the system is less repulsive. This would lead to a smaller

value of the parameter ξ ($\xi < 1.6$) and β. Hence the analysis of reference [85] gives an upper bound. A more quantitative analysis of an accurate experiment with precise information about molecule-molecule scattering length in molecular unitarity of a molecular BEC of fermionic atoms can reveal the correct value of ξ. From the results reported in Table 5.1, most accurate theoretical [76, 77] and experimental [87, 88] estimates for a Fermi gas converge to a value of ξ very close to 0.4. In the present study we will mostly consider $\xi \approx 0.4$. In addition, we also illustrate the sensitivity on our results by varying ξ.

5.2.2 Disk-shaped dipolar condensate

We study a disk-shaped dipolar BEC of 15000 ^{164}Dy atoms with $a_{dd} = 130a_0$ as in the experiment of Lu *et al.* [12].

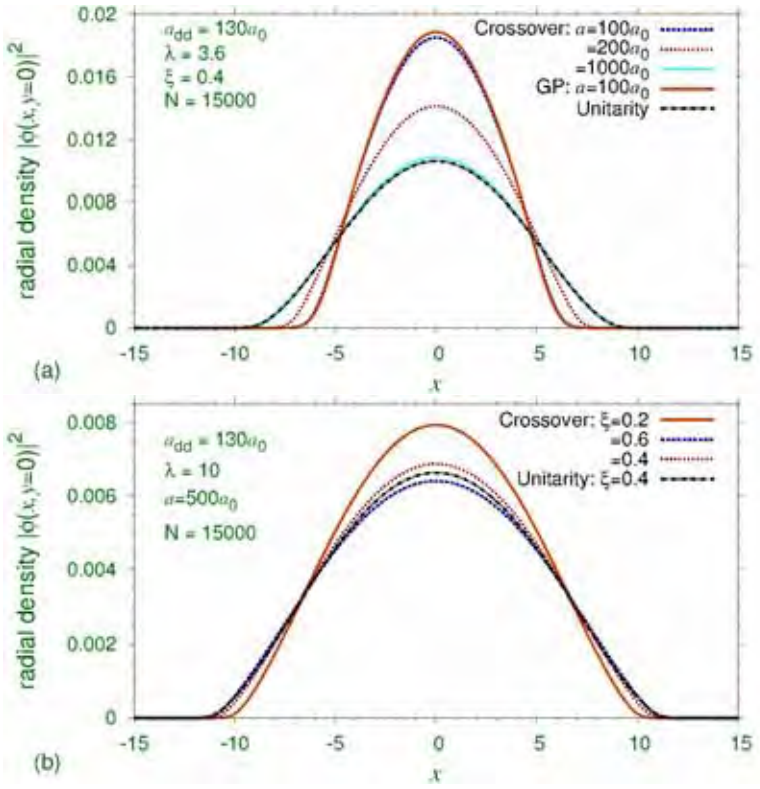

Figure 5.1: Radial density along the x axis $|\Phi(x, y = 0)|^2 = \int dz |\phi(x, y = 0, z)|^2$ of a ^{164}Dy BEC with $a_{dd} = 130a_0$, $N = 15000$, (a) anisotropy trap $\lambda = 3.6$ and $\xi = 0.4$ for $a = 100a_0, 200a_0, 1000a_0$ and at unitarity using Eq.(5.7), the GP limit Eq.(5.6) and the crossover model Eq.(5.9) with $\nu = 1$. (b) The same for $\lambda = 10$, $a = 500a_0$ and $\xi = 0.2, 0.4, 0.6$ using the crossover model Eq.(5.9) and the unitarity Eq.(5.7) for $\xi = 0.4$.

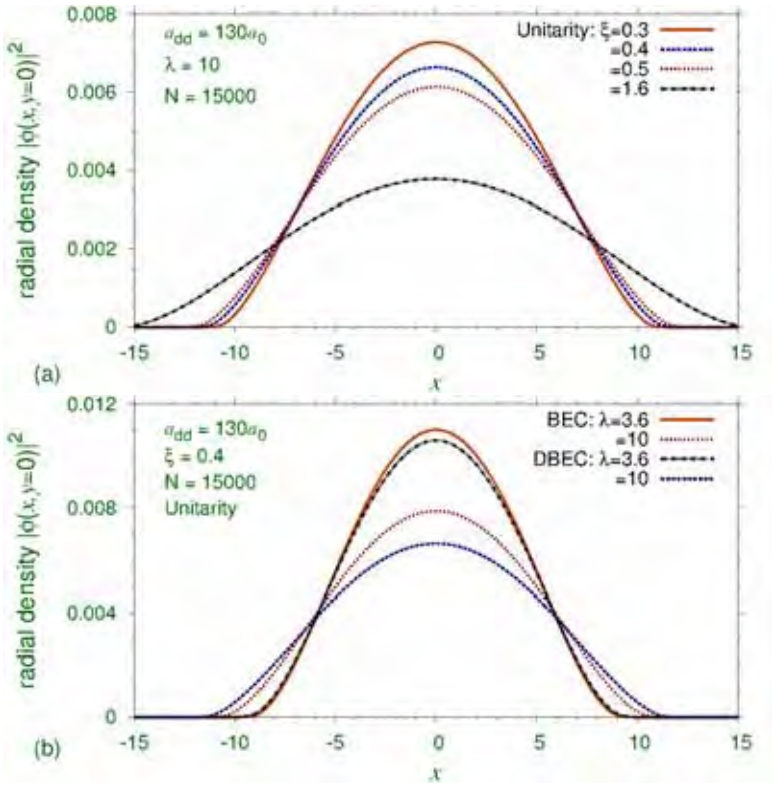

Figure 5.2: Radial density along the x axis $|\Phi(x, y = 0)|^2 = \int dz|\phi(x, y = 0, z)|^2$ of a ^{164}Dy BEC with $a_{dd} = 130a_0$, $N = 15000$ and (a) $\lambda = 10$ for different ξ. (b) The same for $\xi = 0.4$, and two values of $\lambda = 3.6$ and 10. All calculated at unitarity Eq.(5.7) for a dipolar BEC of $a_{dd} = 130a_0$ (DBEC), and $a_{dd} = 0$ (BEC).

The parameter ξ can be extracted from the observables of the dipolar BEC in the strong-coupling regime where the observables would be sensitive to this parameter. In the weak-coupling region, the results would be insensitive to this parameter. For this purpose, in this section, in addition to the numerical study at unitarity, we also present a complete numerical study of the dipolar BEC in the strong-coupling regime for scattering length $a > 100a_0$ using the crossover model Eq.(5.9). Note that $a \approx 100a_0$ is the typical experimental value of the scattering length for a dipolar BEC.

In Figs. 5.1 and 5.2, we plot the radial density of the BEC along the x axis $|\Phi(x, y = 0)|^2$ obtained by integrating out the z dependence of density:

$$|\Phi(x, y)|^2 = \int dz|\phi(x, y, z)|^2. \tag{5.21}$$

In figure 5.1 (a) we show the result for $a = 100a_0$ using the GP model Eq.(5.6) and at unitarity Eq.(5.7) in addition to the results for $a = 100a_0$, $200a_0$, and

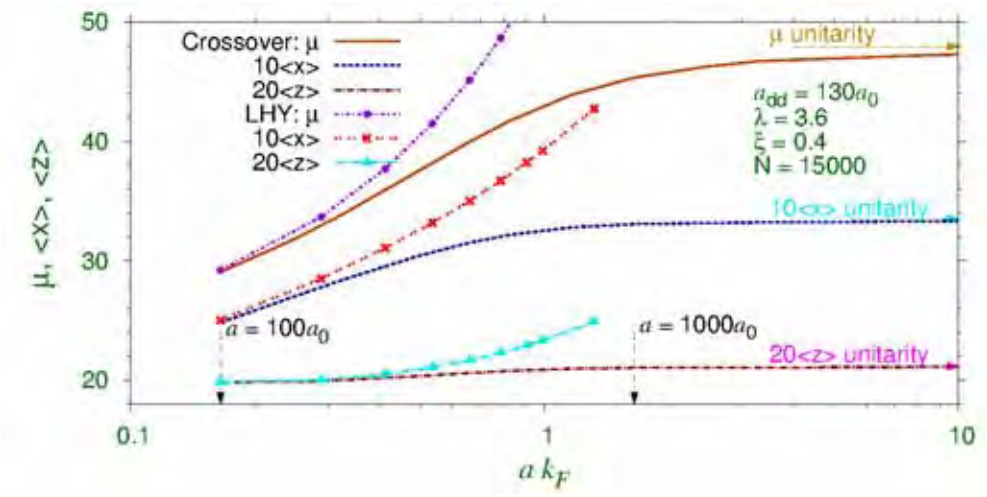

Figure 5.3: The numerical rms sizes $\langle x\rangle$, $\langle z\rangle$, and chemical potential μ of the dipolar BEC with $N = 15000$, $a_{dd} = 130a_0, \xi = 0.4, \nu = 1, \lambda = 3.6$ versus ak_F using the crossover model Eq.(5.9), the Lee-Huang-Yang (LHY) correction Eq.(5.8) as well as at unitarity Eq.(5.7) (arrow).

$1000a_0$ using the BEC-unitarity crossover model Eq.(5.9) with $\xi = 0.4$ and $\nu = 1$. For small a, the density from the crossover model Eq.(5.9) is in agreement with the GP model Eq.(5.6) and hence practically independent of the parameter ξ, whereas for large a it approximates the unitarity limit Eq.(5.7) with the increase of a. In Fig. 5.1 (b) we plot the radial density for $a = 500a_0$ for different ξ using the crossover model Eq.(5.9). The result at unitarity Eq.(5.7) for $\xi = 0.4$ is also shown, and is possible to see that for $\xi = 0.4$ the crossover model yields density in agreement with that at unitarity. Also we find that the density is sensitive to the parameter ξ for $a = 500a_0$ as can be seen from Fig. 5.1 (b) comparing the results for $\xi = 0.2, 0.4$ and 0.6.

The sensitivity of the density on ξ at unitarity is illustrated in Fig. 5.2 (a), where we show the radial density for $\xi = 0.3, 0.4, 0.5$ and 1.6. Finally, in Fig. 5.2 (b) we show the density at unitarity for nondipolar and dipolar BECs for two values of the trap asymmetry $\lambda = 3.6$ and 10. The difference between the two densities is more pronounced for $\lambda = 10$, where the dipolar repulsion is stronger. In Fig. 5.3 we plot the rms sizes $\langle x\rangle$, $\langle z\rangle$, and the chemical potential μ of the dipolar BEC for $\xi = 0.4$, and $a_{dd} = 130a_0$ as calculated using crossover model Eq.(5.9) and the LHY correction Eq.(5.8) versus the dimensionless parameter $k_F a$, where k_F is the Fermi wave vector in a harmonic trap defined [1] such as in

[1] The Fermi wave vector k_F for a ideal gas in the harmonic potential is $k_F = p_F/\hbar = (48N)^{1/6}/a_{ho}$. Here $a_{ho} = \sqrt{\hbar/m\omega_{ho}}$ denotes the harmonic oscillator length for the geometrical average of the three trapping frequencies $\omega_{ho} = (\omega_x\omega_y\omega_z)^{1/3}$ [74].

reference [74]. One can find from Fig. 5.3 how these quantities $-\langle x\rangle$, $\langle z\rangle$, $\mu-$ approach their values at unitarity as a increases. With the increase of a these quantities saturate rapidly to their respective values at unitarity. The use of the LHY correction Eq. (5.8), in place of the crossover model Eq.(5.9), will lead to divergent [45] results at unitarity. Even for $a = 1000a_0$ the LHY correction leads to sizes much larger than the crossover model and also much larger than the value at unitarity as can be seen in Fig. 5.3. In Fig. 5.4 (a), we plot the numerical Eq.(5.7) and variational (v) results for $\langle x\rangle$, $\langle z\rangle$, and μ versus a_{dd} at unitarity, which shows that the results are weakly sensitive to a variation of a_{dd}. In Fig. 5.4 (b) we plot $\langle x\rangle$, $\langle z\rangle$, and μ versus ξ at unitarity, which shows that the results are sensitive to a variation of ξ. Finally, in Fig. 5.4 (c) we plot $\langle x\rangle$, $\langle z\rangle$, and μ versus λ at unitarity showing the strong sensitivity of the results to a variation of λ. From Figs. 5.4 (a), (b), (c) we see that the variational results are in good agreement with the numerical ones.

In a recent experiment, Navon *et al.* [79] were able to make measurements for densities of a very dilute BEC of ^{7}Li for $a = 2150\ a_0$ and extract the parameter ξ from a theoretical analysis using the LHY correction [83, 84]. The very dilute BEC prepared in a weak trap, allowed them to experiment with large $a = 2150\ a_0$. However because of the low density, the BEC remained away from the strong-coupling regime even for $a = 2150a_0$ and was studied by the LHY correction, rather than a full crossover model as in the present study. In this regime the densities are weakly sensitive to the parameter ξ and only an upper limit $\xi < 0.6$ could be obtained from that study [79]. However, with the present scheme using a disk-shaped dipolar BEC, one could perform an experiment much closer to the strong-coupling regime where the densities are more sensitive to ξ and thus extract a more accurate value of this parameter. In contrast to the experiment of Navon *et al.* [79], in the present study a much stronger trap is employed, and for a much smaller value of scattering length $a = 500\ a_0$, the system is much closer to the strong-coupling regime, as can be seen from Fig. 5.1 (b), where an analysis using the LHY correction Eq.(5.8) as in reference [79] would not be appropriate.

In summary, using the BEC-unitarity crossover model Eq.(5.9) we studied the properties of a disk-shaped dipolar BEC in the strong-coupling regime. We find that the density profiles are sensitive to the universal parameter ξ in this regime and a study of density should yield an information about this parameter. We also find that the radial densities are sensitive to the parameter ξ in the strong-coupling regime and hence a study of density is expected to yield information about this parameter. Furthermore to extract the parameter ξ it is not necessary to study the system at unitarity. The density profile of the BEC is sensitive to the parameter ξ for the contact interaction lying between the weak-coupling GP and strong-coupling unitarity limits, so that a study in this regime should reveal information about this parameter.

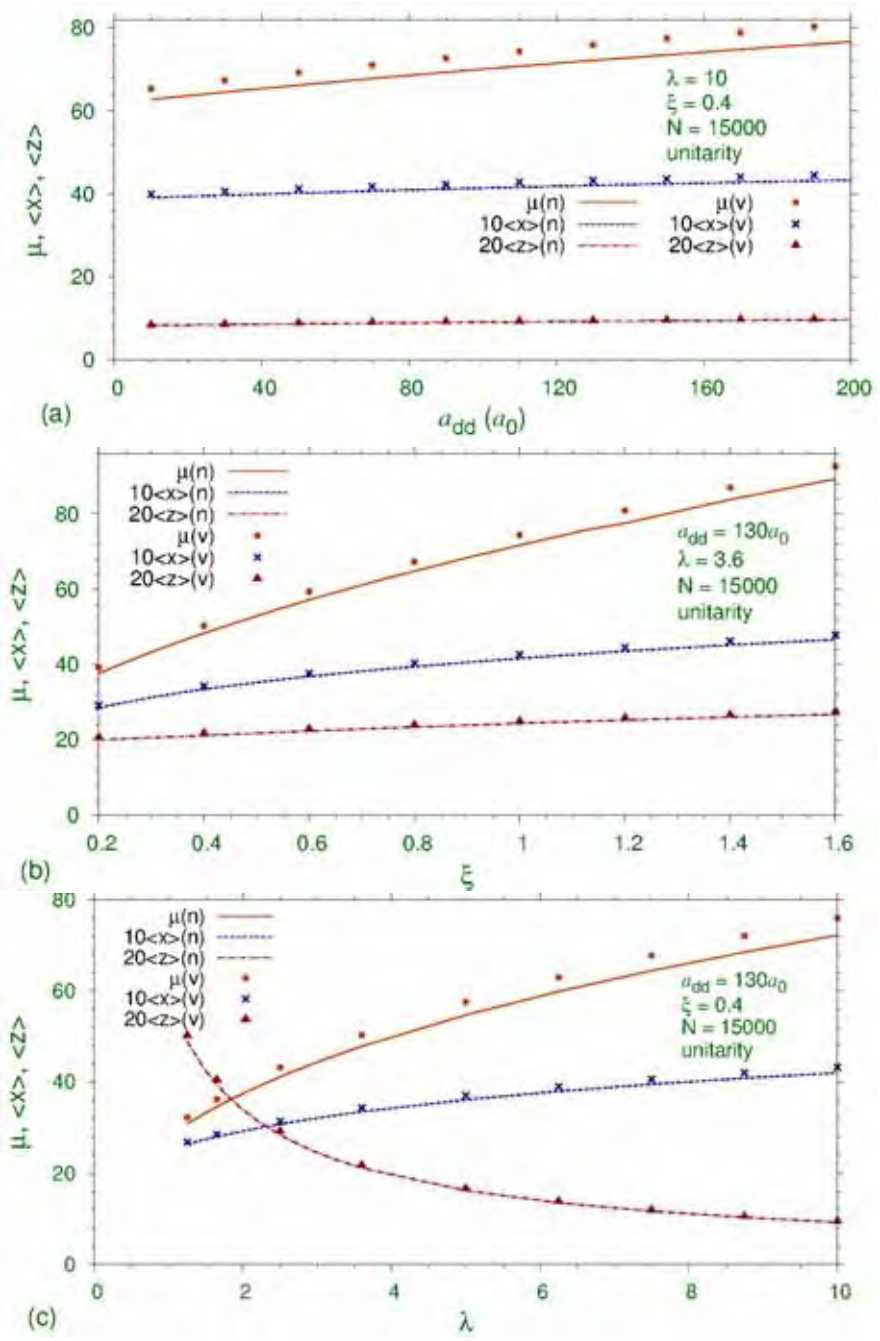

Figure 5.4: The numerical (n) and variational (v) results for rms sizes $\langle x\rangle$, $\langle z\rangle$ and chemical potential μ of the dipolar BEC at unitarity with $N = 15000$, (a) $\xi = 0.4$ and $\lambda = 10$ versus a_{dd}, (b) $a_{dd} = 130a_0$, and $\lambda = 3.6$ versus ξ, (c) $a_{dd} = 130a_0$, and $\xi = 0.4$ versus λ. For all cases numerical (n) corresponds to Eq.(5.7).

6

Binary Dipolar BEC

The experimental realization of a dipolar Bose-Einstein condensate (BEC) with a anisotropic long-range dipolar interaction allows the study of new atomic systems with interactions beyond short-range interaction, used for description of the atomic interaction in a BECs of alkali-metal atoms, and also has many distinct features that can be experimentally modified. To enhance the effect of the anisotropic dipolar interaction in most theoretical studies, the contact interaction could be set equal to zero. We know that in systems of ^{52}Cr atoms, the strength of the repulsive contact interaction is much stronger than that of the dipolar interaction. However, dipolar BECs of atoms such as ^{164}Dy with much larger dipolar interaction can show effects of anisotropic nonlocal dipolar interaction without switching off the contact interaction. Now with available dipolar BECs of different species of atoms, there is the possibility to investigate a binary mixture of two dipolar BECs of two types of dipolar interactions acting on each species, e.g., intra- and inter-species, superposed on intra- and inter-species contact interactions, thus creating a much richer platform to study the effect of dipolar interaction.

In this chapter, we consider binary dipolar BECs composed of ^{164}Dy and ^{52}Cr atoms as well as ^{164}Dy and ^{168}Er atoms. With all the dipole moments aligned along the z axis, the net dipolar interaction is attractive in a cigar shape along the z axis and repulsive in a disk shape confined in the $x-y$ plane, as parallel dipoles in a chain along the z axis attract, and those confined in the $x-y$ plane repeal, each other. Consequently, the binary dipolar BEC with dipoles polarized along the z axis is more stable in the disk shape confined in the $x-y$ plane than the

cigar shape along the z axis which is vulnerable to collapse, and therefore we shall consider only such a disk-shaped binary dipolar BEC in this study. However, even such a disk-shaped binary dipolar BEC is found to be unstable due to collapse instability for dipolar interaction above a critical value controlled by the number of atoms. This is consistent with the similar conclusion that a single-component dipolar BEC for any anisotropic trap collapses above a critical value of dipolar interaction [35, 69].

We study the limits of stability of binary dipolar disk-shaped BECs formed of ^{168}Er and ^{164}Dy atoms and of ^{52}Cr and ^{164}Dy atoms and present the results in terms of stability phase plots which should aid in the experimental preparation and study of binary dipolar BECs. Of all the atomic interactions, the inter- and intra-species dipolar interactions controlled by the known dipole moments of the two species will be considered known. The contact interactions governed by the approximately known intra-species scattering lengths will also be taken as fixed parameters in this study. We then study the stability of the binary mixture by varying the number of atoms in each species and the yet unknown inter-species scattering length a_{12}. For small values of a_{12}, the dipolar binary BEC prefers a mixed configuration and with the augmentation of the inter-species repulsion the system moves into a demixed configuration.

During this process of mixing-demixing, distinct biconcave red-blood-cell-like and Saturn-ring-like shapes are found in the densities of the two components just below the line of stability of the binary dipolar BEC for a certain value of inter-species scattering length. The biconcave structure due to dipolar interaction has previously been studied in detail for BEC with single-component dipolar [36, 89]. The Saturn-ring-like density distribution has never been observed in a single-component dipolar BEC. To enhance the dipolar effect, in these previous studies the repulsive contact interaction was set to zero, whereas in the present study we set all the intra- and inter-species repulsive contact interactions to their large experimental values and yet obtain these special structures because of the larger values of dipole interactions appropriate for ^{164}Dy and ^{168}Er atoms.

6.1 Mean-field model for the binary dipolar BEC

We consider a general two-species dipolar BEC with inter- and intra-species dipolar and contact interactions with the mass, number of atoms, magnetic moment, scattering length denoted by $m_j, N_j, \bar{\mu}_j, a_j, j = 1, 2$, respectively. The angular frequencies for the axially-symmetric trap along x, y and z directions are taken as $\omega_x^{(j)} = \omega_y^{(j)} = \omega_j$ and $\omega_z = \lambda_j \omega_j$. The intra- and inter-species interactions

for two atoms at positions $\mathbf{r}$ and $\mathbf{r}'$ are taken as

$$V_j(\mathbf{R}) = \frac{\mu_0 \bar{\mu}_j^2}{4\pi} U_{dd}(\mathbf{R}) + \frac{4\pi\hbar^2 a_j}{m_j}\delta(\mathbf{R}), \tag{6.1}$$

$$V_{12}(\mathbf{R}) = \frac{\mu_0 \bar{\mu}_1 \bar{\mu}_2}{4\pi} U_{dd}(\mathbf{R}) + \frac{2\pi\hbar^2 a_{12}}{m_R}\delta(\mathbf{R}), \tag{6.2}$$

where $\mathbf{R} = \mathbf{r} - \mathbf{r}'$, μ_0 is the permeability of free space, $U_{dd}(\mathbf{R})$ represents the dipole-dipole interaccion defined in Eq. (3.10), $m_R = m_1 m_2/(m_1 + m_2)$ is the reduced mass of the two species of atoms and a_{12} the interspecies scattering length. Here $\delta(\mathbf{R})$ is the delta function used to define the contact interaction in Eq. (1.5). With these interactions, the coupled Gross-Pitaevskii (GP) equations for the binary dipolar BEC can be written as [46]

$$\begin{aligned} \mathrm{i}\hbar\frac{\partial\phi_1(\mathbf{r},t)}{\partial t} &= \Big[-\frac{\hbar^2}{2m_1}\nabla^2 + U_1(\mathbf{r}) + \frac{4\pi\hbar^2}{m_1} a_1 N_1 |\phi_1(\mathbf{r},t)|^2 \\ &+ N_1 \frac{\mu_0\ \bar{\mu}_1^2}{4\pi} \int U_{dd}(\mathbf{R}) |\phi_1(\mathbf{r}',t)|^2 d\mathbf{r}' + \frac{2\pi\hbar^2}{m_R} a_{12} N_2 |\phi_2(\mathbf{r},t)|^2 \\ &+ N_2 \frac{\mu_0\ \bar{\mu}_1\ \bar{\mu}_2}{4\pi} \int U_{dd}(\mathbf{R}) |\phi_2(\mathbf{r}',t)|^2 d\mathbf{r}' \Big] \phi_1(\mathbf{r},t), \end{aligned} \tag{6.3}$$

$$\begin{aligned} \mathrm{i}\hbar\frac{\partial\phi_2(\mathbf{r},t)}{\partial t} &= \Big[-\frac{\hbar^2}{2m_2}\nabla^2 + U_2(\mathbf{r}) + \frac{4\pi\hbar^2}{m_2} a_2 N_2 |\phi_2(\mathbf{r},t)|^2 \\ &+ N_2 \frac{\mu_0\ \bar{\mu}_2^2}{4\pi} \int U_{dd}(\mathbf{R}) |\phi_2(\mathbf{r}',t)|^2 d\mathbf{r}' + \frac{2\pi\hbar^2}{m_R} a_{12} N_1 |\phi_1(\mathbf{r},t)|^2 \\ &+ N_1 \frac{\mu_0\ \bar{\mu}_1\ \bar{\mu}_2}{4\pi} \int U_{dd}(\mathbf{R}) |\phi_1(\mathbf{r}',t)|^2 d\mathbf{r}' \Big] \phi_2(\mathbf{r},t), \end{aligned} \tag{6.4}$$

where $\mathrm{i} = \sqrt{-1}$,

$$\int d\mathbf{r}\ |\phi_j(\mathbf{r},t)|^2 = 1, \tag{6.5}$$

$$U_j(\mathbf{r}) = \frac{1}{2} m_j \omega_j^2\ (\rho^2 + \lambda_j^2 z^2), \tag{6.6}$$

are the normalization and the harmonic trap for each component $(j = 1, 2)$ respectively with $\rho^2 = x^2 + y^2$. To compare the dipolar and contact interactions, the intra- and inter-species dipolar interactions will be expressed in terms of the length scales $a_{dd}^{(j)}$ and $a_{dd}^{(12)}$, respectively, defined by

$$\frac{\mu_0 \bar{\mu}_j^2}{4\pi} = \frac{3\hbar^2}{m_j} a_{dd}^{(j)}, \quad \frac{\mu_0 \bar{\mu}_1 \bar{\mu}_2}{4\pi} = \frac{3\hbar^2}{m_1} a_{dd}^{(12)}. \tag{6.7}$$

The mass of the corresponding species m_j has been used to define the intra-species dipolar scale $a_{dd}^{(j)}$. To define the inter-species dipolar scale $a_{dd}^{(12)}$, we have used the mass m_1 of the first species. We express the strengths of the dipolar interactions in Eqs. (6.3) and (6.4) by these length scales and transform these equations into the following dimensionless form:

$$\mathrm{i}\frac{\partial\phi_1(\mathbf{r},t)}{\partial t} = \Big[-\frac{\nabla^2}{2} + \frac{1}{2}(\rho^2+\lambda_1^2 z^2) + g_1|\phi_1|^2 + g_{dd}^{(1)}\int U_{dd}(\mathbf{R})|\phi_1(\mathbf{r}',t)|^2 d\mathbf{r}' + g_{12}|\phi_2|^2 + g_{dd}^{(12)}\int U_{dd}(\mathbf{R})|\phi_2(\mathbf{r}',t)|^2 d\mathbf{r}'\Big]\phi_1(\mathbf{r},t), \tag{6.8}$$

$$\mathrm{i}\frac{\partial\phi_2(\mathbf{r},t)}{\partial t} = \Big[-m_{12}\frac{\nabla^2}{2} + \frac{m_w}{2}(\rho^2+\lambda_2^2 z^2) + g_2|\phi_2|^2 + g_{dd}^{(2)}\int U_{dd}(\mathbf{R})|\phi_2(\mathbf{r}',t)|^2 d\mathbf{r}' + g_{21}|\phi_1|^2 + g_{dd}^{(21)}\int U_{dd}(\mathbf{R})|\phi_1(\mathbf{r}',t)|^2 d\mathbf{r}'\Big]\phi_2(\mathbf{r},t), \tag{6.9}$$

where

$$\begin{aligned} m_{12} &= \frac{m_1}{m_2},\ m_w = \frac{\omega_2^2}{m_{12}\omega_1^2},\ g_1 = 4\pi a_1 N_1,\ g_2 = 4\pi a_2 N_2 m_{12}, \\ g_{dd}^{(1)} &= 3N_1 a_{dd}^{(1)},\ g_{dd}^{(2)} = 3N_2 a_{dd}^{(2)} m_{12}, \\ g_{12} &= \frac{2\pi m_1}{m_R} a_{12} N_2,\ g_{21} = \frac{2\pi m_1}{m_R} a_{12} N_1, \\ g_{dd}^{(12)} &= 3N_2 a_{dd}^{(12)},\ g_{dd}^{(21)} = 3N_1 a_{dd}^{(12)}. \end{aligned} \tag{6.10}$$

In Eqs. (6.8) and (6.9), length is expressed in units of oscillator length for the first species $l_0 = \sqrt{\hbar/m_1\omega_1}$, energy in units of oscillator energy $\hbar\omega_1$, density $|\phi_j|^2$ in units of l_0^{-3}, and time in units of $t_0 = \omega_1^{-1}$.

6.2 Same species of atoms in isotropic trap

To test the model and the numerical routine, we consider a simple binary dipolar BEC of the same species of atoms without contact interaction in a spherically-symmetric trap. However, the two components are considered to be oppositely polarized along z and $-z$ directions, respectively. In this model, first considered by Góral and Santos [53],

$$\begin{aligned} m_j = m,\ \omega_j = \omega,\ m_{12} = m_\omega = 1,\ \lambda_j = 1, \\ a_{dd}^{(j)} = -a_{dd}^{(12)} = a_{dd},\ a_j = a_{12} = 0. \end{aligned} \tag{6.11}$$

Consequently, in Eqs. (6.8) and (6.9)

$$g_j = g_{12} = 0,\ g_{dd}^{(j)} = 3N_j a_{dd},\ g_{dd}^{(12)} = -3N_2 a_{dd},\ g_{dd}^{(21)} = -3N_1 a_{dd}. \tag{6.12}$$

Using $\eta = N_1/N$, $\zeta = 3a_{dd}N$, with $N = N_1 + N_2$, we can write Eqs. (6.8) and (6.9) as in reference [53]:

$$\mathrm{i}\frac{\partial \phi_1}{\partial t} = \Big[-\frac{\nabla^2}{2} + \frac{r^2}{2} + \zeta\Big\{\eta V_1(\mathbf{r}) - (1-\eta)V_2(\mathbf{r})\Big\}\Big]\phi_1, \tag{6.13}$$

$$\mathrm{i}\frac{\partial \phi_2}{\partial t} = \Big[-\frac{\nabla^2}{2} + \frac{r^2}{2} + \zeta\Big\{(1-\eta)V_2(\mathbf{r}) - \eta V_1(\mathbf{r})\Big\}\Big]\phi_2, \tag{6.14}$$

where

$$V_j(\mathbf{r}) = \int U_{dd}(\mathbf{R})|\phi_j(\mathbf{r}')|^2 d\mathbf{r}', \quad j = 1, 2. \tag{6.15}$$

For a fixed fraction of atoms on the first component η, the system is stable up to a critical value of net dipolar interaction nonlinearity ζ, e.g. for $\zeta < \zeta_{\rm cr}$, beyond which the system becomes unstable.

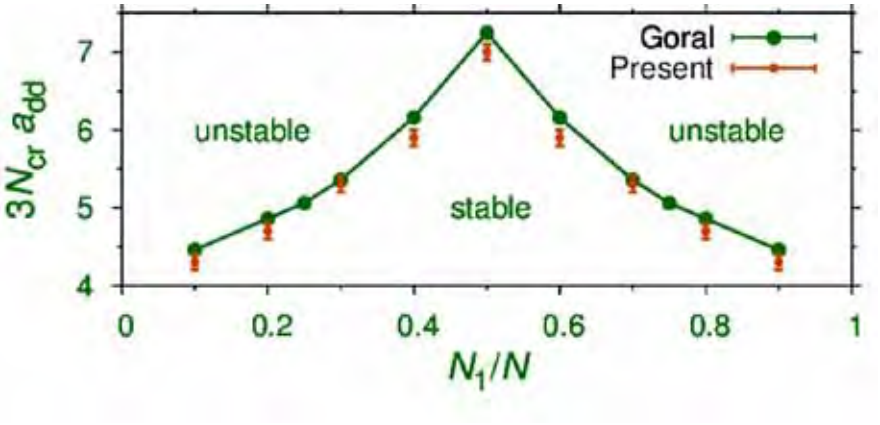

Figure 6.1: The maximum allowed value of net intra-species dipolar nonlinearity $\zeta_{\rm cr}(\equiv 3N_{\rm cr}a_{dd})$ versus fraction of atoms of the first component η $(\equiv N_1/N)$ for a binary dipolar BEC of oppositely polarized dipolar gases in a spherically symmetric trap compared with the findings of Góral and Santos [53].

The stability of the binary system can be expressed in terms of a $\zeta - \eta$ phase diagram. This stability phase diagram for this binary dipolar condensate of the same species of atoms, but of oppositely polarized dipolar moments, in a spherically symmetric trap is shown in Fig. 6.1 in agreement with Góral and Santos [53]. Independent of the composition of the system governed by the parameter η, the system is unstable beyond a critical value of the total number of atoms N.

.

6.3 Different species of atoms in disk trap

We consider two different binary systems of dipolar BECs, ^{168}Er-^{164}Dy and ^{52}Cr-^{164}Dy mixtures, using the coupled set of GP equations (6.8) and (6.9).

Binary ^{168}Er-^{164}Dy mixture:

First, we consider the ^{168}Er-^{164}Dy mixture. In this case we take BEC number 1 as ^{168}Er and BEC number 2 as ^{164}Dy with parameters

$$\bar{\mu}_1 = 7\mu_B,\ \bar{\mu}_2 = 10\mu_B,\ a_{dd}^{(1)} = 66a_0,\ a_{dd}^{(2)} = 131a_0 \tag{6.16}$$

with a_0 the Bohr radius and μ_B the Bohr magneton. From Eq. (6.7), is possible to calculate the parameter $a_{dd}^{(12)}$ as follows

$$a_{dd}^{(12)} = \frac{\mu_0\ \bar{\mu}_1^2\ m_1}{12\pi\hbar^2} \times \frac{\bar{\mu}_2}{\bar{\mu}_1}, \tag{6.17}$$

so, for binary ^{168}Er-^{164}Dy sistem the inter-species dipolar interaction is $a_{dd}^{(12)} = 94a_0$. Without accurate experimental estimates [12, 13] of the intra-species scattering lengths, we use $a_j = 110a_0$. The angular frequencies of the axial trap for ^{164}Dy are taken as $\omega_2 = 2\pi \times 243$ Hz, $\lambda_2 = \sqrt{10} \approx 3.1623$, compared with experimental frequencies [12] $\{f_x, f_y, f_z\} = \{205, 195, 760\}$ Hz with trap aspect ratio $\lambda = 3.8$. We take $m_\omega = 1$, corresponding to $\omega_1 = 2\pi \times 240$ Hz, $\lambda_1 = \sqrt{10}$. The unit of length in this study is $l_0 = \sqrt{\hbar/(m_1\omega_1)} \approx 0.5$ μm and the unit of time $t_0 = \omega_1^{-1} \approx 0.663$ ms.

Binary ^{52}Cr-^{164}Dy mixture:

In this case, taking the condensate number 1 as ^{52}Cr and number 2 as ^{164}Dy, the parameters are:

$$\bar{\mu}_1 = 6\mu_B,\ \bar{\mu}_2 = 10\mu_B,\ a_{dd}^{(1)} = 15a_0,\ a_{dd}^{(2)} = 131a_0,\ a_{dd}^{(12)} = 25a_0. \tag{6.18}$$

We take $a_j = 110a_0$, which approximates their experimental estimates [12, 33, 90]. The angular frequencies of the axial trap for the first dipolar BEC are taken as $\omega_1 = 2\pi \times 195$ Hz, $\lambda_1 = \sqrt{10} \approx 3.1623$, compared with the experimental frequencies [90] $\{f_x, f_y, f_z\} = \{150, 150, \lambda f_x\}$ Hz with trap aspect ratio $\lambda < 10$. We take $m_\omega = 1$, corresponding to $\omega_2 = 2\pi \times 110$ Hz, $\lambda_2 = \sqrt{10}$. The unit of length in this calculation is $l_0 = \sqrt{\hbar/(m_1\omega_1)} \approx 1$ μm and the unit of time $t_0 = \omega_1^{-1} \approx 0.816$ ms.

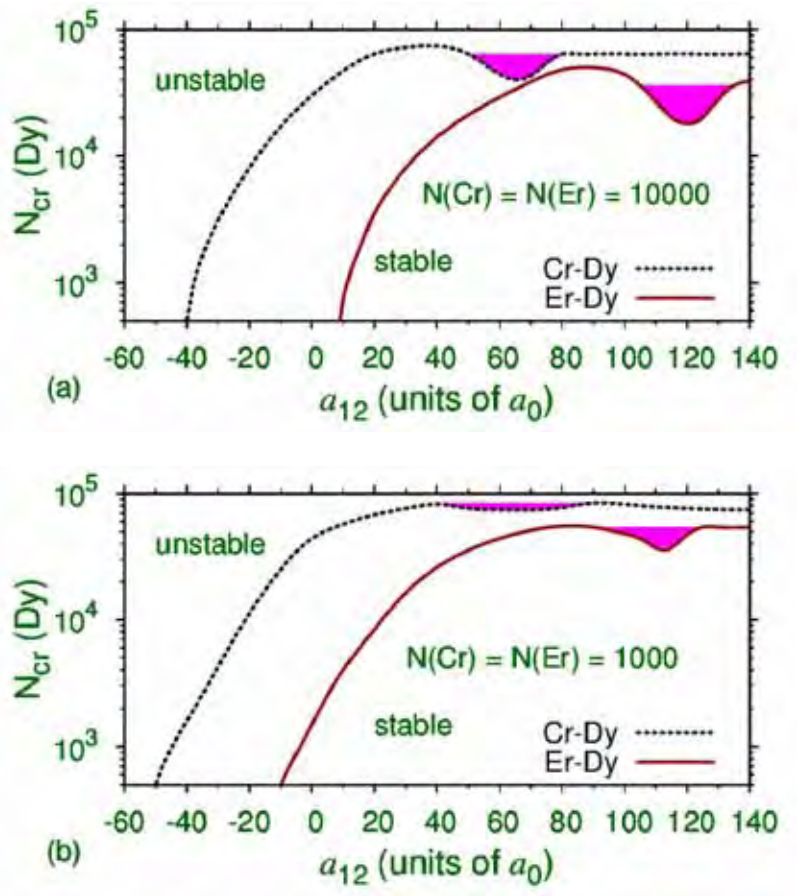

Figure 6.2: Stability phase plot showing the critical number N_{cr}(Dy) of ^{164}Dy atoms in the ^{52}Cr-^{164}Dy and ^{168}Er-^{164}Dy binary mixtures versus inter-species scattering length a_{12} for (a) 10000 and (b) 1000 ^{52}Cr or ^{168}Er atoms, respectively. The system is stable below the respective lines. The shaded dark areas illustrate the domains where biconcave density profiles appear.

6.3.1 Stability phase plot

By solving the coupled set of GP equations (6.8) and (6.9) for the binary mixture of dipolar BECs we find that the system becomes unstable above a certain number of atoms with the total dipolar interaction beyond a limiting value, which concurs with a similar conclusion [35] regarding a single-component dipolar BEC. To perform a systematic study of the stability of the binary dipolar BEC, we solve Eqs. (6.8) and (6.9) with the above parameters, fixing the number of atoms in the first species (^{52}Cr or ^{168}Er) and searching for the critical number of atoms (N_{cr}) of second species (^{164}Dy) beyond which the system becomes unstable for different values of inter-species scattering length a_{12}.

If the binary mixture has a smaller number of atoms of the first species (^{52}Cr or ^{168}Er), it can accommodate a larger number of atoms of the second species (^{164}Dy) while the limiting value of the total dipolar interaction is reached maintaining all other parameters fixed. We present the results of our study in stability phase plots in Fig. 6.2. We show the critical number of ^{164}Dy atoms N_{cr}(Dy) versus a_{12} for Fig. 6.2 (a) 10000, and Fig. 6.2 (b) 1000 atoms of ^{52}Cr or ^{168}Er in binary ^{52}Cr-^{164}Dy and ^{168}Er-^{164}Dy mixtures, respectively. The system is stable below both lines of Fig. 6.2 and unstable above. The system may have distinct structures of density in the shaded regions in this figure. This region is similar to the darker region of reference [35], where the density of a single-component dipolar BEC has a biconcave shape. Stability phase plots of Fig. 6.2 could be relevant for planning future experiments on binary dipolar BECs.

At lower values of a_{12}, the contact repulsion reduces and the system becomes more vulnerable to collapse for a larger number of atoms due to dipolar interaction and hence can accommodate only a small number of ^{164}Dy atoms as can be seen in Fig. 6.2. We shall see below that biconcave and Saturn-ring-like shapes in the density of the components of the binary dipolar BEC may appear in the shaded region in Fig. 6.2.

6.3.2 Mixing, demixing, and structure formation

Next we study in detail the density of the two species of atoms in the binary dipolar BEC to look for mixing (overlapping phases of two components), demixing (separated phases) and distinct structure formation in the shaded regions of the phase plots shown in Fig. 6.2. For low values of a_{12} the inter-atomic contact repulsion between the two species is small and one has a mixed configuration. As a_{12} is increased the inter-species contact repulsion increases and for a large enough value of a_{12} one can have demixing of the two species. In the demixed configuration one of the species occupies the central region and the other the external region. To illustrate this phenomenon, we plot (in Fig. 6.3) the reduced 2D density in the radial direction $|\Phi(x, y = 0)|^2 = \int dz |\phi(x, y = 0, z)|^2$ versus x under different situations in case of the binary ^{168}Er-^{164}Dy mixture. The present structures were obtained by using imaginary time propagation of the coupled mean-field equations with Gaussian profiles for the initial densities[1].

The mixing-demixing is illustrated in Figs. 6.3 (a), (b), and (c) for 10000 ^{168}Er and 20000 ^{164}Dy atoms, respectively, for $a_{12} = 110a_0, 125a_0$, and $130a_0$. In Fig. 6.3 (a) we have a mixed (overlapping) configuration and with the increase

[1] We started with the Gaussian profiles of the linear oscillator states and increased the dipolar and nondipolar nonlinearities in small steps during numerical simulation until the final nonlinearities were reached. In this fashion the structure in density in the shaded regions of phase plots in Fig. 6.2 were obtained.

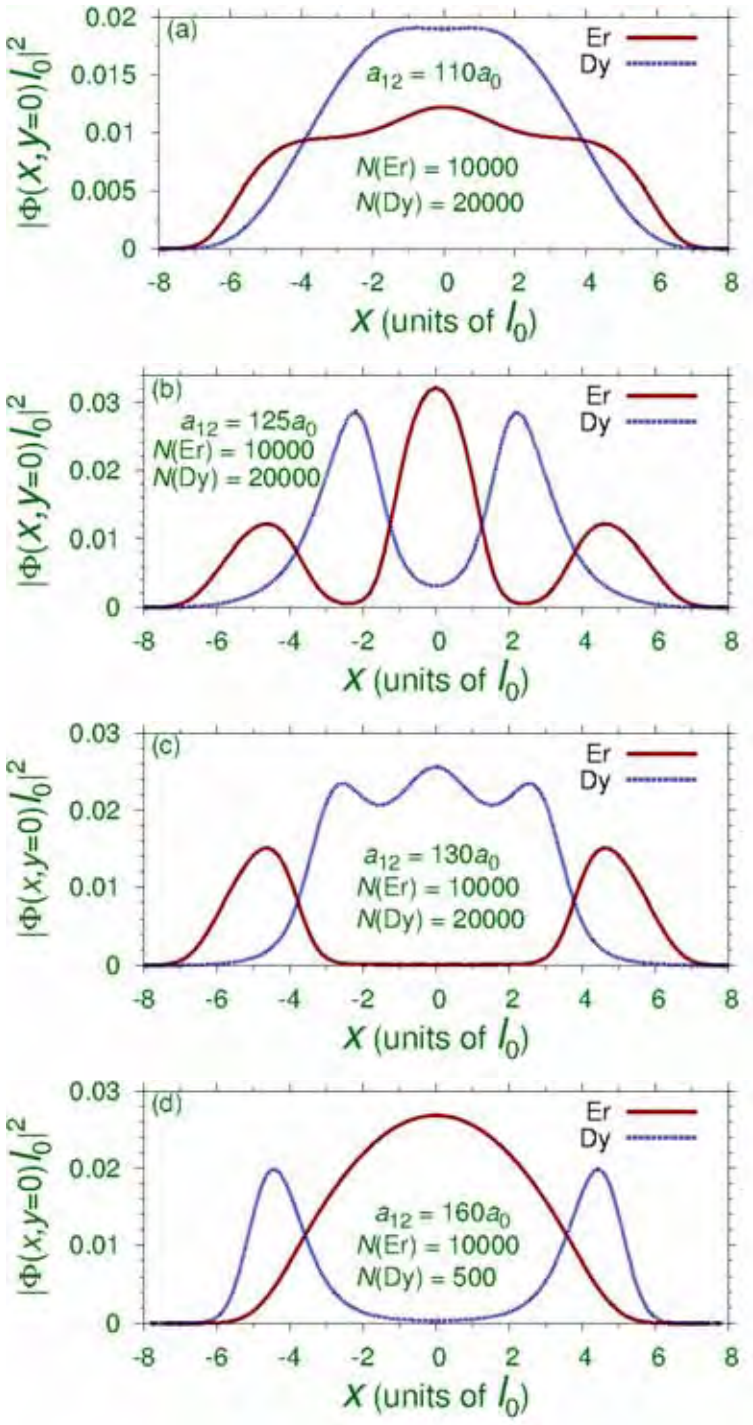

Figure 6.3: Two-dimensional radial density along the x axis $|\Phi_j(x, y = 0)|^2 \equiv \int dz|\phi_j(x, y = 0, z)|^2$ of the binary ^{168}Er-^{164}Dy BEC, for (a) $N(\mathrm{Er}) = 10000$, $N(\mathrm{Dy}) = 20000$, and $a_{12} = 110a_0$; (b) $N(\mathrm{Er}) = 10000$, $N(\mathrm{Dy}) = 20000$, and $a_{12} = 125a_0$; (c) $N(\mathrm{Er}) = 1000$, $N(\mathrm{Dy}) = 20000$, and $a_{12} = 130a_0$; (d) $N(\mathrm{Er}) = 10000$, $N(\mathrm{Dy}) = 500$, and $a_{12} = 160a_0$. For the trap parameters of this study the length scale is $l_0(= 0.5\mu\mathrm{m})$.

of inter-species contact repulsion, in Fig. 6.3 (c) we have a demixed (separated) configuration of the two species. In Fig. 6.3 (b), for $a_{12} = 125a_0$ we have a partially demixed configuration. In the demixed configuration in Fig. 6.3 (c), 20000 ^{164}Dy atoms have a larger contribution to energy of the system and the ^{164}Dy atoms expel the ^{168}Er atoms from the central region due to inter-species repulsion. The opposite phenomenon is also possible for a larger number of ^{168}Er atoms, in which case the ^{168}Er atoms can expel the ^{164}Dy atoms from the central region. Such a situation is illustrated in Fig. 6.3 (d) with 10000 ^{168}Er atoms and 500 ^{164}Dy atoms and with $a_{12} = 160a_0$. In this case ^{168}Er atoms have a larger contribution to the energy of the system and expel the ^{164}Dy atoms from the center.

A careful examination of the transition from the partially mixed configuration of Fig. 6.3 (b) to the demixed configuration of Fig. 6.3 (c) reveals an interesting feature. To study this, we consider the 3D profile of the density $|\phi_j(x, y, z)|^2$ of the two species for the cases depicted in Figs. 6.3 (b) and (c). For this purpose, in Figs. 6.4 (a) and (b) we plot the 3D contours of ^{168}Er and ^{164}Dy BEC profiles for the parameters of Fig. 6.3 (b). The same plots for the parameters of Fig. 6.3 (c) are illustrated in Figs. 6.4 (c) and (d). The density $|\phi(x, y, z)|^2$ on the surface of these plots is $0.0005 l_0^{-3}$. Parameter values of $l_0 = 0.5$ μm, and $N(\text{Er}) = 10000$, and $N(\text{Dy}) = 20000$ lead to atom densities on contour of 40 μm^{-3} for ^{168}Er and of 80 μm^{-3} for ^{164}Dy. The maxima of atom densities in the interior of the BECs of Figs. 6.4 (a) – (d) are, respectively, 800 μm^{-3}, 1160 μm^{-3}, 460 μm^{-3}, and 1000 μm^{-3}. In Figs. 6.4 (a) and (b) the ^{168}Er and ^{164}Dy BECs have Saturn-ring-like and red-blood-cell-like biconcave profiles, respectively. The biconcave profile is a manifestation of the dipolar interaction: the net dipolar repulsion in disk shaped ^{164}Dy drives the dysprosium atoms to a peripheral region thus creating the biconcave shape. The biconcave profile has been found in previous papers related with the single-component case [35]. The Saturn-ring-like ^{168}Er profile in Fig. 6.4 (a) is a manifestation of the inter-species dipolar interaction: the biconcave density distribution of the ^{164}Dy species with a density minimum at the center, due to inter-species repulsion, expels one part of the ^{168}Er BEC to the central region of lower density and another part to the peripheral region, also of lower density, thus creating the Saturn-ring-like profile. Such a profile is not possible in a single-component dipolar BEC, or in a binary BEC without dipolar interaction.

With a further increase of inter-species contact repulsion ($a_{12} = 130a_0$) the contact repulsions dominate over the dipolar interactions and hence play a major role thus creating a simpler situation of demixing, shown in Fig. 6.3 (c) and Figs. 6.4 (c) and (d), where the net inter-species repulsion is so strong that all ^{168}Er atoms are driven to the peripheral region in the form of a ring with the dominant ^{164}Dy atoms occupying the central region. The ring-like structure in Fig. 6.4 (a) as opposed to a shell-like demixed configuration is a consequence of the dipolar

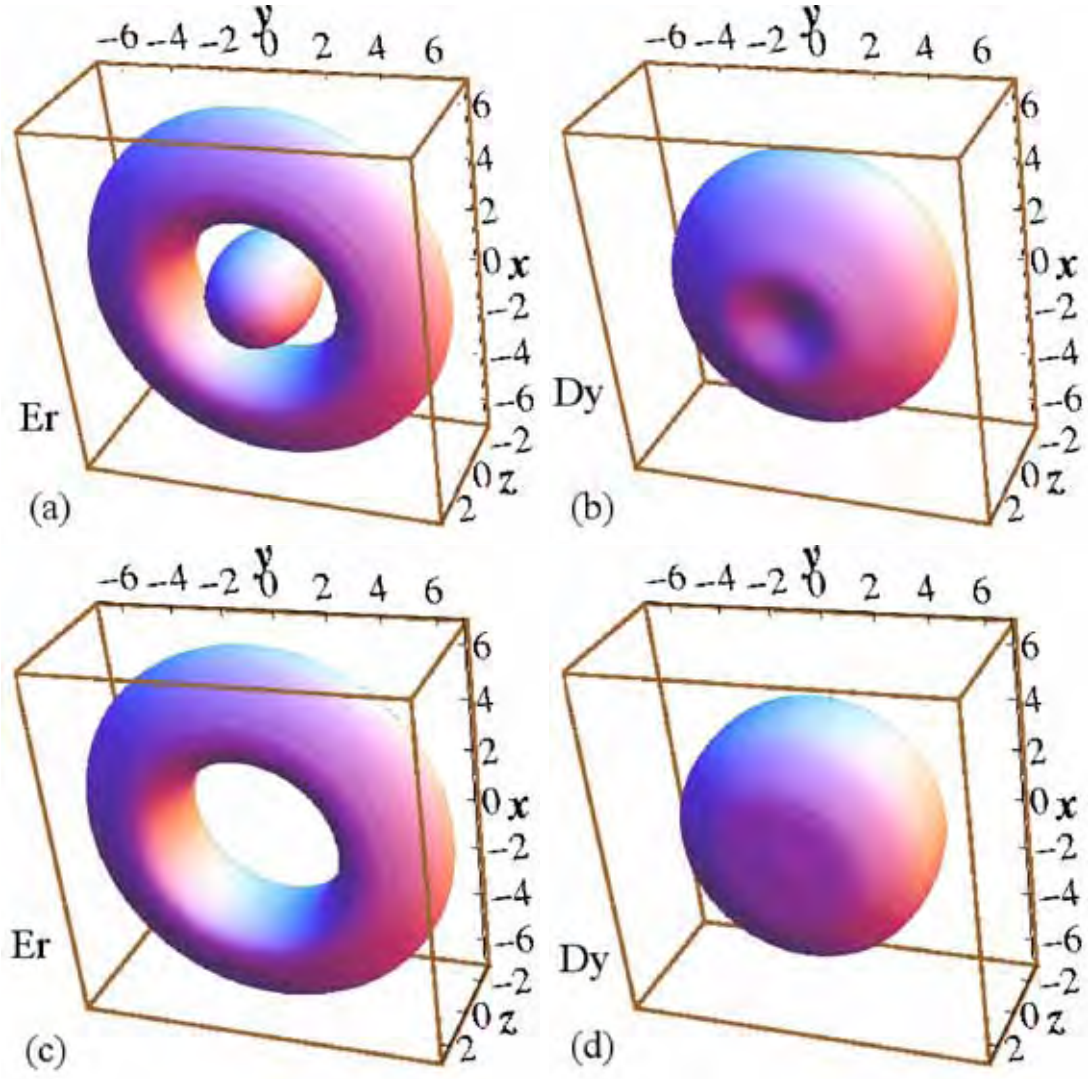

Figure 6.4: Three-dimensional contour plot of the (a) ^{168}Er and (b) ^{164}Dy densities $|\phi_j(x,y,z)|^2$ of the ^{168}Er-^{164}Dy binary BEC of Fig. 6.3 (b) for $a_{12} = 125a_0$. The same for the (c) ^{168}Er and (d) ^{164}Dy densities of the binary BEC of Fig. 6.3 (c) for $a_{12} = 130a_0$. Density on contour = 0.0005, and N(Er) = 10000, N(Dy) = 20000. The lengths x, y and z are in units of $l_0(= 0.5\mu\text{m})$. See text for actual values of density inside and on the surface of the plots.

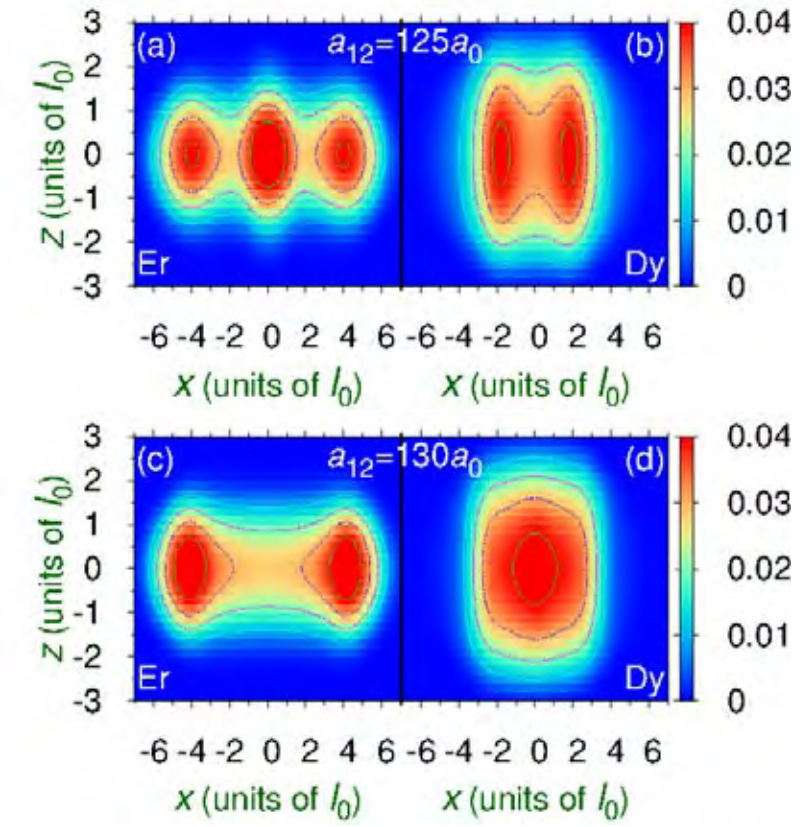

Figure 6.5: Contour plot of 2D densities $|\Phi_j(x,z)|^2 \equiv \int dy |\phi_j(x,y,z)|^2$ of the binary ^{168}Er-^{164}Dy BEC for $N(\mathrm{Er}) = 10000$, $N(\mathrm{Dy}) = 20000$ with $a_{12} = 125a_0$ for (a) ^{168}Er, (b) ^{164}Dy, and with $a_{12} = 130a_0$ for (c) ^{168}Er, and (d) ^{164}Dy. The lengths are expressed in units of $l_0 (= 0.5\ \mu\mathrm{m})$ and the 2D density in units of l_0^{-2}.

interaction: a pure inter-species contact repulsion would have led to a hollow shell-like configuration for ^{168}Er surrounding a compact disk-shaped ^{164}Dy core. The dipolar interaction is attractive in the z direction and this transforms the shell-like configuration into a ring. Such transition from a shell-like configuration to a ring with the increase of dipolar interaction has been demonstrated in a single-component dipolar BEC in a shell-like trap [91]. From Figs. 6.3 we find that for a binary dipolar BEC composed of 10000 ^{168}Er atoms and 20000 ^{164}Dy atoms the transition from a mixed to a demixed configuration occurs at around $a_{12} = 120a_0$. We verified that a similar transition also takes place in a binary dipolar BEC for 10000 ^{168}Er atoms and a reduced number of ^{164}Dy atoms also at $a_{12} \approx 120a_0$. Nevertheless, the biconcave structure in the density of ^{164}Dy is obtained for a small shaded region below the stability line in Fig. 6.2 (a) with a large number of ^{164}Dy atoms. As in the single component case [35], the binary dipolar BEC possessing a biconcave shaped density in the ^{164}Dy BEC

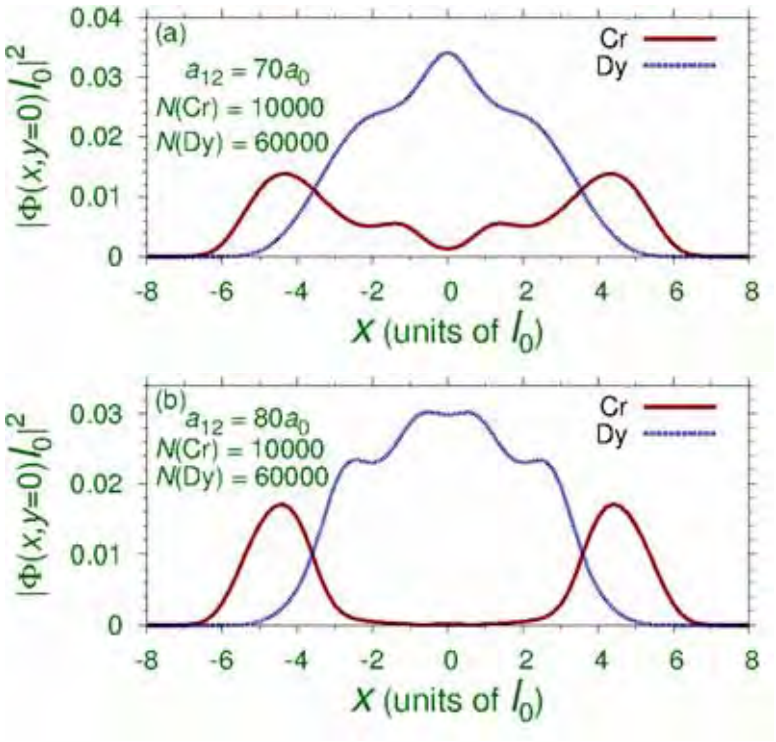

Figure 6.6: Two-dimensional radial density along the x axis $|\Phi_j(x, y = 0)|^2 \equiv \int dz|\phi_j(x, y = 0, z)|^2$ of the binary ^{52}Cr-^{164}Dy BEC for (a) $a_{12} = 70a_0$, (b) $a_{12} = 80a_0$. In these cases $N(\mathrm{Cr}) = 10000$, $N(\mathrm{Dy}) = 60000$. The lengths x, y and z are in units of $l_0(= 1\mu\mathrm{m})$.

in the shaded region in Fig. 6.2 (a) is usually transient and instability appears after crossing the stability lines in Fig. 6.2. In the case of a single-component dipolar BEC a conveniently chosen initial density could be necessary for obtaining a density with a biconcave structure. In imaginary-time propagation the initial density should be chosen as a Gaussian with widths slightly larger than the actual widths of the desired state.

To gain further insight into the density distributions in Figs. 6.4 (a) – (d) we plot in Figs. 6.5 (a) – (d) contour plots of the asymmetric 2D densities $|\Phi(x, z)|^2 = \int dy|\phi(x, y, z)|^2$ of the binary ^{168}Er-^{164}Dy mixtures for parameters corresponding to Figs. 6.4 (a) – (d), respectively. For the double and single special structures in density in the $x - z$ plane in Figs. 6.5 (a) and (b) we have that a minimum in density along the x direction coincides with a maximum in density in the z direction thus creating a called saddle point, which appears as a clear manifestation of the dipolar interaction [54]. Such a density distribution is not possible in the absence of dipolar interaction and to the best of our knowledge has not been demonstrated even in the single-component dipolar BEC.

In Fig. 6.5 (a), for $a_{12} = 125a_0$, we have two saddle points on the x axis in the density of ^{168}Er and one saddle point in the density of ^{164}Dy. Similarly, for $a_{12} = 130a_0$, we have a single saddle point only in the density of ^{168}Er and none in ^{164}Dy. These saddle points have curvatures consistent with saddle-shaped dipolar interaction [54] with negative curvature along the direction of magnetization (z axis) and positive curvature orthogonal to it (x axis).

With this study of the binary ^{168}Er-^{164}Dy BEC, we also considered a detailed investigation of the binary ^{52}Cr-^{164}Dy BEC. Similar mixing, demixing, and structure formation are also found in this second case, although the quantitative results and estimates are different. We only report here the studies on the interesting structure formation in the binary ^{52}Cr-^{164}Dy BEC. Indeed we find that one can obtain a biconcave shaped condensate in this case. In Figs. 6.6 (a) and (b) we plot the linear density in the $x-y$ plane along the x direction $|\Phi(x, y = 0)|^2$, as in Fig. 6.3, for a binary mixture of 10000 ^{52}Cr atoms and 60000 ^{164}Dy atoms for $a_{12} = 70a_0$ and $80a_0$, respectively. Fig. 6.6 (a) illustrates a case similar to Fig. 6.3 (b), denoting a transition from a mixed state to a demixed state. For $a_{12} < 60a_0$, we have a fully mixed configuration of the two condensates as in Fig. 6.3 (a). For $a_{12} = 70a_0$ a biconcave shape appears in the density of ^{52}Cr. For $a_{12} > 75a_0$, a completely demixed configuration appears as illustrated in Fig. 6.6 (b) for $a = 80a_0$, where the ^{52}Cr atoms are expelled from the central region which is therefore occupied solely by ^{164}Dy atoms.

In Figs. 6.7 (a) and (b) we show the 3D contour of the densities $|\phi(x, y, z)|^2$ of the ^{52}Cr and ^{164}Dy BECs corresponding to the parameters of Fig. 6.6 (a) with the density $0.0005 l_0^{-3}$ on contour. This corresponds to the number of densities on the contour of 5 μm^{-3} and 30 μm^{-3} in ^{52}Cr and ^{164}Dy, respectively, for $l_0 = 1$ μm. The ^{52}Cr BEC shows a pronounced biconcave shape which is a direct manifestation of the dipolar interaction. However, we could not find a biconcave shape in the density of the ^{164}Dy BEC, as in the case of a binary dipolar ^{168}Er-^{164}Dy mixture, possibly because the inter-species dipole interaction in the ^{52}Cr-^{164}Dy system is much weaker than in the binary ^{168}Er-^{164}Dy system and is therefore unable to create the biconcave shaped density in the presence of dominating large contact repulsions acting on ^{164}Dy.

The much larger dipole interactions in ^{164}Dy might be responsible for the biconcave shaped density in Fig. 6.4 (b). Even in the single-component case, the biconcave profile of the density appears for certain values of the trap aspect ratio [35], and it is also possible that for other values of trap aspect ratio the biconcave profile might appear in the density of ^{164}Dy in the present binary ^{52}Cr-^{164}Dy mixture. However, the dipolar interaction leaves its signature in a different fashion as can be seen in Figs. 6.7 (c) and (d), where we plot the same densities as in Figs. 6.7 (a) and (b) but now with the density $0.0025 l_0^{-3}$ on the contour.

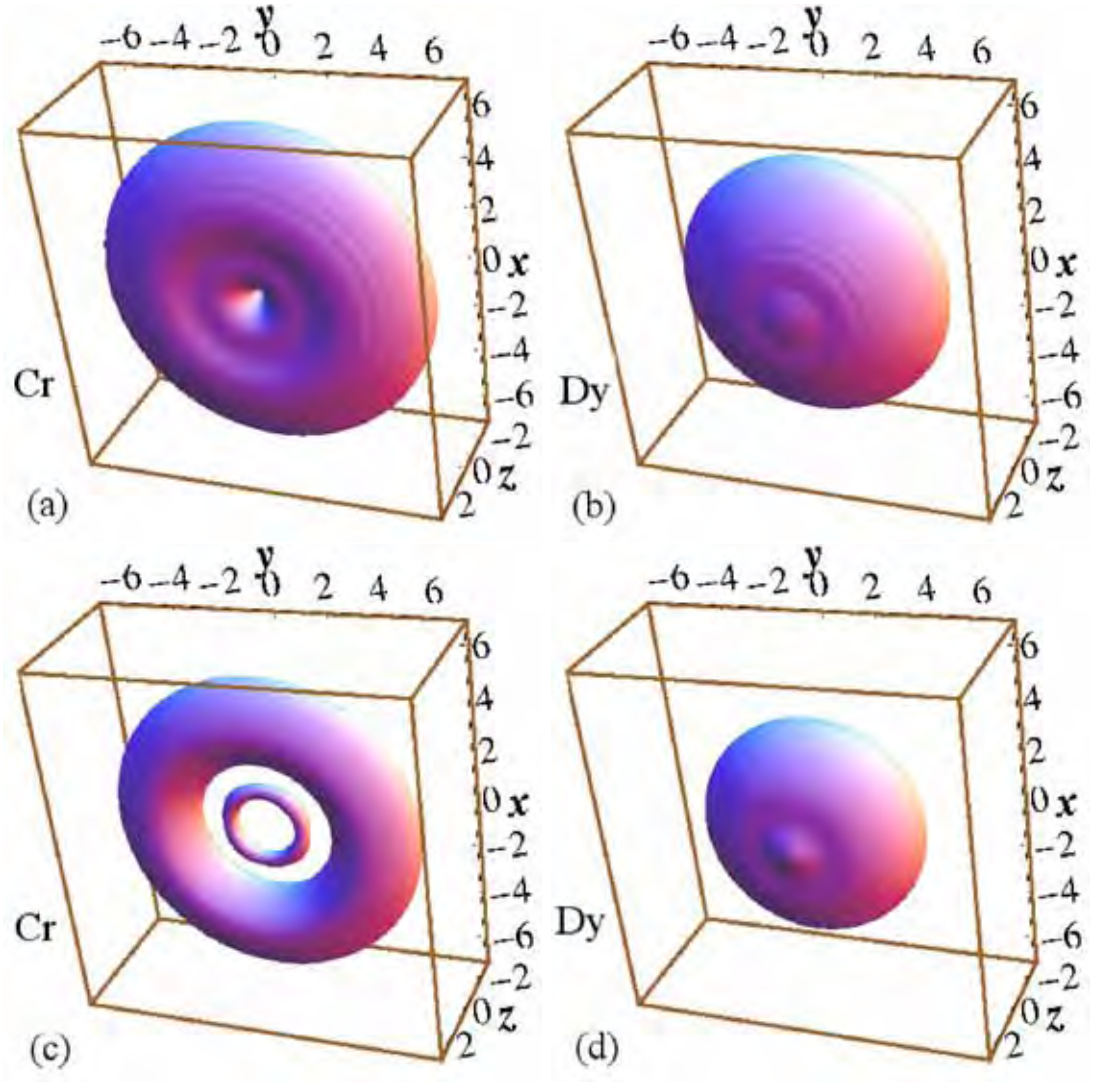

Figure 6.7: Three-dimensional contour plot of the (a) ^{52}Cr and (b) ^{164}Dy densities $|\phi_j(x,y,z)|^2$ of the binary BEC for $a_{12} = 70a_0$ with the cut-off density on contour of 0.0005. The same densities of (c) ^{52}Cr and (d) ^{164}Dy with the cut-off density on contour of 0.0025. In all cases $N(\mathrm{Cr}) = 10000$, $N(\mathrm{Dy}) = 60000$. The lengths x, y and z are in units of $l_0(= 1\mu\mathrm{m})$.

This corresponds to a number of the densities on the contour of 25 μm^{-3} and 150 μm^{-3} in ^{52}Cr and ^{164}Dy, respectively, for $l_0 = 1$ μm.

The Figs. 6.7 (c) and (d) thus show the structure in the interior of the BECs illustrated in Figs. 6.7 (a) and (b). Along the radial direction in the x-y plane, we find in Figs. 6.7 (c) and (d) that the maximum density of one component is accompanied by the minimum density of the other component due to interspecies contact repulsion and the density of one component may have several local maxima. The global maxima in the densities of Figs. 6.7 (c) and (d) are $0.0064 l_0^{-3}$ and $0.013 l_0^{-3}$, respectively, corresponding to a number of the densities of 64 μm^{-3} and 780 μm^{-3} for ^{52}Cr and ^{164}Dy.

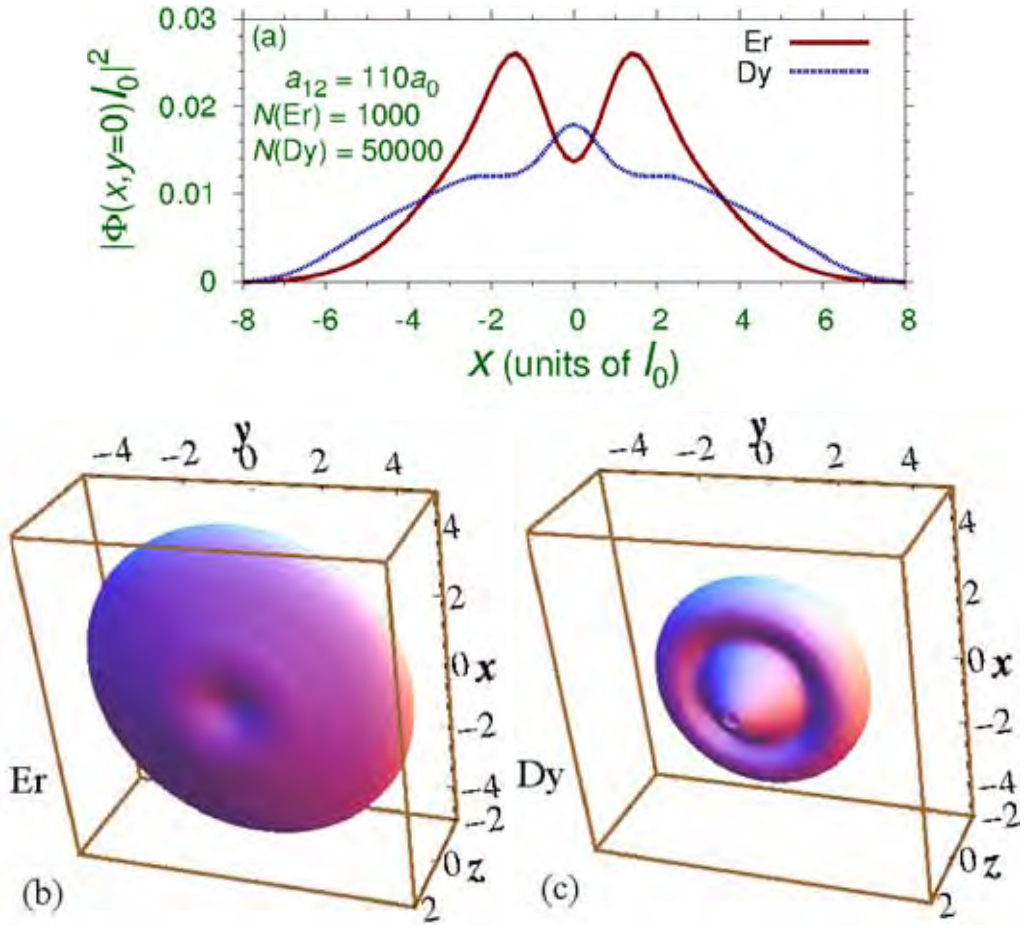

Figure 6.8: Two-dimensional radial density along the x axis $|\Phi_j(x, y = 0)|^2 \equiv \int dz |\phi_j(x, y = 0, z)|^2$ of the binary ^{168}Er-^{164}Dy BEC of N(Er) = 1000, N(Dy) = 50000, for (a) $a_{12} = 110a_0$. Three-dimensional contour plot of the (b) ^{168}Er and (c) ^{164}Dy density $|\phi_j(x, y, z)|^2$ of the binary BEC of (a). Density on 3D contour = 0.0025. The lengths x, y and z are in units of $l_0 (= 0.5 \mu$m).

We study the distinct structure of the densities of binary dipolar BECs with a smaller number of ^{168}Er atoms in the shaded region of Fig. 6.2 (b). In particular we consider the partially mixed configuration with $a_{12} = 110a_0, N(\mathrm{Er}) = 1000$, $N(\mathrm{Dy}) = 50000$. For this binary ^{168}Er-^{164}Dy BEC, in Fig. 6.8 (a), we illustrate the 2D radial density along the x axis

$$|\Phi(x, y = 0)|^2 \equiv \int dz |\phi(x, y = 0, z)|^2. \tag{6.19}$$

In Figs. 6.8 (b) and (c) the contour plots of the corresponding 3D densities of ^{168}Er and ^{164}Dy are shown with a cut-off density $0.0025 l_0^{-3}$ on the contour. The maximum densities inside the ^{168}Er and ^{164}Dy BECs are $0.014 l_0^{-3}$ and $0.0038 l_0^{-3}$, respectively. In this case a biconcave shape has appeared in the density profile of the ^{168}Er BEC in Fig. 6.8 (b). A Saturn-anel-like profile in the density of the ^{164}Dy BEC is shown in Fig. 6.8 (c). The central high-density region of the ^{164}Dy BEC has expelled the ^{168}Er BEC from the central region, thus creating a biconcave shape in the density. If we compare Figs. 6.4 (a) and (b) with Figs. 6.8 (b) and (c), we find that the roles of ^{164}Dy and ^{168}Er BECs have interchanged. In Fig. 6.4 (a), the ^{168}Er BEC has a Saturn-anel-like profile, whereas, in Fig. 6.8 (c), the ^{164}Dy BEC has a similar profile.

Finally, we emphasize that these type of profiles, where the contact interaction is diminished with respect to the long range interaction, are a consequence of the anisotropic nature in dipole-dipole interaction, and with this purpose we study carefully the binary system for the cases depicted in Fig. 6.3 (b), without dipolar interaction, this means for $a_{dd}^{(1)} = a_{dd}^{(2)} = a_{dd}^{(12)} = 0$. In Fig. 6.9 (a) is illustrated the reduced 2D density in the radial direction for the binary ^{168}Er-^{164}Dy mixture for 10000 ^{168}Er and 20000 ^{164}Dy atoms, corresponding with Fig. 6.3 (b) for $a_{12} = 125a_0$ without dipolar interaction. The Fig. 6.9 (a) reveals a new demixed configuration, showing that without dipolar interaction the partially demixed structure of Fig. 6.3 (b) disappears. In Figs. 6.9 (b) and (c) we plot the 3D contours of ^{168}Er and ^{164}Dy BEC profiles for the parameters of Fig. 6.9 (a). The density $|\phi(x, y, z)|^2$ on the surface of these plots is $0.0005 l_0^{-3}$. In this case without dipolar interaction the special structures, that previously we showed in Figs. 6.4 (a) and (b), of Saturn-ring-like and red-blood-cell-like biconcave profiles disappears and we have just a demixed configuration. It is important to emphasize that with current technology, these structures for dipolar BECs could be created in the laboratory and our theoretical results verified.

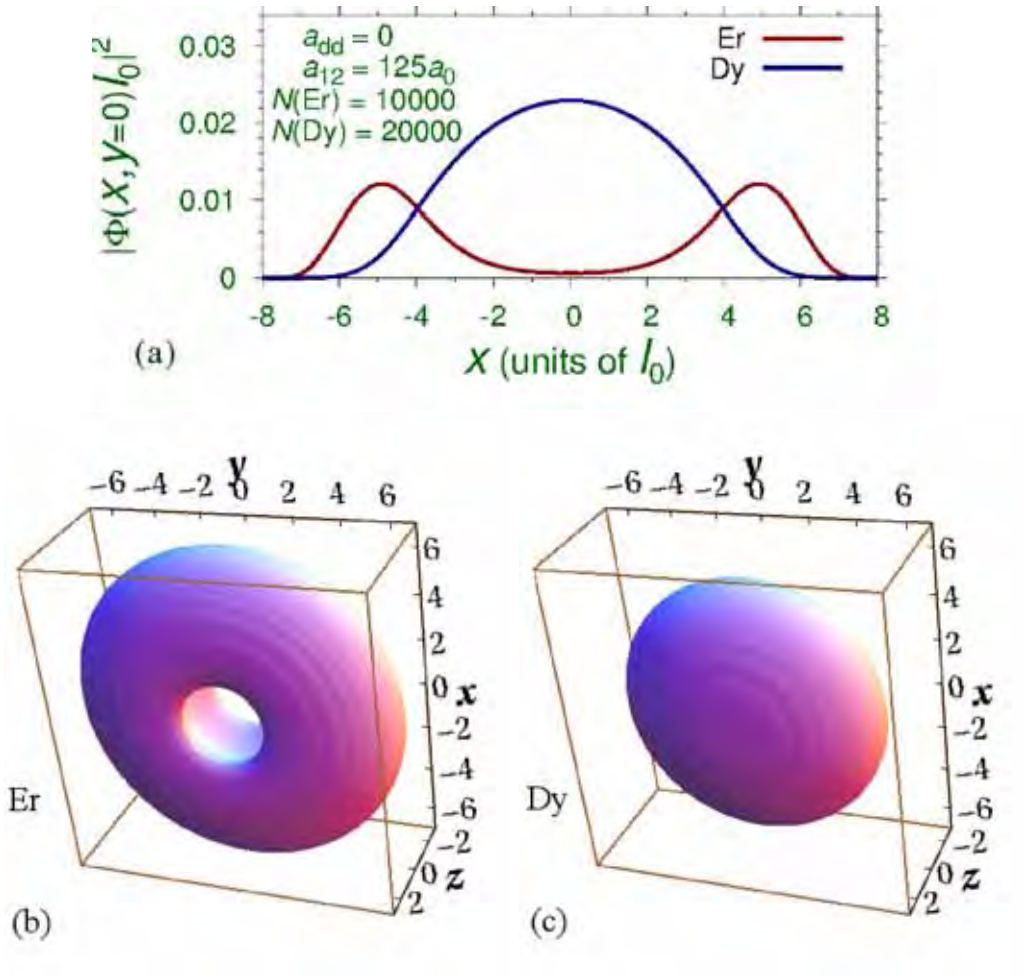

Figure 6.9: Binary ^{168}Er-^{164}Dy BEC of $N(\mathrm{Er}) = 10000$, $N(\mathrm{Dy}) = 20000$, for $a_{12} = 125a_0$ without dipolar interaction $a_{dd}^{(1)} = a_{dd}^{(2)} = a_{dd}^{(12)} = 0$. (a) Two-dimensional radial density along the x axis $|\Phi_j(x, y = 0)|^2 \equiv \int dz |\phi_j(x, y = 0, z)|^2$. Three-dimensional contour plot of the (b) ^{168}Er and (c) ^{164}Dy density $|\phi_j(x, y, z)|^2$ of the binary BEC of (a). Density on 3D contour = 0.0005. The lengths x, y and z are in units of $l_0 (= 0.5\mu\mathrm{m})$. This case without dipolar interaction reveals a new demixed configuration showing that the partially demixed structure of Fig. 6.3 (b) and the special structures that previously we showed in Figs. 6.4 (a) and (b), of Saturn-ring-like and red-blood-cell-like biconcave profiles disappears.

7

Bound Dipolar Droplet in a Trapped Condensate

An untrapped three-dimensional (3D) Bose-Einstein Condensate (BEC) with attractive interaction does not exist in nature due to collapse instability [15]. However, the collapse of an untrapped BEC can be avoided due to interspecies contact interaction in a binary mixture with a trapped BEC. The shape of such a stable droplet bound in a trapped BEC is controlled by the inter−species interactions, whereas that of a trapped BEC is determined by the underlying trap. Here we consider such a dipolar droplet bound in a trapped nondipolar BEC. The effect of the underlying atomic interaction, especially the anisotropic dipolar interaction, will easily manifest itself in such a dipolar droplet. These droplets will be termed quasi-free as they can easily move around inside the larger trapped BEC responsible for their binding. By taking the trapped BEC to be nondipolar, one can easily study the effect of intra-species dipolar interaction on the quasi-free droplet in the absence of any inter-species dipolar interaction.

Dipolar BECs are immediately distinguishable from those with purely contact interactions by their strong shape and stability dependence [35, 38–41] on trapping geometry. Here, we are proposing a new way to trap a dipolar BEC in the form of a quasi-free dipolar droplet, using an attractive inter-species mean-field potential, which introduces a unique trapping geometry that results in further interesting shape and stability characteristics of dipolar BECs. We study the statics and dynamics of a quasi-free dipolar droplet using numerical solutions and variational approximations of a mean-field model [28, 37, 92]. For this pur-

pose we consider a binary mixture of nondipolar ^{87}Rb [1] and dipolar ^{164}Dy where the trapped nondipolar ^{87}Rb BEC could be in a cigar- or disk-shape. The dipole moments of the ^{164}Dy atoms are considered polarized along the axial z direction. Among the available dipolar BECs [12, 13, 90], ^{164}Dy atoms have the largest (magnetic) dipolar interaction strength [46, 71]. The existence of stable 3D ^{164}Dy droplets is illustrated by stability plots of the number of atoms of the two species and the inter-species scattering length.

For a fixed number N(Rb) of ^{87}Rb atoms the dipolar droplet could be bound below a critical number N(Dy) of ^{164}Dy atoms between two limiting values of inter-species attraction. If the inter-species attraction is too small, the ^{164}Dy atoms in the droplet cannot be bound, and for a very large inter-species attraction the droplet is destroyed by collapse instability. Usually, the dipolar droplet has the same shape as the trap acting on the nondipolar BEC. However, for a large number of ^{164}Dy atoms, as the inter-species attraction approaches the level of collapse instability, the dipolar droplet is always cigar shaped even if the external trap is disk shaped and eventually the dipolar droplet collapses on the axial z direction from the cylindrical configuration. For a small number of atoms, the dipolar droplet collapses to the center maintaining its shape rather than moving along the z axis.

In this chapter the variational approximation to the sizes and chemical potentials of the stationary droplets is compared with the numerical solution of the mean-field model. The numerical study of the breathing oscillation of the stable dipolar droplet is found to be in reasonable agreement with a time-dependent variational model calculation. We also demonstrate a viable experimental way of creating a ^{164}Dy droplet bound in a trapped ^{87}Rb BEC, e.g., by slowly removing the trap on a trapped binary ^{164}Dy-^{87}Rb mixture, while the trapped ^{164}Dy BEC evolves into a quasi-free droplet.

7.1 Mean-field model for a quasi-free dipolar droplet

We consider a binary BEC, where one of the species is dipolar and the other nondipolar, interacting via inter- and intra-species interactions with the mass, number of atoms, magnetic dipole moment, and scattering length for the two species $j = 1, 2$, denoted by m_j, N_j, $\bar{\mu}_j$, a_j, respectively. The first species (^{87}Rb) is taken to be nondipolar ($\bar{\mu}_1 = 0$) and trapped while the second species (^{164}Dy) is dipolar ($\bar{\mu}_2 \neq 0$) and polarized along the axial z direction. The angular frequencies for the axially-symmetric trap on ^{87}Rb along the x, y and z directions are taken as $\omega_x = \omega_y = \omega_1$ and $\omega_z = \lambda_1\omega_1$. The inter ($V_{12}$) and intra-species ($V_j$)

[1] We have taken ^{87}Rb as a typical example, because Rubidium was the first element to be Bose condensed, and is still most commonly used species for ultracold boson experiments.

interactions for two atoms at positions $\mathbf{r}$ and $\mathbf{r}'$ are taken as

$$V_{12}(\mathbf{R}) = \frac{2\pi\hbar^2 a_{12}}{m_R}\delta(\mathbf{R}), \quad V_1(\mathbf{R}) = \frac{4\pi\hbar^2 a_1}{m_1}\delta(\mathbf{R}), \tag{7.1}$$

$$V_2(\mathbf{R}) = \frac{\mu_0\bar{\mu}_2^2}{4\pi}U_{dd}(\mathbf{R}) + \frac{4\pi\hbar^2 a_2}{m_2}\delta(\mathbf{R}), \tag{7.2}$$

where $\mathbf{R} = \mathbf{r} - \mathbf{r}'$, $U_{dd}(\mathbf{R})$ represents the dipole-dipole interaccion defined in Eq. (3.10), $\delta(\mathbf{R})$ is the delta function used to define the contact interaction in Eq. (1.5), μ_0 is the permeability of free space, m_R is the reduced mass of the two species of atoms and a_{12} is the interspecies scattering length. With these interactions, the coupled Gross-Pitaevskii (GP) equations for the binary BEC can be written as [28]

$$i\hbar\frac{\partial\phi_1(\mathbf{r},t)}{\partial t} = \Big[-\frac{\hbar^2}{2m_1}\nabla^2 + \frac{1}{2}m_1\omega_1^2(\rho^2+\lambda_1^2 z^2) + \frac{4\pi\hbar^2}{m_1}a_1N_1|\phi_1(\mathbf{r},t)|^2 + \frac{2\pi\hbar^2}{m_R}a_{12}N_2|\phi_2(\mathbf{r},t)|^2\Big]\phi_1(\mathbf{r},t), \tag{7.3}$$

$$i\hbar\frac{\partial\phi_2(\mathbf{r},t)}{\partial t} = \Big[-\frac{\hbar^2}{2m_2}\nabla^2 + \frac{4\pi\hbar^2}{m_2}a_2N_2|\phi_2(\mathbf{r},t)|^2 + \frac{2\pi\hbar^2}{m_R}a_{12}N_1|\phi_1(\mathbf{r},t)|^2 + N_2\frac{\mu_0\ \bar{\mu}_2^2}{4\pi}\int U_{dd}(\mathbf{R})|\phi_2(\mathbf{r}',t)|^2 d\mathbf{r}'\Big]\phi_2(\mathbf{r},t), \tag{7.4}$$

where $i=\sqrt{-1}$, $\rho^2 = x^2+y^2$ and

$$\int d\mathbf{r}\ |\phi_j(\mathbf{r},t)|^2 = 1, \tag{7.5}$$

is the normalization for each component ($j = 1,2$). To compare the dipolar and contact interactions, we define the length a_{dd} (wich measures the strength of dipolar interaction) in terms of the second species

$$a_{dd} = \frac{\mu_0\bar{\mu}_2^2 m_2}{12\pi\hbar^2}. \tag{7.6}$$

We express the strength of the dipolar interaction in Eq. (7.4) by this length scale and transform Eqs. (7.3) and (7.4) into the following dimensionless form [28]:

$$i\frac{\partial\phi_1(\mathbf{r},t)}{\partial t} = \Big[-\frac{\nabla^2}{2} + \frac{1}{2}(\rho^2+\lambda_1^2 z^2) + g_1|\phi_1|^2 + g_{12}|\phi_2|^2\Big]\phi_1(\mathbf{r},t), \tag{7.7}$$

$$i\frac{\partial\phi_2(\mathbf{r},t)}{\partial t} = \Big[-m_{12}\frac{\nabla^2}{2} + g_2|\phi_2|^2 + g_{21}|\phi_1|^2 + g_{dd}\int U_{dd}(\mathbf{R})|\phi_2(\mathbf{r}',t)|^2 d\mathbf{r}'\Big]\phi_2(\mathbf{r},t), \tag{7.8}$$

where

$$m_{12} = \frac{m_1}{m_2},\ g_1 = 4\pi a_1 N_1,\ g_2 = 4\pi a_2 N_2 m_{12},$$
$$g_{12} = \frac{2\pi m_1}{m_R} a_{12} N_2,\ g_{21} = \frac{2\pi m_1}{m_R} a_{12} N_1,\ g_{dd} = 3N_2 a_{dd} m_{12}. \tag{7.9}$$

In Eqs. (7.7) and (7.8), length is expressed in units of oscillator length of the first species $l_0 = \sqrt{\hbar/m_1\omega_1}$, energy in units of oscillator energy $\hbar\omega_1$, density $|\phi_j|^2$ in units of l_0^{-3}, and time in units of $t_0 = \omega_1^{-1}$. Now, we propose the following Lagrangian density for a binary BEC of Eq. (7.7) and (7.8)

$$\mathcal{L} = \mathcal{L}_1 + \mathcal{L}_2 + \mathcal{L}_{12}, \tag{7.10}$$

where the intra and interspecies Lagrangian density is

$$\mathcal{L}_1 = \frac{1}{2}\Big[iN_1\left(\phi_1\ \partial_t\phi_1^\star - \phi_1^\star\ \partial_t\phi_1\right) + N_1|\nabla\phi_1(\mathbf{r},t)|^2 + N_1(\rho^2 + \lambda_1^2 z^2)|\phi_1(\mathbf{r},t)|^2 + N_1\ g_1|\phi_1(\mathbf{r},t)|^4\Big], \tag{7.11}$$

$$\mathcal{L}_2 = \frac{1}{2}\Big[iN_2\left(\phi_2\ \partial_t\phi_2^\star - \phi_2^\star\ \partial_t\phi_2\right) + m_{12}N_2|\nabla\phi_2(\mathbf{r},t)|^2 + N_2\ g_2|\phi_2(\mathbf{r},t)|^4\Big] + \frac{N_2}{2}g_{dd}\int U_{dd}(\mathbf{R})|\phi_2(\mathbf{r}',t)|^2|\phi_2(\mathbf{r},t)|^2 d\mathbf{r}', \tag{7.12}$$

$$\mathcal{L}_{12} = N_1 g_{12}|\phi_1(\mathbf{r},t)|^2|\phi_2(\mathbf{r},t)|^2, \tag{7.13}$$

where ∂_t denotes time derivative. It is straightforward to verify that Eqs. 7.7 and 7.8 are the Euler-Lagrange equations for the Lagrangian density 7.10. We find the equation for each component by deriving for $\phi_j^\star$

$$\frac{d}{dt}\left(\frac{\partial\mathcal{L}}{\partial\dot{\phi}_j^\star}\right) - \frac{\partial\mathcal{L}}{\partial\phi_j^\star} = \ 0, \tag{7.14}$$

For example, deriving for $\phi_2^\star$ in Eq. (7.14), and using Eq. (7.10), we have for the second dipolar BEC

$$-\frac{1}{2}\Big\{-iN_2\ \partial_t\phi_2 + m_{12}\ N_2\frac{\partial}{\partial\phi_2^\star}[(\nabla\phi_2^\star)(\nabla\phi_2)] + 2N_2\ g_2|\phi_2(\mathbf{r},t)|^2\phi_2(\mathbf{r},t)\Big\}$$
$$+\frac{i}{2}N_2\partial_t\phi_2 - N_1\ g_{12}|\phi_1|^2\phi_2 - N_2\ g_{dd}\int U_{dd}(\mathbf{R})\ |\phi_2(\mathbf{r}',t)|^2 d\mathbf{r}'\phi_2(\mathbf{r},t) = 0, \tag{7.15}$$

using $|\nabla\phi|^2 = (\nabla\phi^\star)(\nabla\phi) = \nabla(\phi^\star\nabla\phi) - \phi^\star\nabla^2\phi$ and $N_1\ g_{12} = N_2\ g_{21}$ we have

$$i\partial_t\phi_2(\mathbf{r},t) = \Big[-\frac{m_{12}}{2}\nabla^2 + g_2|\phi_2(\mathbf{r},t)|^2 + g_{21}|\phi_1(\mathbf{r},t)|^2 + g_{dd}\int U_{dd}(\mathbf{R})\ |\phi_2(\mathbf{r}',t)|^2 d\mathbf{r}'\Big]\phi_2(\mathbf{r},t), \tag{7.16}$$

finally, the last mathematical expression corresponds to dynamics equation for second BEC: Eq. (7.8).

7.2 Numerical Results

7.2.1 Stable States

We solve Eqs. (7.7) and (7.8) with a split-step Crank-Nicolson discretization scheme described in reference [21] using a space step of 0.1 and the time step 0.001. The contribution of the dipolar interaction is calculated in momentum space by Fourier transformation [53]. For both species of atoms ^{87}Rb and ^{164}Dy we take the intra-species scattering length as $a_j = 110a_0$, and the strength of dipolar interaction as $a_{dd} = 131a_0$ [12, 15]. The yet unknown inter-species scattering length a_{12} is taken as a variable. The variation of a_{12} can be achieved experimentally by the Feshbach resonance technique [65]. We consider the angular frequency $\omega_1 = 2\pi \times 115$ Hz, so that the length scale $l_0 \equiv \sqrt{\hbar/m_1\omega_1} = 1$ μm and time scale $t_0 \equiv \omega_1^{-1} = 1.38$ ms.

We find that a quasi-free ^{164}Dy droplet is achievable for a moderately attractive inter-species attraction (negative a_{12}) and at appropriate numbers of atoms of the two species N_1 and N_2. We illustrate the domain of existence of a stable ^{164}Dy droplet in the stability plots of Figs. 7.1 (a), (b) and (c) for N(Rb) = 2000, 10000 and 50000, and for $\lambda = 4$ (disk-shaped trap) and 0.25 (cigar-shaped trap). We consider cigar- and disk-shaped ^{164}Dy droplets in this study, where the effect of dipolar interaction is expected to be more prominent, and not spherically symmetric ones where the effect of dipolar interaction is expected to be minimal [33, 46].

In all the plots of Figs. 7.1, for a fixed N(Rb), the ^{164}Dy droplet can be bound for a maximum N(Dy). This maximum N(Dy) increases with N(Rb), all other parameters remaining fixed. For a fixed N(Rb), the disk-shaped trap can accommodate a larger maximum number of ^{164}Dy atoms than the cigar-shaped trap. For N(Dy) smaller than this maximum number, the ^{164}Dy droplet can be bound for $|a_{12}|$ between two limiting values. For $|a_{12}|$ above the upper limit, there is too much inter-species attraction on the ^{164}Dy droplet leading to its collapse. For $|a_{12}|$ below the lower limit, there is not enough attraction and the ^{164}Dy droplet cannot be bound.

The lower limit of $|a_{12}|$ is small and tends to zero as N(Rb) tends to infinity. For fixed values of N(Rb) and N(Dy) and for small $|a_{12}|$ near the lower limit, the disk-shaped configuration is favored and it can bind the ^{164}Dy droplet for smaller values of $|a_{12}|$. However, for a fixed N(Rb) and large $|a_{12}|$ near the upper limit, the disk-shaped configuration is favored only for a large N(Dy) allowing a ^{164}Dy droplet for larger $|a_{12}|$, whereas the cigar-shaped configuration is favored for a small N(Dy), because it allows a ^{164}Dy droplet for larger $|a_{12}|$.

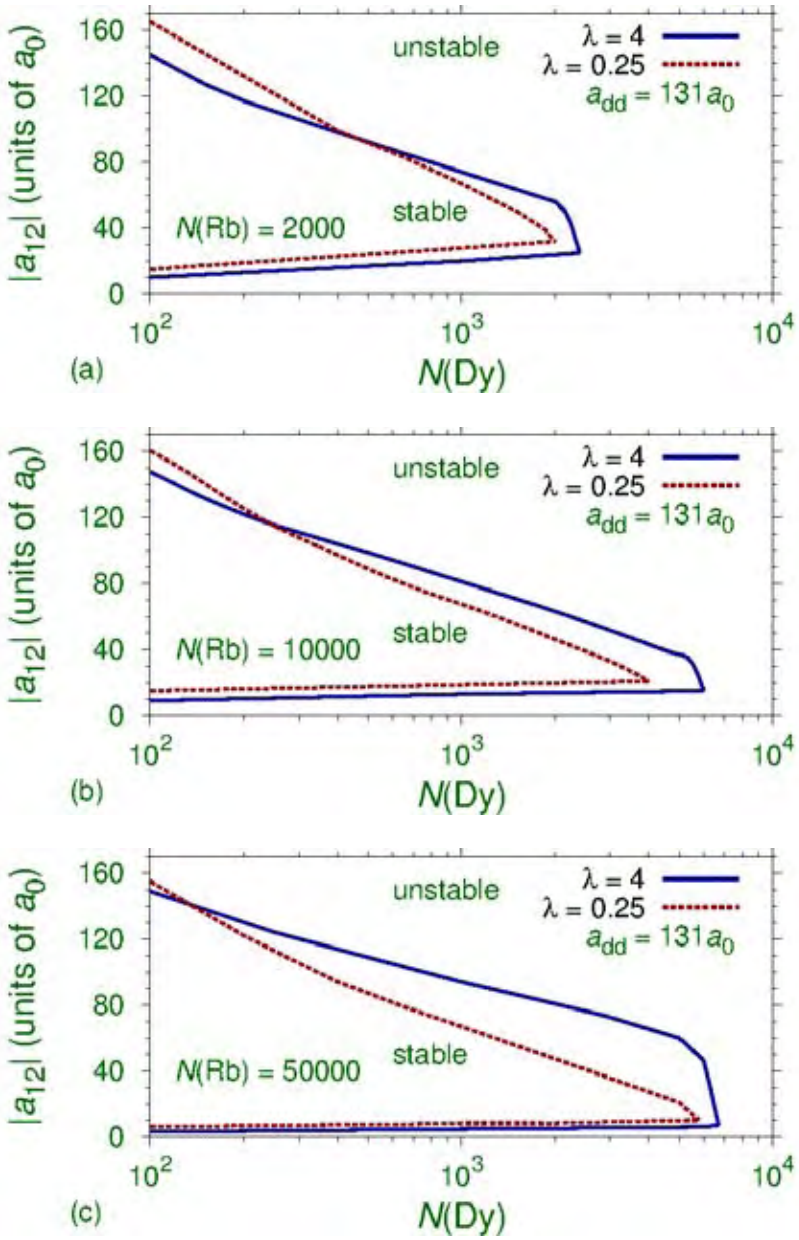

Figure 7.1: Stability phase plot showing the interspecies scattering length $|a_{12}|$ versus the number N(Dy) of ^{164}Dy atoms. Here is showing the domain of stable ^{164}Dy droplet in a binary ^{87}Rb$-^{164}$Dy mixture for: (a) N(Rb) = 2000, (b) N(Rb) = 10000, and (c) N(Rb) = 50000, all for $\lambda = 0.25$ (red) and $\lambda = 4$ (blue). The intra-species scattering lengths are taken as $a_1 = a_2 = 110a_0$ and the strength of dipolar interaction for Dy is $a_{dd} = 131a_0$.

7.2.2 Analytic Variational Solution

Using Eq. (7.10), the effective Lagrangian ($L \equiv \int \mathcal{L}\, d\mathbf{r}$) has the form

$$\begin{aligned} L = \int d\mathbf{r} \frac{1}{2}\Big\{ \sum_j \Big[iN_j(\phi_j \partial_t \phi_j^\star - \phi_j^\star \partial_t \phi_j) + N_j g_j |\phi_j(\mathbf{r})|^4 \Big] \\ + N_1 |\nabla \phi_1(\mathbf{r})|^2 + m_{12} N_2 |\nabla \phi_2(\mathbf{r})|^2 + N_1(\rho^2 + \lambda_1^2 z^2) \times |\phi_1(\mathbf{r})|^2 \Big\} \\ + N_1 g_{12} \int d\mathbf{r} |\phi_1(\mathbf{r})|^2 |\phi_2(\mathbf{r})|^2 + \frac{N_2}{2} g_{dd} \int\int U_{dd}(\mathbf{R}) |\phi_2(\mathbf{r}')|^2 |\phi_2(\mathbf{r})|^2 d\mathbf{r}' d\mathbf{r}. \end{aligned} \tag{7.17}$$

Convenient analytic variational approximation to Eqs. (7.7) and (7.8) can be obtained with the following ansatz for the wave functions [24, 53, 69]:

$$\phi_j(\mathbf{r}, t) = \frac{\pi^{-3/4}}{w_{\rho j}\sqrt{w_{zj}}} \exp\Big[-\frac{\rho^2}{2w_{\rho j}^2} - \frac{z^2}{2w_{zj}^2} + i\alpha_j \rho^2 + i\beta_j z^2 \Big] \tag{7.18}$$

where $\mathbf{r} = \{\rho, z\}$, $\rho = \{x, y\}$, $w_{\rho j}$ and w_{zj} are the widths and α_j and β_j are additional variational parameters. In this form, the effective Lagrangian for the binary system Eq. (7.17) is

$$\begin{aligned} L = \sum_{j=1}^{2} \frac{N_j}{2}(2w_{\rho j}^2 \dot{\alpha}_j + w_{zj}^2 \dot{\beta}_j) + \frac{N_1}{2}\left[\frac{1}{w_{\rho 1}^2} + \frac{1}{2w_{z1}^2} + 4w_{\rho 1}^2 \alpha_1^2 + 2w_{z1}^2 \beta_1^2 \right] \\ + \frac{N_2 m_{12}}{2}\left[\frac{1}{w_{\rho 2}^2} + \frac{1}{2w_{z2}^2} + 4w_{\rho 2}^2 \alpha_2^2 + 2w_{z2}^2 \beta_2^2 \right] + \frac{N_1}{2}\left[w_{\rho 1}^2 + \lambda_1^2 \frac{w_{z1}^2}{2} \right] \\ + \frac{N_1^2 a_1}{\sqrt{2\pi} w_{\rho 1}^2 w_{z1}} + \frac{N_2^2 m_{12}}{\sqrt{2\pi} w_{\rho 2}^2 w_{z2}} [a_2 - a_{dd} f(\kappa)] + \frac{C N_1 N_2}{2AB^{1/2}}, \end{aligned} \tag{7.19}$$

with

$$\kappa = \frac{w_{\rho 2}}{w_{z2}}, \quad f(\kappa) = \frac{1 + 2\kappa^2 - 3\kappa^2 d(\kappa)}{1 - \kappa^2}, \quad d(\kappa) = \frac{\operatorname{atan}(\sqrt{\kappa^2 - 1})}{\sqrt{\kappa^2 - 1}}, \tag{7.20}$$

where $A = w_{\rho 1}^2 + w_{\rho 2}^2$, $B = w_{z1}^2 + w_{z2}^2$ and $C = 4a_{12} m_1/(\sqrt{\pi} m_R)$. In these equations the overhead dot denotes time derivative. The Euler-Lagrange variational equations for the widths of the effective Lagrangian (7.17), obtained in the usual

fashion [24], are:

$$\ddot{w}_{\rho 1} + w_{\rho 1} = \frac{1}{w_{\rho 1}^3} + \frac{1}{\sqrt{2\pi}} \frac{2N_1 a_1}{w_{\rho 1}^3 w_{z1}} + \frac{CN_2 w_{\rho 1}}{A^2 B^{1/2}}, \tag{7.21}$$

$$\ddot{w}_{z1} + \lambda_1^2 w_{z1} = \frac{1}{w_{z1}^3} + \frac{1}{\sqrt{2\pi}} \frac{2N_1 a_1}{w_{\rho 1}^2 w_{z1}^2} + \frac{CN_2 w_{z1}}{AB^{3/2}}, \tag{7.22}$$

$$\ddot{w}_{\rho 2} = \frac{m_{12}}{w_{\rho 2}^3} + \frac{N_2 m_{12}[2a_2 - a_{dd} g(\kappa)]}{\sqrt{2\pi} w_{\rho 2}^3 w_{z2}} + \frac{CN_1 w_{\rho 2}}{A^2 B^{1/2}}, \tag{7.23}$$

$$\ddot{w}_{z2} = \frac{m_{12}}{w_{z2}^3} + \frac{2N_2 m_{12}[a_2 - a_{dd} h(\kappa)]}{\sqrt{2\pi} w_{\rho 2}^2 w_{z2}^2} + \frac{CN_1 w_{z2}}{AB^{3/2}}, \tag{7.24}$$

$$g(\kappa) = \frac{2 - 7\kappa^2 - 4\kappa^4 + 9\kappa^4 d(\kappa)}{(1-\kappa^2)^2}, \quad h(\kappa) = \frac{1 + 10\kappa^2 - 2\kappa^4 - 9\kappa^2 d(\kappa)}{(1-\kappa^2)^2}. \tag{7.25}$$

The solution of the time-dependent Eqs. (7.21) − (7.24) gives the dynamics of the variational approximation. If μ_j is the chemical potential with which the stationary wave function propagates in time, e.g. $\phi_j(\mathbf{r}, t) \sim \exp(-i\mu_j t)\phi_j(\mathbf{r})$, then the variational estimate for μ_j is:

$$\mu_1 = \frac{1}{2}\left[\frac{1}{w_{\rho 1}^2} + \frac{1}{2w_{z1}^2}\right] + \frac{1}{2}\left[w_{\rho 1}^2 + \lambda_1^2 \frac{w_{z1}^2}{2}\right] + \frac{2N_1 a_1}{\sqrt{2\pi} w_{\rho 1}^2 w_{z1}} + \frac{CN_2}{2AB^{1/2}}, \tag{7.26}$$

$$\mu_2 = \frac{m_{12}}{2}\left[\frac{1}{w_{\rho 2}^2} + \frac{1}{2w_{z2}^2}\right] + \frac{2N_2 m_{12}}{\sqrt{2\pi} w_{\rho 2}^2 w_{z2}}[a_2 - a_{dd} f(\kappa)] + \frac{CN_1}{2AB^{1/2}}. \tag{7.27}$$

The energy of the system is given by

$$\begin{aligned} E =& \frac{N_1}{2}\left[\frac{1}{w_{\rho 1}^2} + \frac{1}{2w_{z1}^2}\right] + \frac{N_1}{2}\left[w_{\rho 1}^2 + \lambda_1^2 \frac{w_{z1}^2}{2}\right] + \frac{N_2 m_{12}}{2}\left[\frac{1}{w_{\rho 2}^2} + \frac{1}{2w_{z2}^2}\right] \\ &+ \frac{N_1^2 a_1}{\sqrt{2\pi} w_{\rho 1}^2 w_{z1}} + \frac{N_2^2 m_{12}}{\sqrt{2\pi} w_{\rho 2}^2 w_{z2}}[a_2 - a_{dd} f(\kappa)] + \frac{CN_1 N_2}{2AB^{1/2}}. \end{aligned} \tag{7.28}$$

The widths of the stationary state can be obtained from the solution of Eqs. (7.21) − (7.24) setting the time derivatives of the widths equal to zero. This procedure is equivalent to a minimization of the energy (7.28), provided the stationary state is stable and corresponds to a energy minimum. In Figs. 7.2 we illustrate the numerical and variational results for the chemical potentials and root-mean-square (rms) sizes $\langle x \rangle$ and $\langle z \rangle$ of the trapped ^{87}Rb BEC of 10000 atoms and of the bound ^{164}Dy droplet versus N(Dy) for (a) $\lambda = 4$ and (b) 0.25. Considering that the ^{164}Dy droplet may not have a Gaussian shape as assumed in the variational approximation, the agreement between the numerical and variational results is quite satisfactory. The existence of the quasi-free ^{164}Dy droplet can be studied

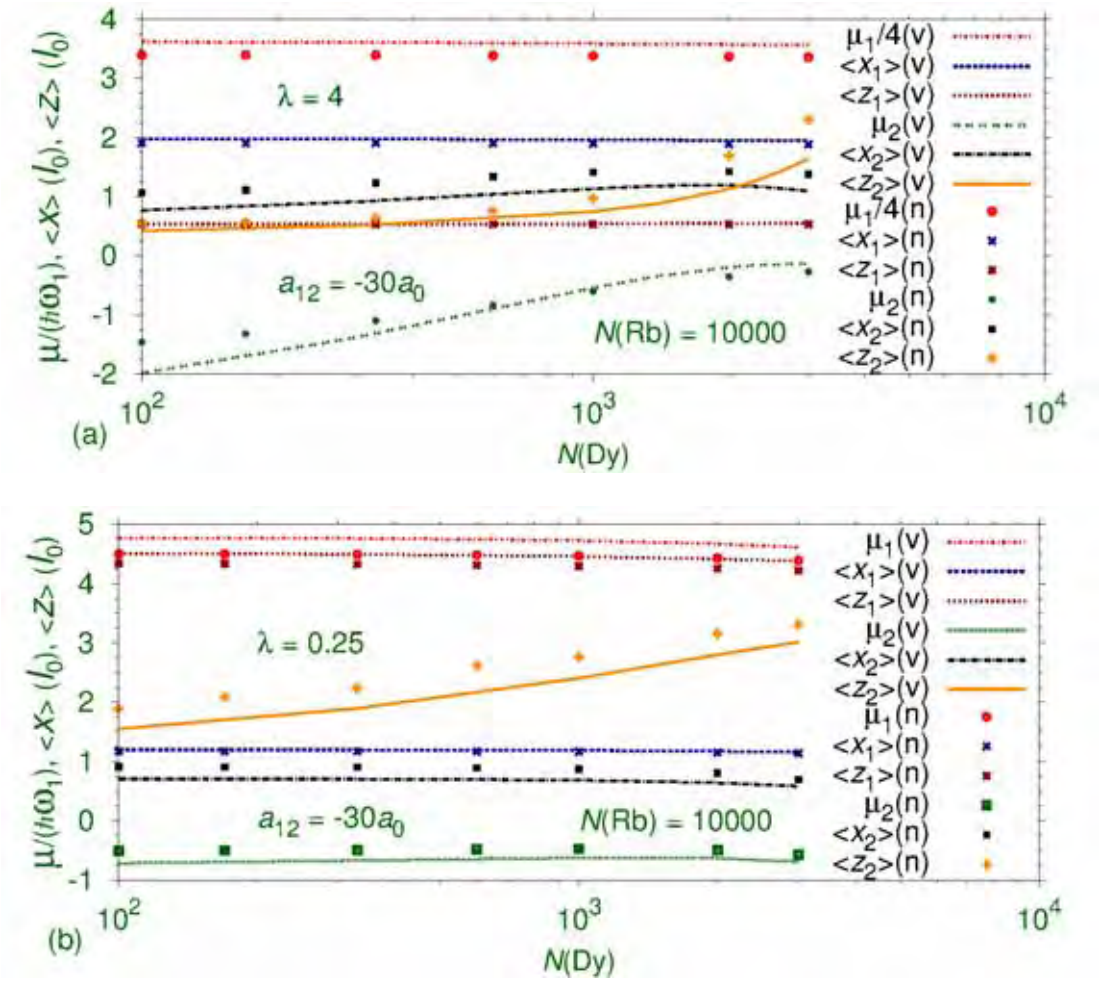

Figure 7.2: Variational (v) and numerical (n) results for chemical potential μ_1 and rms sizes $\langle x_1\rangle, \langle z_1\rangle$ for the trapped ^{87}Rb BEC of 10000 atoms and μ_2, $\langle x_2\rangle, \langle z_2\rangle$ for the bound ^{164}Dy droplet versus the number of ^{164}Dy atoms for (a) $\lambda = 4$ and (b) $\lambda = 0.25$. The inter-species scattering length is $a_{12} = -30a_0$. The numerical and variational results of chemical potential and rms sizes of disk- and cigar-shaped to be in good agreement with each other.

qualitatively by a minimization of the energy Eq. (7.28). However, the widths of the ^{87}Rb BEC for a fixed N(Rb) do not vary much as N(Dy) or a_{12} are altered. Hence for a qualitative understanding of the existence of a stable ^{164}Dy droplet for a fixed N(Rb), we can make a further approximation of the system energy (7.28) and take the widths of the trapped ^{87}Rb BEC to be the same as the widths of the ^{87}Rb BEC in the absence of ^{164}Dy atoms under otherwise identical conditions. The widths of the ^{164}Dy droplet so obtained (approx) for N(Rb) = 50000 are compared in Table 7.1 for several values of a_{12}, N(Dy), and λ with the widths

Table 7.1: Root-mean-square sizes of the binary ^{87}Rb-^{164}Dy system of 50000 ^{87}Rb atoms from variational approximation (7.21) − (7.24) (var). The values (approx) corresponds to an approximate energy minimization taking the widths of the trapped ^{87}Rb BEC to be fixed.

	a_{12}	N(Dy)	λ	$\langle x_1\rangle$	$\langle z_1\rangle$	$\langle x_2\rangle$	$\langle z_2\rangle$
approx	-40a_0	1000	4	2.7597	0.7106	1.0755	0.4847
var	-40a_0	1000	4	2.7475	0.7091	1.0703	0.4834
approx	-80a_0	1000	0.25	2.2780	8.9525	0.6468	2.5799
var	-80a_0	1000	0.25	2.2549	8.8558	0.6378	2.5525
approx	-60a_0	500	4	2.7597	0.7106	0.8478	0.3768
var	-60a_0	500	4	2.7492	0.7090	0.8443	0.3757
approx	-100a_0	100	0.25	2.2780	8.9525	0.6384	1.5803
var	-100a_0	100	0.25	2.2752	8.9392	0.6373	1.5779

obtained from exact energy minimization (var), setting the time derivatives of the widths equal to zero in Eqs. (7.21) − (7.24). We find in Table 7.1 that the sizes of the ^{87}Rb for a fixed N(Rb) remain reasonably constant with respect to the variation of N(Dy) and a_{12} and that the approximate energy minimization with fixed widths for the ^{87}Rb BEC leads to a good approximation of the widths of the ^{164}Dy droplet. In the numerical solution of the binary GP equations (7.7) and (7.8) we also verified that the shape and size of the trapped ^{87}Rb BEC are fairly independent of the presence or absence of the ^{164}Dy droplet. Hence in the study of the shape, size and dynamics of the dipolar ^{164}Dy droplet bound in the trapped ^{87}Rb BEC, the trapped BEC will only have a passive role and we shall highlight only the shape, size and dynamics of the ^{164}Dy droplet in the following.

7.2.3 Dipolar droplet close to the instability

We consider the shape of a stable ^{164}Dy droplet in the stability plots of Figs. 7.1 and study its change as collapse instability is approached. In Fig. 7.3 (a) we show the isodensity contour plot (density $|\phi_1(\mathbf{r})|^2$) of a disk-shaped ($\lambda = 4$) ^{87}Rb BEC of 10000 atoms and that of the bound ^{164}Dy droplet in Figs. 7.3 (b) for N(Dy) = 1000 ($a_{12} = -30a_0$), (c) for N(Dy) = 1000 ($a_{12} = -80a_0$), and in (d) for N(Dy) = 4000 ($a_{12} = -30a_0$). The isodensity of the ^{87}Rb BEC is practically the same in all three cases. Of the isodensities of the ^{164}Dy droplet, the one in Fig. 7.3 (b) is the deepest inside the stability region and furthest away from collapse instability. The parameters of Figs. 7.3 (c) and (d) are close to the region of collapse instability. Of these two, Fig. 7.3 (c) corresponds to a medium number of ^{164}Dy atoms and Fig. 7.3 (d) to a large number. Independent of the initial shape, a ^{164}Dy droplet with a medium number of ^{164}Dy atoms always collapses towards the center with shrinking size.

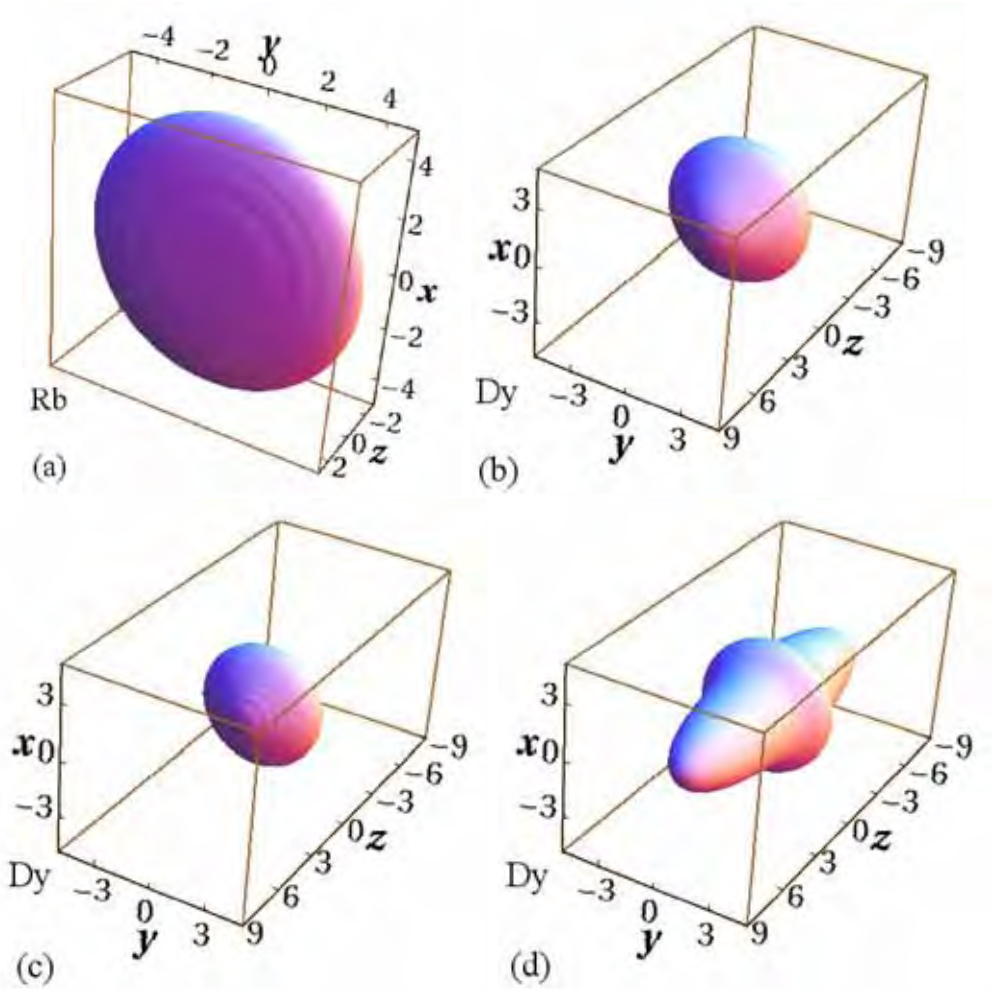

Figure 7.3: The density contour plot $|\phi_j(x, y, z)|^2$ of (a) a disk-shaped ($\lambda = 4$) ^{87}Rb BEC of 10000 atoms and that of the bound ^{164}Dy droplet of (b) 1000 atoms ($a_{12} = -30a_0$), (c) 1000 atoms ($a_{12} = -80a_0$), (d) 4000 atoms ($a_{12} = -30a_0$). The isodensity contour of the ^{87}Rb BEC is practically the same in all three cases. In all cases the density on the contour is $0.001 l_0^{-3}$, length is measured in units of l_0 ($= 1$ μm), the intra-species scattering lengths are taken as $a_1 = a_2 = 110a_0$ and the strength of dipolar interaction for Dy is $a_{dd} = 131a_0$.

However, a ^{164}Dy droplet containing a large number of atoms, independent of the associated trap symmetry, always first takes a cigar shape and then collapses on the axial z direction. A strong dipolar interaction prohibits a collapse to center of a large ^{164}Dy droplet and favors a cigar shape. In Figs. 7.3 the trap is disk-shaped. The medium-sized ^{164}Dy droplet of Fig. 7.3 (c) collapses to the center, but maintains its disk shape due to lower net dipolar interaction. The large ^{164}Dy droplet in Fig. 7.3 (d) has changed from the supporting disk-shaped

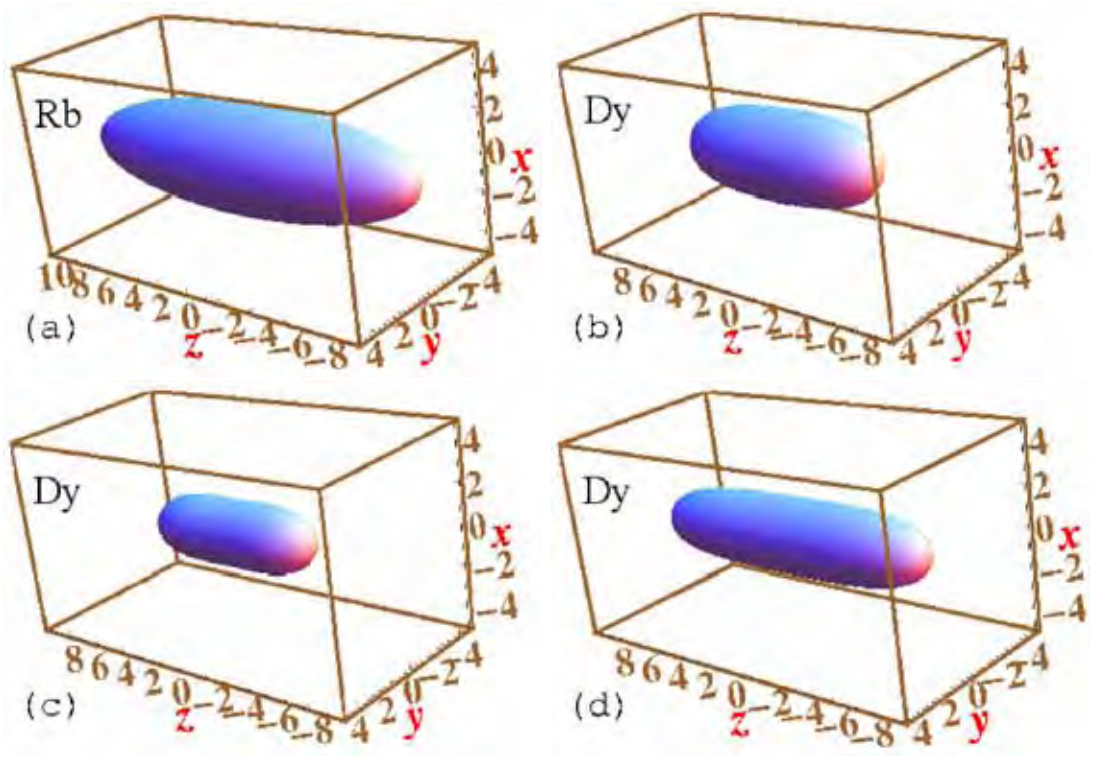

Figure 7.4: Three-dimensional contour plot of densities $|\phi_j(x, y, z)|^2$ for (a) a cigar-shaped ($\lambda = 0.25$) ^{87}Rb BEC of 10000 atoms and that of the bound ^{164}Dy droplet of (b) 1000 atoms ($a_{12} = -30a_0$), (c) 1000 atoms ($a_{12} = -65a_0$), (d) 3000 atoms ($a_{12} = -30a_0$). The isodensity contour of the ^{87}Rb BEC is practically the same in all three cases. The density on the contour in all cases is $0.001\, l_0^{-3}$ and length is measured in units of l_0 ($= 1\ \mu$m).

trap to a cigar shape. If the attraction is further increased (by increasing $|a_{12}|$) the ^{164}Dy droplet of Fig. 7.3 (d) would collapse from the cigar shape on the axial z direction. In Fig. 7.4 (a) we illustrate the isodensity contour of a cigar-shaped ($\lambda = 0.25$) ^{87}Rb BEC of 10000 atoms and the same of the ^{164}Dy droplet are shown in Figs. 7.4 (b) for $N(\text{Dy}) = 1000$ ($a_{12} = -30a_0$), (c) for $N(\text{Dy}) = 1000$ ($a_{12} = -65a_0$), and in (d) for $N(\text{Dy}) = 3000$ ($a_{12} = -30a_0$). The density of the ^{87}Rb BEC is virtually the same in all three cases. Of the three ^{164}Dy droplets, the one in Fig. 7.4 (b) is deepest inside the stability region and furthest away from collapse instability. The parameters for Figs. 7.4 (c) and (d) are close to the region of collapse instability. In all cases the ^{164}Dy droplet maintains the cigar shape of the accompanying trap acting on the ^{87}Rb BEC. The size of the ^{164}Dy droplet in Fig. 7.4 (b) is larger than that of Fig. 7.4 (c) with the same number of atoms due to a strong inter-species attraction acting on the latter. The ^{164}Dy droplet of Fig. 7.4 (d) is larger than those in Figs. 7.4 (b) and (c) due to its

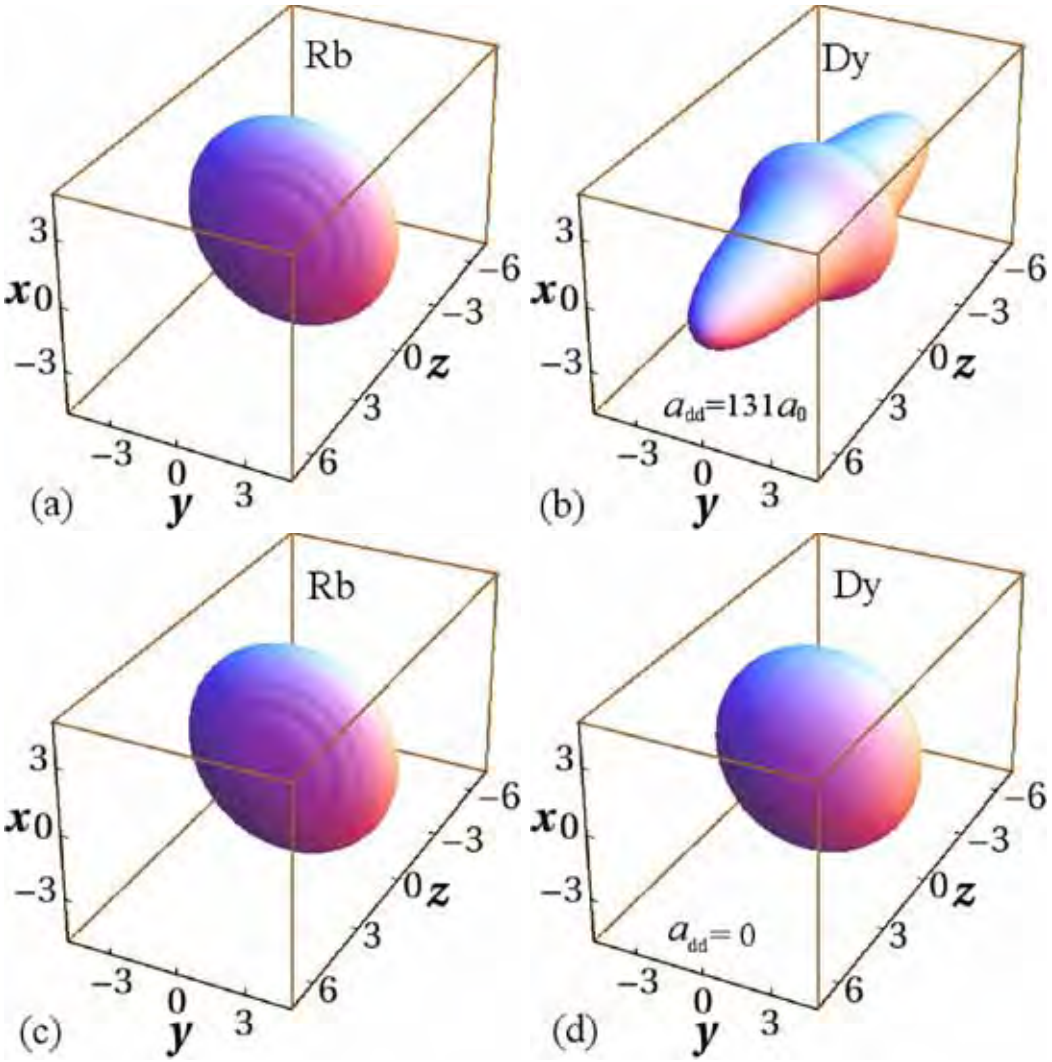

Figure 7.5: Three-dimensional contour plot of densities $|\phi_j(x, y, z)|^2$ for a (a) disk-shaped ^{87}Rb BEC and that of the (b) bound ^{164}Dy droplet with $a_{dd} = 131a_0$. Lower panel the same plot without dipolar interaction (c) disk-shaped ^{87}Rb BEC and that of the (d) bound ^{164}Dy droplet for $a_{dd} = 0$. Without dipolar interaction the special structures showing a change for the condensate aspect disappears. In all cases, the density on the contour is $0.001 l_0^{-3}$, the inter-species scattering length is $a_{12} = -30a_0$, a disk-shaped ($\lambda = 4$) of $N(\text{Rb}) = 10000$ atoms, the bound droplet of $N(\text{Dy}) = 4000$ atoms and length is measured in units of l_0 ($= 1$ μm).

higher number of ^{164}Dy atoms. Here, we emphasize the result of Fig. 7.3 (d) where the dipolar interaction, manifests itself in an elongation of the condensate along the magnetization direction giving in a change for the condensate aspect ratio. These type of profiles, are a consequence of the anisotropic nature in

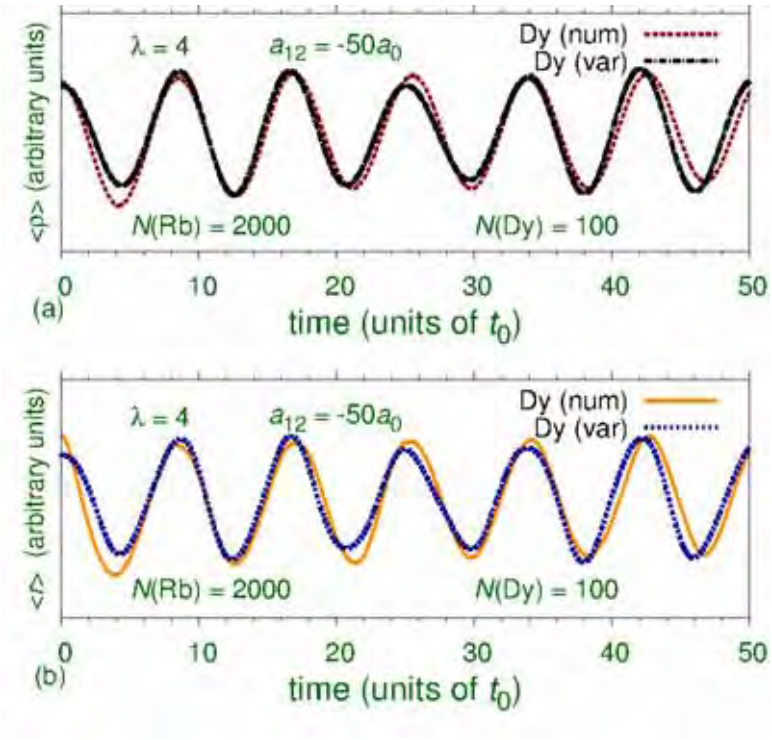

Figure 7.6: The rms sizes (a) $\langle\rho\rangle$ and (b) $\langle r\rangle$ from numerical simulation (num) and variational approximation (var) during breathing oscillation initiated by $a_{12} \to 1.01 \times a_{12}$ versus time in units of t_0 (= 1.38 ms) of a ^{164}Dy droplet of 100 atoms bound in a trapped ^{87}Rb BEC of 2000 atoms for $a_{12} = -50$ and $\lambda = 4$.

dipole-dipole interaction such as in reference [11] where the contact interaction is diminished with respect to the long range interaction. In this point, we study the binary system for the case depicted in Fig. 7.3 (d) without dipolar interaction, this means for $a_{dd} = 0$. In Figs. 7.5 is illustrated the 3D contours of disk-shaped ($\lambda = 4$) ^{87}Rb and the bound droplet of ^{164}Dy BEC profiles for 10000 ^{87}Rb and 4000 ^{164}Dy atoms with $a_{12} = -30a_0$. The Figs. 7.5 (a) and (b) corresponding to parameters of Fig. 7.3 (d). We plot the same case in Figs. 7.5 (c) and (d) without dipolar interaction ($a_{dd} = 0$). The density $|\phi(x, y, z)|^2$ on the surface of these plots is $0.001 l_0^{-3}$. It is important to emphasize that in the case without dipolar interaction the special structures that previously showed, in Fig. 7.5 (b), a change for the condensate aspect disappears and we have just a disk-shape symmetry for the BEC in Fig. 7.5 (d).

7.2.4 Dynamics Results

We investigate the dynamics of a bound ^{164}Dy droplet in a trapped ^{87}Rb BEC. First, to test the present scheme we consider a small ^{164}Dy droplet of 100 atoms

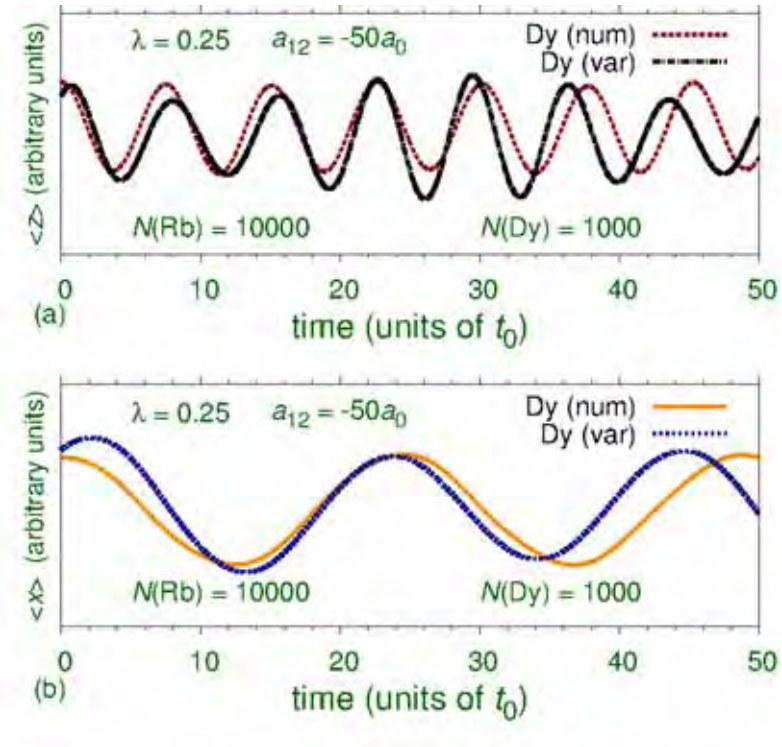

Figure 7.7: The rms sizes (a) $\langle z \rangle$ and (b) $\langle x \rangle$ from numerical simulation (num) and variational approximation (var) during breathing oscillation initiated by the sudden change $a_{12} \to 1.01 \times a_{12}$ versus time in units of t_0 (= 1.38 ms) of a ^{164}Dy droplet of 1000 atoms bound in a trapped ^{87}Rb BEC of 10000 atoms for $a_{12} = -50$ and $\lambda = 0.25$.

bound in a disk-shaped ($\lambda = 4$) ^{87}Rb BEC of 2000 atoms with $a_{12} = -50a_0$. This corresponds to the stable region of Fig. 7.1 (a). In real-time evolution of the system, the scattering length a_{12} is suddenly changed to $1.01 \times a_{12}$ thus starting the breathing oscillation. In Figs. 7.6 we show the resultant oscillation of the rms sizes (a) $\langle \rho \rangle$ and (b) $\langle r \rangle$ during time evolution as obtained from numerical solution of Eqs. (7.7) and (7.8) and variational approximation (7.21) – (7.24). After obtaining a satisfactory results on the dynamics with a small system, we proceed to a larger system of greater experimental interest: a stable ^{164}Dy droplet of 1000 atoms bound in a cigar-shaped ($\lambda = 0.25$) ^{87}Rb BEC of 10000 atoms with $a_{12} = -50a_0$, which corresponds to the stable region of Fig. 7.1 (b). In real-time evolution of the system, the scattering length a_{12} is again suddenly changed to $1.01 \times a_{12}$ thus starting the breathing oscillation. In Figs. 7.7 we show the resultant oscillation of the rms sizes (a) $\langle z \rangle$ and (b) $\langle x \rangle$ during time evolution as obtained from a numerical solution of Eqs. (7.7) and (7.8) and variational approximation (7.21) – (7.24). The agreement between the numerical simulation

and variational approximation in both cases of breathing oscillation illustrated in Figs. 7.6 and 7.7 for disk- and cigar-shapes is quite satisfactory considering:

- During oscillation the bound ^{164}Dy droplet might have a density distribution different from the Gaussian distribution assumed in the variational approximation.
- The large nonlinearity in the ^{87}Rb BEC will also make its density distribution non-Gaussian.

The stable oscillation under small perturbation as shown in Figs. 7.6 and 7.7 confirms the dynamical stability of the ^{164}Dy droplet for both disk and cigar type environments.

7.2.5 Experimental Path

The present quasi-free dipolar droplet is not just of theoretical interest, but can be realized experimentally by initially preparing a binary ^{87}Rb-^{164}Dy mixture where both components are harmonically trapped. The trap on ^{164}Dy can then be ramped to zero exponentially during a few milliseconds. The ^{164}Dy cloud will initially expand and finally form the quasi-free ^{164}Dy droplet. To numerically illustrate the viability of this procedure, we consider an initial ^{87}Rb-^{164}Dy binary mixture with the following parameters: $N(\mathrm{Rb}) = 10000$, $N(\mathrm{Dy}) = 1000$, $a_{12} = -50a_0$. We take the same axial trap with $\lambda = 4$ acting on both components. Then we perform real-time propagation of the binary GP equation with this initial state and ramp down the ^{164}Dy trap by $V_{\mathrm{trap}}(\mathrm{Dy}) \to \exp[-(t-10)]V_{\mathrm{trap}}(\mathrm{Dy})$ for time $t > 10$. The trap on ^{164}Dy is practically zero for times $t \geq 20$. The trapped ^{164}Dy BEC first expands for $t > 10$ and eventually it emerges as the quasi-free ^{164}Dy droplet. The time evolution of the rms sizes of the ^{164}Dy droplet is shown in Fig. 7.8 (a). The widths of the ^{164}Dy droplet first increase and eventually show small oscillations, thus describing a stable ^{164}Dy droplet. To investigate the shape of the ^{164}Dy droplet, we plot in Figs. 7.8 (b) and (c) the one-dimensional (1D) densities $|\varphi(z)|^2 \equiv \int\int dxdy|\phi(x,y,z)|^2$ and $|\varphi(x)|^2 \equiv \int\int dydz|\phi(x,y,z)|^2$ at times $t = 20, 40, 60, 80$, and 100 along with the corresponding numerical densities of the stationary droplet calculated from the solution of Eqs. (7.7) and (7.8).

The 1D numerical densities of the stationary ^{164}Dy droplet are in agreement with the densities obtained from dynamical simulation of the passage of the trapped ^{164}Dy BEC to a quasi-free droplet. In Figs. 7.8 (b) and (c) one can easily identify the small oscillation of the evolving dynamical droplet around its stationary shape.

Finally we should highlight that dipolar interaction among atoms is quite different from normal short-range atomic interaction and manifests itself in different ways in a trapped dipolar BEC. However, in a trapped dipolar BEC, the confining

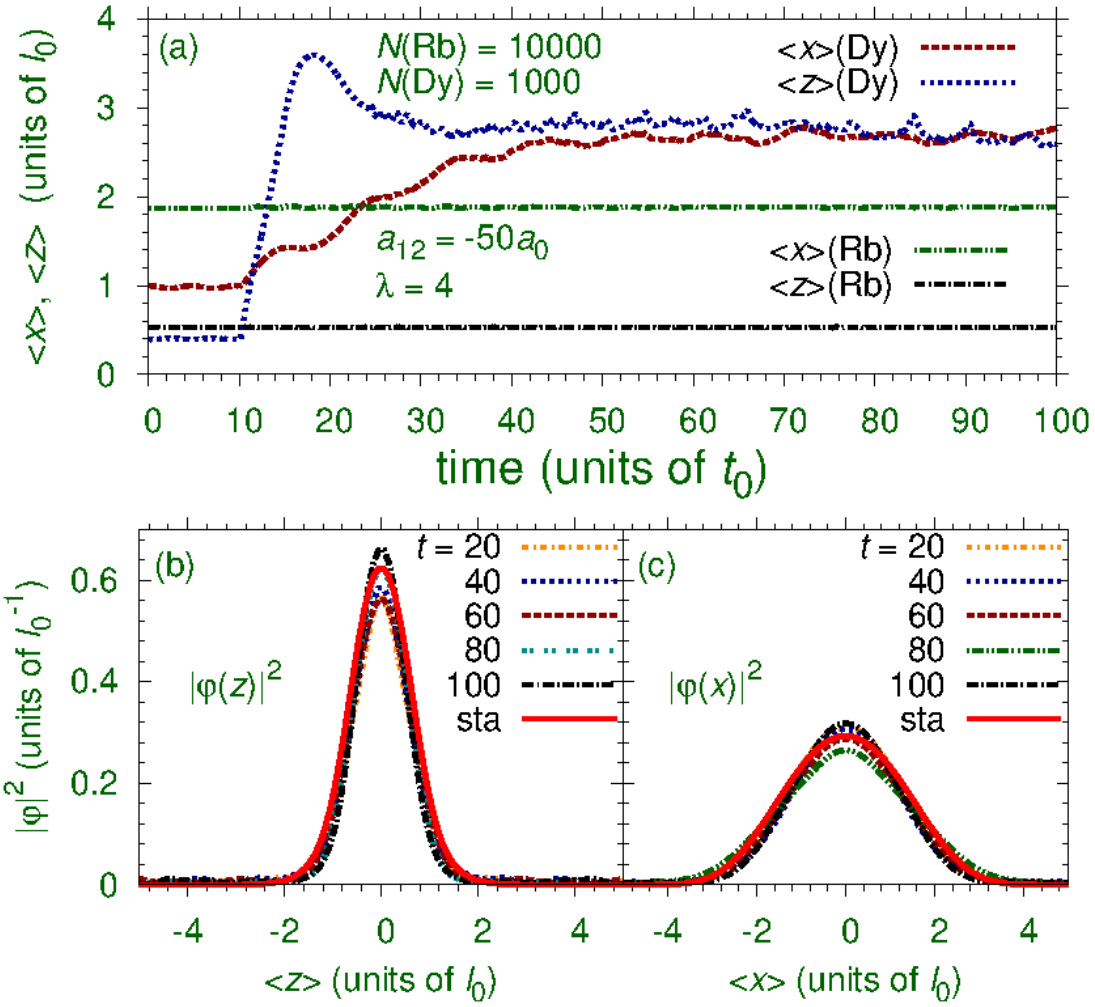

Figure 7.8: (a) The rms sizes $\langle x\rangle$ and $\langle z\rangle$ of the ^{164}Dy and ^{87}Rb BECs versus time during the passage of the trapped ^{164}Dy BEC in the binary ^{87}Rb-^{164}Dy mixture with $N(\mathrm{Rb}) = 10000$, $N(\mathrm{Dy}) = 1000$, $a_{12} = -50a_0$ and $\lambda = 4$ as the confining trap on the ^{164}Dy BEC is relaxed for $t > 10$ exponentially as $V_{\mathrm{trap}} \to \exp[-(t-10)]V_{\mathrm{trap}}$, so that this trap is practically zero for $t > 20$. The linear 1D densities (b) $|\varphi(z)|^2$ and (c) $|\varphi(x)|^2$ at times $t = 20, 40, 60, 80, 100$ (in units of $t_0 = 1.38$ms) during the expansion together with the numerically calculated density of the stationary (sta) ^{164}Dy droplet.

constraints could be too strong and thus make the effect of dipolar interaction difficult to observe. Special experimental set up and theoretical formulation might be necessary to study the effect of dipolar interaction. However, it will be much easier to see the effect of dipolar interaction in the present binary mixture of nondipolar trapped ^{87}Rb and dipolar ^{164}Dy without an specific trap. Our results show that strong dipolar interaction in the axial polarization z direction should elongate the dipolar BEC along this direction thus transforming it to a cigar shape. However, it will be difficult to observe this change in the presence of a harmonic trap along z. The effect of dipolar interaction is clearly seen in the present quasi-free ^{164}Dy droplet of Fig. 7.3 (d) where, due to a strong dipolar interaction, the shape of the ^{164}Dy droplet has changed from the disk shape (the shape of the ^{87}Rb BEC of Fig. 7.3 (a) responsible for its binding) to the cigar shape. The thin disk-shaped ^{87}Rb BEC stays only near the central $z = 0$ plane of the ^{164}Dy droplet. Most of the ^{164}Dy atoms lying outside the ^{87}Rb BEC are bound due to the intra-species dipolar interaction. In the dipolar ^{164}Dy droplet of Fig. 7.3 (d) the dipolar interaction plays a more important role in its binding and shape.

In summary, the present quasi-free dipolar droplet may also find other interesting applications in the BEC phenomenology. Among the interesting features in a trapped dipolar BEC, one can mention its peculiar shape and stability properties [35, 38–41], anisotropic soliton and vortex soliton [26, 42, 43], as well as super-fluid soliton states. It would be of great interest to discover how these features and properties of a trapped dipolar BEC would manifest themselves in a 3D quasi-free dipolar droplet. For example, a quasi-free dipolar droplet could be used in the experimental study of anisotropic sound and shock-wave propagation [93], collapse dynamics [34], formation of vortex dipoles and vortex lattice [44], etc, in a different setting of confinement, which will facilitate the observation of the effect of anisotropic dipolar interaction.

8

Summary and Conclusions

In summary, the present thesis studied the physical features of quantum systems associated with Bose-Einstein condensation (BEC), including mixtures of two components, and dipolar gases. Initially, we presented a introduction of the key concepts for BECs (chapter 1) and, more specifically, a theoretical understanding of mean-field theory, and then we applied these ideas in some cases of great interest to theoretical and experimental physics.

We realize the description of a binary BEC where the components are subject to distinct trap symmetries belonging to two different spatial dimensions (chapter 2). In particular, we considered the possibility that the first component is in 1D (cigar shape) and the second in 2D (disk shape). We found the numerically solutions for this system using a 3D binary Gross-Pitaevskii (GP) equation, in the coupled 1D-2D case where the cigar-shaped component is in the z direction and the disk-shaped component remains in the (x, y) plane. Then we calculated the density profiles and dynamics for small oscillation of this binary 1D-2D BEC, initiated by a sudden change of the radial angular frequency of the disk shape component, for different values of nonlinearities. We consider the 3D profile of the density showing that for attractive interspecies interaction the two components have the highest value of density in the center of system conforming the mixing state and for the case with repulsive interspecies interaction both BECs are moving away from each other in agreement with the demixing state. In this form, we found that there are effects on the unperturbed BEC because of the presence of interspecies coupling, giving us an important background for the study of more complex coupled systems.

After a brief introduction to dipolar BEC (chapter 3) we suggested the possibility of bright solitons in dipolar BECs for *repulsive* short-range interaction when the scatterins length a is positive and for N below a critical number (N_{crit}) of atoms. These solitons with $a > 0$ have never been observed, nevertheless, with modern techniques of now could be produced in the laboratory. We studied the statics (root-mean square (rms) sizes and chemical potential) and dynamics (collision) properties of such solitons (chapter 4). In this case, numerical results in the stability phase plot of the bright solitons are in good agreement with variational calculations. We found that the collision between two solitons is quasi-elastic at high velocities ($\sim$ 1 cm/s) and independent of the initial phase. At a very low ($\sim$ 0) initial velocity, two equal-phase solitons placed side-by-side at rest coalesce to form a stable bound soliton molecule [57] due to dipolar attraction. With current technology, this soliton molecule could be created in the laboratory and our theoretical results verified. This theoretical study of solitons could be extended for Fermi gases or Bose-Fermi mixtures using a recent study where we have demonstrated that bright solitons (self-localized ground states) can be created in the spin-balanced gas of fermions with repulsion between the spin components, merging the spatial growth of the s-wave scattering length (which accounts for the repulsion between the components) in one or two directions, and the external harmonic confining potential, acting in the other directions [18].

On the other hand, we present the mean-field and beyond-mean-field models used to study a dipolar BEC under weak interaction and strong-coupling regime (unitarity) as well as along the BEC-unitarity crossover as the scattering length a is increased (chapter 5). We present a Gaussian variational formulation for its solution at unitarity and also the results of numerical and variational studies of density, rms sizes and chemical potential of a disk-shaped dipolar BEC. In this study we used a dipolar BEC of 15000 ^{164}Dy atoms in a disk-shaped trap of anisotropy $\lambda = 3.6$, as in the experiment of reference [12], and also $\lambda = 10$. We have suggested this scheme for extracting the universal parameter ξ, that relates the energy of the noninteracting and unitary gases, from a study of the density profile of a strongly dipolar disk-shaped BEC under the strong-coupling regime. In this setting, the dipolar atoms are strongly repulsive which should suppress three-body loss by molecule formation. However, an experiment with a nondipolar BEC at unitarity to extract this parameter is seriously undermined because of three-body loss by molecule formation. In chapter 5 we find that the radial densities are sensitive to the universal parameter ξ under the strong-coupling regime and hence a study of density is expected to yield information about this parameter. Away from the strong-coupling regime the results are not be sensitive to ξ. In conclusion, an anisotropy of $\lambda = 10$, or larger, and a BEC with strong dipole interaction is preferred for an experimental study. Furthermore, we can contribute two important points:

- It is crucial that, to study BEC-unitarity crossover, we use the crossover

model Eq. (5.9), as the GP model Eq. (5.6) and LHY correction Eq. (5.8) would lead to divergent unphysical results.

- To extract the parameter ξ it is not necessary to perform the experiment at unitarity. The density profile of the BEC is sensitive to the parameter ξ for atomic short-range interaction lying between the weak-coupling GP and strong-coupling unitarity limits, and so a study under this regime should reveal this parameter.

Furthermore, we used a mean-field description to study the static properties of the binary disk-shaped dipolar BECs ^{168}Er-^{164}Dy and ^{52}Cr-^{164}Dy, in order to search for the effect of inter- and intra-species dipolar interactions, employing realistic values of inter- and intra-species dipolar interactions and intra-species scattering lengths (chapter 6). In this study, the yet unknown inter-species scattering length is considered as a variable parameter. The binary system is found to be stable for a number of atoms below a critical value, and the stability domain for the system is illustrated in convenient phase plots involving the number of atoms of the species and the inter-species scattering length a_{12}.

In the same way, as an important characteristic for this binary sistem with small values of a_{12} a mixed state (with overlapping phase) of the two species emerges and this state transforms into a demixed state (with separated phase) at larger a_{12}. Just below the stability line, in the region of transition from the mixed to a demixed configuration, distinct structures in 3D densities may appear in the form of the Saturn-ring-like shape or red-blood-cell-like biconcave shape. With current experimental techniques these states could be realized in a laboratory.

Finally, we demonstrate the existence of a stable dipolar ^{164}Dy droplet bound by inter-species attraction in a trapped nondipolar BEC of ^{87}Rb atoms, using variational approximation and numerical solution of a set of coupled mean-field GP equations (chapter 7). The domain of stability of the ^{164}Dy droplet is highlighted in stability plots of the number of ^{164}Dy atoms and inter-species scattering length a_{12} for both cigar- and disk-shaped traps acting on the ^{87}Rb BEC. In these phase diagrams we found that a trapped nondipolar BEC, of a fixed number of atoms, can only bind a dipolar droplet containing atoms less than a critical number of atoms, and with an inter-species scattering length between two critical values. The dipolar droplet collapses when inter-species attraction is above the upper limit and escapes to infinity when inter-species attraction is below the lower limit. Results of variational approximation and numerical solution (for the statics and dynamics) of the ^{164}Dy droplet are found to be in satisfactory agreement with each other.

We also demonstrate numerically that such droplets can be obtained experimentally by considering a trapped binary ^{87}Rb-^{164}Dy BEC and then removing the trap on ^{164}Dy. The ^{164}Dy BEC then expands and transforms into a bound

dipolar droplet. Therefore, we suggested that this system is not just of theoretical interest, but can be realized experimentally to see the effect of dipolar interaction. Specifically, in our results due to a strong dipolar interaction the shape of the quasi-free dipolar ^{164}Dy droplet has changed from the disk shape (the shape of the ^{87}Rb BEC responsible for its binding) to the cigar shape. However, in a trapped dipolar BEC, the confining constraints could be too strong and thus make the effect of dipolar interaction difficult to observe.

Consequently, the results of the present thesis and other studies realized during the last three years, which are widely interesting for the theoretical and experimental community, have been extended in **seven (7)** different publications cited in Appendix C.

New works could be realized for these exotic BECs. In particular, we could study an extension of the statics and the dynamics of dipolar BECs by using a variational method and the numerical solution of the time-dependent mean-field nonlinear Gross-Pitaevskii equation. More specifically, we could explore the stability properties of dipolar condensates with respect to s-wave and dipolar interactions for many different trap geometries and any numbers of atoms.

Furthermore, studies of the properties of two interacting BECs could be extended: one or both of them could be dipolar, using coupled mean-field equations to describe these binary mixtures. We could extend this work to understand the dynamics of these systems in fascinating areas such as dipolar BECs on optical lattices, anisotropic sound and supersonic waves in a dipolar BEC, inter alia.

A

Dimensional Reduction of a Binary BEC

It is now well established that, at ultralow temperature, dilute a Bose-Einstein condensate (BEC) can be accurately described by the three-dimensional (3D) Gross-Pitaevskii (GP) equation [2, 16]. Some years ago it has been found that, starting from the 3D GP equation and using a Gaussian variational approach [61], it is possible to derive effective one-dimensional (1D) or two-dimensional (2D) wave equations which describes the dynamics of quasi-1D or quasi-2D BECs as appropriate for cigar or disk shapes [94]. For instance, in that derivation of the effective 1D equation the trapping potential is harmonic and isotropic in the transverse direction and generic in the axial one. The effective 1D equation, which is a time-dependent nonpolynomial Schrödinger equation (NPSE) [94], has been used to model a cigar-shaped condensate by many experimental and theoretical groups.

Starting from a binary 3D GP equation, presented in chapter 2, we derive a binary nonpolynomial Schrödinger equation (BNPSE) in reduced dimensions by using a Lagrangian variational approach. The BNPSE represent a set of coupled nonlinear differential equations with nonpolynomial non-power-law nonlinearities. The BNPSEs depend on the geometry of the system and also on the inter-species interaction. In fact, the main difference with respect to the case of a single BEC is the coupling between the two BECs, which gives rise, quite generally, to a integral term in the reduced wave equations. We use the BNPSE to study numerically the static properties of a 1D-2D binary BEC where the first quasi-1D component lies along the z axis and the quasi-2D component in the (x, y) plane. For small and larger values of nonlinearities the BNLSE yielded results for density in good

agreement with the full 3D result. We used the following binary 3D GP equation

$$i\hbar\partial_t\psi_1 = \Big[-\frac{\hbar^2}{2m_1}\nabla^2_{\mathbf{r}} + U_1(\mathbf{r}) + g_1|\psi_1|^2 + g_{12}|\psi_2|^2\Big]\psi_1 \ , \tag{A.1}$$

$$i\hbar\partial_t\psi_2 = \Big[-\frac{\hbar^2}{2m_2}\nabla^2_{\mathbf{r}} + U_2(\mathbf{r}) + g_2|\psi_2|^2 + g_{12}|\psi_1|^2\Big]\psi_2 \ . \tag{A.2}$$

These two coupled partial differential equations are both in 3+1 (space-time) dimensions. In the general case, these can be solved numerically in a routine fashion, such as in chapter 2. However, in many situations of interest, when one or both of the BEC components have extreme distinct cigar and disk shapes and when we are interested in density and dynamics in axial and radial directions, respectively, the following reduction procedures are of particular use. Let us suppose that the confining potential of the first BEC, with cylindrical symmetry, is

$$U_1(\mathbf{r}) = \frac{1}{2}m_1\omega^2_{1\rho}\rho^2 + V_1(z). \tag{A.3}$$

where $V_1(z)$ is a generic potential in z direction. In this case we impose cylindrical symmetry i.e. $\omega_{1\rho} = \omega_{1x} = \omega_{1y}$ in the harmonic potential acting on the first BEC, is the angular frequencies of the harmonic trap along radial direction, with $\rho^2 = x^2 + y^2$. The radial harmonic potentials are assumed to be so strong that the first BEC is quasi-1D, i.e. in an elongated cigar-shaped configuration. An interesting possibility is a binary system where the cigar-shaped BEC is perpendicular to the plane of the two-dimensional BEC. This kind of configuration can be obtained by considering the following trapping potential, with cylindrical symmetry, acting on the second BEC

$$U_2(\mathbf{r}) = W_2(\rho) + \frac{1}{2}m_2\omega^2_{2z}z^2, \tag{A.4}$$

where $W_2(\rho) = W_2(x, y)$ is a generic potential in (x, y) plane, while the harmonic potential of angular frequency ω_{2z} along the z axis is so strong that the second BEC is a quasi-2D in the (x, y) plane. For the first BEC, we can then use the variational wave function [94]

$$\psi_1(\mathbf{r}, t) = \frac{e^{-\rho^2/(2\sigma^2(z,t))}}{\pi^{1/2}\sigma(z, t)}\ f_1(z, t), \tag{A.5}$$

for the first BEC, where $\sigma \equiv \sigma(z, t)$ is its width, which can be quite different from the characteristic harmonic length $a_\rho = \sqrt{\hbar/(m_1\omega_{1\rho})}$ of the transverse confinement. We assume, consistent with the philosophy of the reduction scheme, that in Eq. (A.5) the z and t derivatives act only on f_1. While for the second BEC we adopt the following variational wave function [94]

$$\psi_2(\mathbf{r}, t) = \frac{e^{-z^2/(2\eta^2(\rho,t))}}{\pi^{1/4}\eta^{1/2}(\rho, t)}h_2(\rho, t), \tag{A.6}$$

where the width $\eta \equiv \eta(\rho, t)$ can be quite different from the characteristic harmonic length along the z direction and the ρ and t derivatives are supposed to act only on h_2. Consequently, the action of the system can now be written as

$$A = \int \hat{L}_1 \; dzdt + 2\pi \int \bar{L}_2 \; \rho d\rho \; dt + \int \bar{\mathcal{L}}_{12} \; d^3\mathbf{r} \; dt \; , \tag{A.7}$$

where

$$\begin{aligned} \hat{L}_1 = & \, i\frac{\hbar}{2}(f_1^* \partial_t f_1 - f_1 \partial_t f_1^*) - \frac{\hbar^2}{2m_1}|\partial_z f_1|^2 - V_1(z)|f_1|^2 \\ & - \left(\frac{\hbar^2}{2m_1\sigma^2} + \frac{m_1\omega_{1\rho}^2\sigma^2}{2} \right) |f_1|^2 - \frac{g_1}{4\pi\sigma^2}|f_1|^4, \end{aligned} \tag{A.8}$$

$$\begin{aligned} \bar{L}_2 &= i\frac{\hbar}{2}(h_2^* \partial_t h_2 - h_2 \partial_t h_2^*) - \frac{\hbar^2}{2m_2}|\nabla_\rho h_2|^2 - W_2(\rho)|h_2|^2 \\ &- \frac{1}{2}\left(\frac{\hbar^2}{2m_2\eta^2} + \frac{m_2\omega_{2z}^2\eta^2}{2} \right) |h_2|^2 - \frac{g_2}{2\eta\sqrt{2\pi}}|h_2|^4, \end{aligned} \tag{A.9}$$

$$\bar{\mathcal{L}}_{12} = -\frac{g_{12}}{\pi^{3/4}\eta\sigma^2} e^{-\rho^2/\sigma^2} e^{-z^2/\eta^2} |f_1|^2 |h_2|^2, \tag{A.10}$$

where we have neglected, in the spirit of the reduction scheme, the spatial derivative of σ and η. We now extremize the action A with respect to f_1^*, h_2^*, σ and η to get the desired equations

$$\begin{aligned} i\hbar\partial_t f_1 = \Big[& -\frac{\hbar^2}{2m_1}\partial_z^2 + V_1(z) + \frac{g_1}{2\pi\sigma^2}|f_1|^2 + \left(\frac{\hbar^2}{2m_1\sigma^2} + \frac{m_1\omega_{1\rho}^2\sigma^2}{2} \right) \\ & + \frac{2g_{12}e^{-z^2/\eta^2}}{\pi^{1/2}\sigma^2\eta} \int_0^\infty e^{-\rho^2/\sigma^2} |h_2(\rho,t)|^2 \rho d\rho \Big] f_1 \; , \end{aligned} \tag{A.11}$$

$$\begin{aligned} i\hbar\partial_t h_2 = & \Big[-\frac{\hbar^2}{2m_2}\nabla_\rho^2 + W_2(\rho) + \frac{1}{2}\left(\frac{\hbar^2}{2m_2\eta^2} + \frac{m_2\omega_{2z}^2\eta^2}{2} \right) \\ & + \frac{g_2}{(2\pi)^{1/2}\eta}|h_2|^2 + g_{12}\frac{e^{-\rho^2/\sigma^2}}{\pi^{3/2}\sigma^2\eta} \int_{-\infty}^\infty e^{-z^2/\eta^2} |f_1(z,t)|^2 dz \Big] h_2 \; , \end{aligned} \tag{A.12}$$

$$\begin{aligned} m_1\omega_{1\rho}^2\sigma^4 &= \frac{\hbar^2}{m_1} + \frac{g_1}{2\pi}|f_1|^2 \\ &+ 4g_{12}\pi^{1/4} \int_0^\infty d\rho\rho \frac{1}{\eta} e^{-\rho^2/\sigma^2} e^{-z^2/\eta^2} |h_2|^2 \left(1 - \frac{\rho^2}{\sigma^2} \right) \; . \end{aligned} \tag{A.13}$$

$$\begin{aligned} m_2\omega_{2z}^2\eta^4 &= \frac{\hbar^2}{m_2} + \frac{g_2\eta}{2\sqrt{2\pi}}|h_2|^2 \\ &+ \frac{g_{12}\eta}{\pi^{3/4}} \int_{-\infty}^\infty dz \frac{1}{\sigma^2} e^{-\rho^2/\sigma^2} e^{-z^2/\eta^2} |f_1|^2 \left(1 - 2\frac{z^2}{\eta^2} \right) \; . \end{aligned} \tag{A.14}$$

Equations (A.11) and (A.12) constitute the BNPSE, where the first one is integro-differential in 1+1 dimensions, the second is integro-differential in 2+1 dimensions (but in 1+1 variables). Equations (A.13) and (A.14) integro-algebraic and determines the widths σ and η as functions of $|f_1|^2$ and $|h_2|^2$. If we set the coupling term $g_{12} = 0$ in Eqs. (A.13) and (A.14), Eqs. (A.11) and (A.12) reduce to previously studied models in reference [94] for a cigar- and disk-shaped BECs, respectively. We shall present results for the coupled 1D-2D case when the cigar-shaped BEC is perpendicular to the disk-shaped BEC. The potentials $V_1(z)$ and $W_2(\rho)$ in Eqs. (A.11) and (A.12) are taken as

$$V_1(z) = \frac{1}{2} m_1 \omega_{1z}^2 z^2; \quad W_2(\rho) = \frac{1}{2} m_2 \omega_{2\rho}^2 \rho^2. \tag{A.15}$$

The cigar-shaped BEC, labeled 1, lies along the z axis and has angular frequencies satisfying $\omega_{1\rho}/\omega_{1z} = 10$. The disk-shaped BEC, labeled 2, lies in the (x, y) plane and has trapping frequencies satisfying $\omega_{2z}/\omega_{2\rho} = 10$. For the cigar-shaped BEC we take $\omega_{1\rho} = 10$ and $\omega_{1z} = 1$; for the disk-shaped BEC we take $\omega_{2z} = 10$, and $\omega_{2\rho} = 1$. For the cigar-shaped BEC 1, the harmonic oscillator lengths are $l_{1z} \equiv \sqrt{\hbar/(m\omega_{1z})} = 1$ and $l_{1\rho} \equiv \sqrt{\hbar/(m\omega_{1\rho})} = 1/\sqrt{10}$. For the disk-shaped BEC 2, the harmonic oscillator lengths are $l_{2z} \equiv \sqrt{\hbar/(m\omega_{2z})} = 1/\sqrt{10}$ and $l_{2\rho} \equiv \sqrt{\hbar/(m\omega_{2\rho})} = 1$. The linear and radial densities are calculated from the solution of Eqs. (A.1) and (A.2) via

$$|f_1(z)|^2 = 2\pi \int_0^\infty \rho d\rho |\psi_1(\mathbf{r})|^2, \tag{A.16}$$

$$|h_2(\rho)|^2 = \int_{-\infty}^\infty dz |\psi_1(\mathbf{r})|^2, \tag{A.17}$$

to be compared with the solutions of Eqs. (A.11) and (A.12). To solve the coupled GP equations in three and reduced dimensions we employ the split-step Crank-Nicolson discretization technique [21–23] with real and imaginary time propagation. We essentially use the Fortran programs provided in reference [21]. The convergence of the numerical result was tested by varying the space (typically ~ 0.05) and time (typically ~ 0.001) steps and the total number of spatial and temporal discretization points. In Figs. A.1 (a) and (b) we plot the linear and radial densities $|f_1(z)|^2$ and $h_2(\rho)|^2$, respectively, obtained from the 3D equations (A.1) and (A.2) as well as the BNPSEs (A.11) and (A.12) for $Ng_1 = 4\pi$ and $Ng_2 = 400\pi$ and for different Ng_{12}.

In this case there is some difference between the results of the binary 3D GP equation and the BNPSE. This difference is consistent with the previous studies [94]. The agreement between the densities obtained from the binary 3D GP equation and the BNPSE continues to be good. The small discrepancy between the results of the binary 3D GP equation and the BNPSE continues as a nonzero g_{12} is introduced. This discrepancy does not increase as g_{12} is increased to moderate

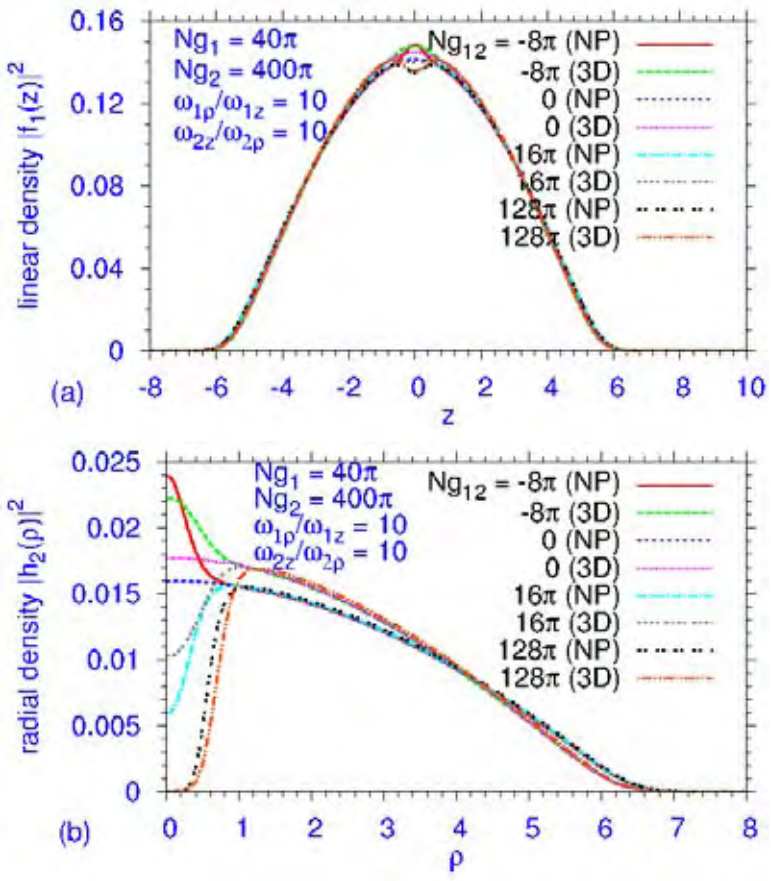

Figure A.1: Plot of (a) linear $|f_1(z;t)|^2 = 2\pi \int_0^\infty \rho \; d\rho |\psi_1(\rho, z; t)|^2$ and (b) radial $|h_2(\rho; t)|^2 = \int_{-\infty}^{\infty} dz |\psi_2(\rho, z; t)|^2$ densities of a binary perpendicular cigar-disk mixture as obtained from the 3D GP equations (A.1-A.2) (3D) and the reduced 1D-2D binary nonpolynomial Schrödinger equation (A.11-A.14) (NP) in dimensionless units for $Ng_1 = 4\pi$, $Ng_2 = 400\pi$, and different Ng_{12}. Both densities are normalized to unity.

values as we see from Fig. A.1. From the results displayed in Fig. A.1 we find that the BNPSE (A.11) and (A.12) provide an excellent account, when compared with the full 3D binary GP equation(A.1) and (A.2), for small nonlinearities and specially good results can be obtained from the BNPSE especially for larger values of nonlinearities.

B

Numerical Method for Dipolar Equation

Many of the static and dynamic properties of an atomic Bose-Einstein condensate (BEC) are usually studied by solving the mean-field Gross-Pitaevskii (GP) equation, which is a nonlinear partial differential equation for short-range atomic interaction. More recently, BEC of atoms with long-range dipolar atomic interaction are used in theoretical and experimental studies. Let us recollect some important expressions about this. To include the dipolar effects we introduce the following additional nonlinearity into the GP equation

$$F_{dd}(\mathbf{r},t) = K \int U_{dd}(\mathbf{r}-\mathbf{r}')|\psi(\mathbf{r}',t)|^2 d\mathbf{r}', \tag{B.1}$$

where $|\psi(\mathbf{r},t)|^2$ is the density of condensate, K is a coupling constant defined such as in Eq. (3.1) and the dipolar interaction U_{dd} is given by

$$U_{dd}(\mathbf{r}-\mathbf{r}') = \frac{1-3\cos^2\theta}{|\mathbf{r}-\mathbf{r}'|^3}, \tag{B.2}$$

such as in Eq. (3.10). Due to this dipolar atomic interaction, the GP equation is a partial integro-differential equation, requiring complex algorithm for its numerical solution. Different approaches to the numerical solution of the dipolar GP equation have been suggested [34, 53, 69, 95]. Yi and You [69] solve the dipolar GP equation for axially-symmetric trap while they perform the angular integral of the dipolar term in the GP equation, thus reducing it to one in axial (z, z') and radial (ρ, ρ') variables involving standard Elliptical integrals. The dipolar term is regularized by a cut-off at small distances and then evaluated numerically. The

dipolar GP equation is then solved by imaginary-time propagation. Gòral and Santos [53] treat the dipolar term by a convolution theorem without approximation, thus transforming it to an inverse Fourier transformation of a product of the Fourier transformation of the dipolar potential and the condensate density. The Fourier and inverse Fourier transformations are then numerically evaluated by standard fast Fourier transformation routines in Cartesian coordinates. The ground state of the system is obtained by employing a standard split-operator technique in imaginary time. Lahaye *et al.* use Fourier transformation in x, y, and z to evaluate the dipolar term and employ imaginary- and real-time propagation after Crank-Nicolson discretization for stationary and nonstationary solution of the dipolar GP equation [34].

The inclusion of the dipolar integral term in the GP equation in coordinate space is not straightforward due to the divergence at short distances. However, this has been tackled by evaluating the dipolar term in the momentum (k) space. The integral can be simplified in Fourier space by means of convolution as

$$\int U_{dd}(\mathbf{r}-\mathbf{r}')|\psi(\mathbf{r}',t)|^2 d\mathbf{r}' = \mathcal{F}^{-1}\{\mathcal{F}[U_{dd}](\mathbf{k})\mathcal{F}[|\psi|^2](\mathbf{k})\}(\mathbf{r}), \tag{B.3}$$

where $\mathcal{F}[\,]$ and $\mathcal{F}^{-1}\{\}$ are the Fourier transform (FT) and inverse FT, respectively. The FT of the dipole potential can be obtained analytically [40, 53]. In spherical-polar variables (r, θ, ϕ), with the polar axis along momentum variable $\mathbf{k}$ (with $\mathbf{k}^2 = k_x^2 + k_y^2 + k_z^2$) and the dipole moment in the $y = 0$ plane making an angle α with $\mathbf{k}$, the FT of the dipole interaction is

$$\begin{aligned} \mathcal{F}[U_{dd}](\mathbf{k}) &= \tilde{U}_{dd}(\mathbf{k}) = \int\int\int \exp(-ikr\cos\theta) \\ &\times \frac{[1-3(\sin\alpha\sin\theta\cos\phi+\cos\alpha\cos\theta)^2]}{r}\sin\theta dr d\theta d\phi. \end{aligned} \tag{B.4}$$

After a change of variable to $x = \cos\theta$ and integrating over ϕ we obtain

$$\tilde{U}_{dd}(\mathbf{k}) = \pi\int_b^\infty \frac{dr}{r}\int_{-1}^1 \exp(-ikrx)(3\cos^2\alpha - 1)(1-3x^2)dx, \tag{B.5}$$

where we introduced a cut-off in r to avoid divergence. After integrating over x we get

$$\tilde{U}_{dd}(\mathbf{k}) = 4\pi(1-3\cos^2\alpha)\int_{kb}^\infty \left[\frac{\sin u}{u^2} + \frac{3\cos u}{u^3} - \frac{3\sin u}{u^4}\right] du, \quad u = kr. \tag{B.6}$$

The integral over u can be performed by parts and has the result $[kb\cos(kb) - \sin(kb)]/(kb)^3$, where the limit $b \to 0$ can be taken leading to the result $-1/3$, so that

$$\tilde{U}_{dd}(\mathbf{k}) = \frac{4\pi}{3}(3\cos^2\alpha - 1) = \frac{4\pi}{3}\left(\frac{3k_z^2}{\mathbf{k}^2} - 1\right), \tag{B.7}$$

In this form, the divergence of the dipolar term at short distances has been handled by treating this term in momentum ($\mathbf{k}$) space. The FT of density $|\psi(\mathbf{r},t)|^2$ is evaluated numerically by means of a standard fast FT (FFT) algorithm.

In this thesis we presented numerical results for both stationary and non-stationary solutions of the full three-dimensional GP equation for a single dipolar BEC as well as for a binary mixture of two types of dipolar or nondipolar BECs. For these solutions we employed the split-step Crank-Nicolson method with real and imaginary time propagations, respectively, for the numerical solution of the GP equation for dynamic and static properties of a dipolar BEC, using split-step Crank-Nicolson scheme for the nondipolar part as in references [21–23]. The results for dipolar integral in Eq. (B.1) involving the FT of density multiplied by FT of dipolar interaction are evaluated by the convolution theorem (B.3). The inverse FT is taken by means of a standard FFT algorithm. The FFT algorithm is carried out in Cartesian coordinates and hence the GP equation is solved in 3D irrespective of the symmetry of the trapping potential. Usually, the programs used in solutions for dipolar BECs have the same structure as in references [21, 23] with added subroutines to calculate the dipolar integrals. A general instruction to use these programs in the nondipolar case can be found in references [21, 23] and we refer the interested reader to this article for the same.

Bibliography

[1] C. J. Pethick and H. Smith. *Bose-Einstein Condensation in Dilute Gases*. University Press, Cambridge, 2002. 11, 12, 13, 14, 40

[2] A. J. Leggett. *Quantum Liquids. Bose Condensation and Cooper Pairing in Condensed-Matter Systems*. Oxford Univ. Press, Oxford, 2006. 11, 14, 101

[3] M. H. Anderson *et. al.* Observation of Bose-Einstein condensation in a dilute atomic vapor. *Science*, **269**:198, 1995. 11

[4] K. B. Davis *et. al.* Bose-Einstein condensation in a gas of sodium atoms. *Phys. Rev. Lett.*, **75**:3969, 1995. 11

[5] C. C. Bradley, C. A. Sackett and R. G. Hulet. Bose-Einstein condensation of lithium: Observation of limited condensate number. *Phys. Rev. Lett.*, **78**: 985, 1997. 12

[6] G. Modugno *et. al.* Bose-Einstein condensation of potassium atoms by sympathetic cooling. *Science*, **294**:1320, 2001. 12

[7] T. Weber *et. al.* Bose-Einstein condensation of cesium. *Science*, **299**:232, 2003. 12

[8] Y. Takasu *et. al.* Spin-singlet Bose-Einstein condensation of two-electron atoms. *Phys. Rev. Lett.*, **91**:040404, 2003. 12

[9] S. Kraft *et. al.* Bose-Einstein condensation of alkaline earth atoms: ^{40}Ca. *Phys. Rev. Lett.*, **103**:130401, 2009. 12

[10] S. Stellmer *et. al.* Bose-Einstein condensation of strontium. *Phys. Rev. Lett.*, **103**:200401, 2009. 12

[11] T. Lahaye *et. al.* Strong dipolar effects in a quantum ferrofluid. *Nature*, **448**: 672, 2007. 12, 27, 28, 30, 32, 36, 50, 92

[12] M. Lu *et. al.* Strongly dipolar Bose-Einstein condensate of dysprosium. *Phys. Rev. Lett.*, **107**:190401, 2011. 12, 27, 42, 50, 54, 56, 66, 80, 83, 98

[13] K. Aikawa *et. al.* Bose-Einstein condensation of Erbium. *Phys. Rev. Lett.*, **108**:210401, 2012. 12, 27, 42, 50, 66, 80

[14] M. H. G. de Miranda *et al.* Controlling the quantum stereodynamics of ultracold bimolecular reactions. *Nature Phys.*, **7**:502, 2011. 12, 27

[15] F. Dalfovo *et. al.* Theory of Bose-Einstein condensation in trapped gases. *Rev. Mod. Phys.*, **71**:463, 1999. 12, 13, 14, 79, 83

[16] L. Pitaevskii and S. Stringari. *Bose-Einstein Condensation*. Clarendon Press: Oxford, 2003. 14, 101

[17] D. M. Stamper-Kurn and J. H. Thywissen. *Contemporary Concepts of Condensed Matter Science; Bose gas. Chapter 1: Experimental Methods of Ultracold Atomic Physics*. Elsevier B.V., 2012. 14

[18] L. E. Young-S., L. Salasnich and B. A. Malomed. Self-trapping of Fermi and Bose gases under spatially modulated repulsive nonlinearity and transverse confinement. *Phys. Rev. A*, **87**:043603, 2013. 15, 35, 98

[19] G. Lamporesi *et. al.* Scattering in mixed dimensions with ultracold gases. *Phys. Rev. Lett.*, **104**:153202, 2010. 15, 16, 19

[20] A. L. Fetter and C. J. Foot. *Contemporary Concepts of Condensed Matter Science; Bose gas. Chapter 2: Theory and Experiment*. Elsevier B.V., 2012. 15, 27

[21] P. Muruganandam and S. K. Adhikari. Fortran programs for the time-dependent Gross-Pitaevskii equation in a fully anisotropic trap. *Comput. Phys. Commun.*, **180**:1888, 2009. 16, 21, 22, 32, 40, 54, 83, 104, 109

[22] A. Gammal, T. Frederico and L. Tomio. Improved numerical approach for time-independent Gross-Pitaevskii nonlinear Schröedinger equation. *Phys. Rev. E*, **60**:2421, 1999.

[23] D. Vudragović *et. al.* C programs for solving the time-dependent Gross-Pitaevskii equation in a fully anisotropic trap. *Comput. Phys. Commun.*, **183**:2021, 2012. 16, 21, 22, 32, 104, 109

[24] V. M. Pérez-García *et. al.* Dynamics of Bose-Einstein condensates: Variational solutions of the Gross-Pitaevskii equations. *Phys. Rev. A*, **56**:1424, 1997. 16, 53, 85, 86

[25] L. E. Young-S., L. Salasnich and S. K. Adhikari. Dimensional reduction of a binary Bose-Einstein condensate in mixed dimensions. *Phys. Rev. A*, **82**: 053601, 2010. 17, 26

[26] L. E. Young-S., P. Muruganandam and S. K. Adhikari. Dynamics of quasi-one-dimensional bright and vortex solitons of a dipolar Bose-Einstein condensate with repulsive atomic interaction. *J. Phys. B*, **44**:101001, 2011. 27, 50, 53, 96

[27] L. E. Young-S., S. K. Adhikari and P. Muruganandam. Dipolar Bose-Einstein condensates with large scattering length. *Phys. Rev. A*, **85**:033619, 2012. 52

[28] L. E. Young-S. and S. K. Adhikari. Mixing, demixing, and structure formation in a binary dipolar Bose-Einstein condensate. *Phys. Rev. A*, **86**:063611, 2012. 33, 79, 81

[29] L. E. Young-S. and S. K. Adhikari. Dipolar droplet bound in a trapped Bose-Einstein condensate. *Phys. Rev. A*, **87**:013618, 2013. 17, 33

[30] E. Timmermans. Phase separation of Bose-Einstein condensates. *Phys. Rev. Lett.*, **81**:5718, 1998. 19

[31] P. Kuopanportti *et. al.* Exotic vortex lattices in two-species Bose-Einstein condensates. *Phys. Rev. A*, **85**:043613, 2012. 19

[32] D. Frantzeskakis G. Kevrekidis and R. Carretero-González. *Emergent Nonlinear Phenomena in Bose-Einstein Condensates*. Springer, Berlin, 2008. 20, 35

[33] T. Koch *et. al.* Stabilization of a purely dipolar quantum gas against collapse. *Nature*, **4**:218, 2008. 27, 30, 36, 50, 51, 66, 83

[34] T. Lahaye *et. al.* d-wave collapse and explosion of a dipolar Bose-Einstein condensate. *Phys. Rev. Lett.*, **101**:080401, 2008. 30, 36, 50, 96, 107, 108

[35] S. Ronen, D. C. E. Bortolotti and J. L. Bohn. Radial and angular rotons in trapped dipolar gases. *Phys. Rev. Lett.*, **98**:030406, 2007. 28, 62, 67, 68, 70, 72, 74, 79, 96

[36] R. M. Wilson *et. al.* Manifestations of the roton mode in dipolar Bose-Einstein condensates. *Phys. Rev. Lett.*, **100**:245302, 2008. 62

[37] H. Saito, Y. Kawaguchi and M. Ueda. Ferrofluidity in a two-component dipolar Bose-Einstein condensate. *Phys. Rev. Lett.*, **102**:230403, 2009. 27, 79

[38] N. G. Parker *et. al.* Structure formation during the collapse of a dipolar atomic Bose-Einstein condensate. *Phys. Rev. A*, **79**:013617, 2009. 27, 79, 96

[39] R. M. Wilson , S. Ronen and J. L. Bohn. Angular collapse of dipolar Bose-Einstein condensates. *Phys. Rev. A*, **80**:023614, 2009.

[40] L. Santos *et. al.* Bose-Einstein condensation in trapped dipolar gases. *Phys. Rev. Lett.*, **85**:1791, 2000. 50, 108

[41] A. Junginger *et. al.* Symmetry-breaking thermally induced collapse of dipolar Bose-Einstein condensates. *Phys. Rev. A*, **86**:023632, 2012. 27, 79, 96

[42] S. K. Adhikari and P. Muruganandam. Two-dimensional dipolar Bose-Einstein condensate bright and vortex solitons on a one dimensional optical lattice. *J. Phys. B*, **45**:045301, 2012. 27, 96

[43] P. Köberle *et. al.* Creating two-dimensional bright solitons in dipolar Bose-Einstein condensates. *Phys. Rev. A*, **85**:023630, 2012. 27, 96

[44] R. K. Kumar and P. Muruganandam. Vortex dynamics of rotating dipolar Bose-Einstein condensate. *J. Phys. B*, **45**:215301, 2012. 27, 96

[45] S. K. Adhikari and L. Salasnich. Nonlinear Schrödinger equation for a superfluid Bose gas from weak coupling to unitarity: Study of vortices. *Phys. Rev. A*, **77**:033618, 2008. 27, 33, 49, 50, 52, 59

[46] T. Lahaye *et. al.* The physics of dipolar bosonic quantum gases. *Rep. Prog. Phys.*, **72**:126401, 2009. 27, 30, 31, 32, 40, 63, 80, 83

[47] A. Griesmaier *et. al.* Comparing contact and dipolar interactions in a Bose-Einstein condensate. *Phys. Rev. Lett.*, **97**:250402, 2006. 30, 32, 36

[48] A. Gammal , T. Frederico and L. Tomio. Critical number of atoms for attractive Bose-Einstein condensates with cylindrically symmetrical traps. *Phys. Rev. A*, **64**:055602, 2001. 32

[49] Y.-L. Lee and Y.-W. Lee. The universality and stability for a dilute Bose gas with a Feshbach resonance. *Phys. Rev. A*, **81**:063613, 2010. 55

[50] V. S. Shchesnovich and V. V. Konotop. Nonlinear tunneling of Bose-Einstein condensates in an optical lattice : Signatures of quantum collapse and revival. *Phys. Rev. A*, **75**:063628, 2007.

[51] F. Kh. Abdullaev *et. al.* Controlling collapse in Bose-Einstein condensates by temporal modulation of the scattering length,. *Phys. Rev. A*, **67**:013605, 2003.

[52] F. Kh. Abdullaev *et. al.* Stability of trapped Bose-Einstein condensates. *Phys. Rev. A*, **63**:043604, 2001. 32

[53] K. Góral and L. Santos. Ground state and elementary excitations of single and binary Bose-Einstein condensates of trapped dipolar gases. *Phys. Rev. A*, **66**:023613, 2002. 32, 64, 65, 83, 85, 107, 108

[54] J. Stuhler *et. al.* Observation of dipole-dipole interaction in a degenerate quantum gas. *Phys. Rev. Lett.*, **95**:150406, 2005. 32, 73, 74

[55] S. K. Adhikari and L. Salasnich. Superfluid Bose Fermi mixture from weak coupling to unitarity. *Phys. Rev. A*, **78**:043616, 2008. 33, 50, 52

[56] D. Bazeia *et. al.* Solitons with cubic and quintic nonlinearities modulated in space and time. *Phys. Rev. E*, **79**:025602, 2009. 35

[57] U. Al Khawaja *et. al.* Bright soliton trains of trapped Bose-Einstein condensates. *Phys. Rev. Lett.*, **89**:200404, 2002. 36, 45, 47, 98

[58] A. M. Kamchatnov *et. al.* Formation of soliton trains in Bose-Einstein condensates as a nonlinear Fresnel diffraction of matter waves. *Phys. Lett. A*, **319**:406, 2003.

[59] V. S. Shchesnovich *et. al.* Solitons in tunnel-coupled repulsive and attractive condensates. *Phys. Rev. A*, **69**:033609, 2004.

[60] D. Bazeia *et. al.* Solitons of two-component Bose-Einstein condensates modulated in space and time. *Phys. Lett. A*, **374**:2356, 2010.

[61] V. M. Pérez-García *et. al.* Bose-Einstein solitons in highly asymmetric traps. *Phys. Rev. A*, **57**:3837, 1998. 36, 101

[62] D. Bazeia *et. al.* Modulation of breathers in cigar-shaped Bose-Einstein condensates. *Phys. Lett. A*, **374**:2640, 2010. 35

[63] K. E. Strecker *et. al.* Formation and propagation of matter-wave soliton trains. *Nature*, **417**:150, 2002. 35

[64] S. L. Cornish *et. al.* Formation of bright matter-wave solitons during the collapse of attractive Bose-Einstein condensates. *Phys. Rev. Lett.*, **96**:170401, 2006. 35, 36

[65] S. Inouye *et. al.* Observation of Feshbach resonances in a Bose-Einstein condensate. *Nature*, **392**:151, 1998. 35, 50, 83

[66] S. Giovanazzi *et. al.* Tuning the dipolar interaction in quantum gases. *Phys. Rev. Lett.*, **89**:130401, 2002. 35

[67] S. Sinha and L. Santos. Cold dipolar gases in quasi-one-dimensional geometries. *Phys. Rev. Lett.*, **99**:140406, 2007. 36

[68] J. Cuevas *et. al.* Solitons in quasi one-dimensional Bose-Einstein condensates with competing dipolar and local interactions. *Phys. Rev. A*, **79**:053608, 2009. 36

[69] S. Yi and L. You. Trapped condensates of atoms with dipole interactions. *Phys. Rev. A*, **63**:053607, 2001. 36, 62, 85, 107

[70] S. Yi and L. You. Calibrating dipolar interaction in an atomic condensate. *Phys. Rev. Lett.*, **92**:193201, 2004. 37

[71] M. Lu, S. H. Youn and B. L. Lev. Trapping ultracold dysprosium: A highly magnetic gas for dipolar physics. *Phys. Rev. Lett.*, **104**:063001, 2010. 42, 50, 80

[72] L. Salasnich, B. A. Malomed and F. Toigo. Matter-wave vortices in cigar-shaped and toroidal waveguides. *Phys. Rev. A*, **76**:063614, 2007. 43

[73] F. Dalfovo and S. Stringari. Bosons in anisotropic traps: Ground state and vortices. *Phys. Rev. A*, **53**:2477, 1996. 43

[74] S. Giorgini, L. P. Pitaevskii and S. Stringari. Theory of ultracold atomic Fermi gases. *Rev. Mod. Phys.*, **80**:1215, 2008. 49, 50, 58, 59

[75] J. M. Diederix *et. al.* Ground state of a resonantly interacting Bose gas. *Phys. Rev. A*, **84**:033618, 2011. 49, 51, 55

[76] G. E. Astrakharchik *et. al.* Equation of state of a Fermi gas in the BCS-BEC crossover: A quantum Monte Carlo study. *Phys. Rev. Lett.*, **93**:200404, 2004. 49, 55, 56

[77] J. Carlson and S. Reddy. Asymmetric two-component fermion systems in strong coupling. *Phys. Rev. Lett.*, **95**:060401, 2005. 49, 55, 56

[78] J. T. Stewart *et. al.* Potential energy of a ^{40}K Fermi gas in the BCS-BEC crossover. *Phys. Rev. Lett.*, **97**:220406, 2006. 55

[79] N. Navon *et. al.* Dynamics and thermodynamics of the low-temperature strongly interacting Bose gas. *Phys. Rev. Lett.*, **107**:135301, 2011. 49, 50, 55, 59

[80] M. Bartenstein *et. al.* Crossover from a molecular Bose-Einstein condensate to a degenerate Fermi gas. *Phys. Rev. Lett.*, **92**:120401, 2004. 49, 55

[81] S. E. Pollack *et. al.* Extreme tunability of interactions in a ^{7}Li Bose-Einstein condensate. *Phys. Rev. Lett.*, **102**:090402, 2009. 50

[82] C. Ticknor, R. M. Wilson and J. L. Bohn. Anisotropic superfluidity in a dipolar Bose gas. *Phys. Rev. Lett.*, **106**:065301, 2011. 50

[83] T. D. Lee, K. Huang and C. N. Yang. Eigenvalues and eigenfunctions of a Bose system of hard spheres and its low-temperature properties. *Phys. Rev. A*, **106**:1135, 1957. 50, 52, 59

[84] A. Fabrocini and A. Polls. Bose-Einstein condensates in the large gas parameter regime. *Phys. Rev. A*, **64**:063610, 2001. 52, 59

[85] S. K. Adhikari. BCS-BEC crossover in a trapped Fermi superfluid using a density functional equation. *J. Phys. B*, **43**:085304, 2010. 52, 55, 56

[86] A. Perali, P. Pieri and G. C. Strinati. Quantitative comparison between theoretical predictions and experimental results for the BCS-BEC crossover. *Phys. Rev. Lett.*, **93**:100404, 2004. 55

[87] N. Navon *et. al.* The equation of state of a low temperature Fermi gas with tunable interactions. *Science*, **328**:729, 2010. 55, 56

[88] L. Luo and J. E. Thomas. Thermodynamic measurements in a strongly interacting Fermi gas. *Journal of Low Temperature Physics*, **154**:1, 2009. 55, 56

[89] M. A.-uz-Zaman and D. Blume. Modification of roton instability due to the presence of a second dipolar Bose-Einstein condensates. *Phys. Rev. A*, **83**: 033616, 2011. 62

[90] K. Góral *et. al.* Bose-Einstein condensation with magnetic dipole dipole forces. *Phys. Rev. A*, **61**:051601, 2000. 66, 80

[91] S. K. Adhikari. Dipolar Bose-Einstein condensate in a ring or in a shell. *Phys. Rev. A*, **85**:053631, 2012. 72

[92] R. M. Wilson *et. al.* Roton immiscibility in a two-component dipolar Bose gas. *Phys. Rev. A*, **86**:033606, 2012. 79

[93] P. Muruganandam and S. K. Adhikari. Anisotropic sound and shock waves in dipolar Bose-Einstein condensate. *Phys. Lett. A*, **376**:480, 2012. 96

[94] L. Salasnich *et. al.* Effective wave equations for the dynamics of cigar-shaped and disk-shaped Bose condensates. *Phys. Rev. A*, **65**:043614, 2002. 101, 102, 104

[95] W. Bao, Y. Cai and H. Wanga. Efficient numerical methods for computing ground states and dynamics of dipolar Bose-Einstein condensates. *J. Comput. Phys.*, **229**:7874, 2010. 107

C

List of Publications

1. Luis E. Young-S., L. Salasnich and S. K. Adhikari. Dimensional reduction of a binary Bose-Einstein condensate in mixed dimensions. *Phys. Rev. A*, **82**:053601, 2010.

2. Luis E. Young-S., P. Muruganandam and S. K. Adhikari. Dynamics of quasi-one-dimensional bright and vortex solitons of a dipolar Bose-Einstein condensate with repulsive atomic interaction. *J. Phys. B*, **44**:101001, 2011.

3. Luis E. Young-S., S. K. Adhikari and P. Muruganandam. Dipolar Bose-Einstein condensates with large scattering length. *Phys. Rev. A*, **85**:033619, 2012.

4. Luis E. Young-S. and S. K. Adhikari. Mixing, demixing, and structure formation in a binary dipolar Bose-Einstein condensate. *Phys. Rev. A*, **86**:063611, 2012.

5. Luis E. Young-S. and S. K. Adhikari. Dipolar droplet bound in a trapped Bose-Einstein condensate. *Phys. Rev. A*, **87**:013618, 2013.

6. Luis E. Young-S., L. Salasnich and Boris A. Malomed. Self-trapping of Fermi and Bose gases under spatially modulated repulsive nonlinearity and transverse confinement. *Physical Review A*, **87**:043603, 2013.

7. R. Kishor Kumar, Luis E. Young-S., Dušan Vudragović, Antun Balaž, P. Muruganandam and S. K. Adhikari. Fortran and C programs for the time-dependent dipolar Gross-Pitaevskii equation in an anisotropic trap. In preparation for publication in *Comput. Phys. Commun.*, 2013.

PHYSICAL REVIEW A **82**, 053601 (2010)

Dimensional reduction of a binary Bose-Einstein condensate in mixed dimensions

Luis E. Young-S.,[1,*] L. Salasnich,[2,3,†] and S. K. Adhikari[1,‡]

[1]*Instituto de Física Teórica, UNESP–Universidade Estadual Paulista, 01.140-070 São Paulo, São Paulo, Brazil*

[2]*INO-CNR, Research Unit at the Dipartimento di Fisica "Galileo Galilei", Università di Padova, Via Marzolo 8, I-35131 Padova, Italy*

[3]*CAMTP, University of Maribor, Krekova 2, SLO-2000 Maribor, Slovenia*

(Received 30 August 2010; published 1 November 2010)

We present effective reduced equations for the study of a binary Bose-Einstein condensate (BEC), where the confining potentials of the two BEC components have distinct asymmetry so that the components belong to different space dimensions as in a recent experiment [G. Lamporesi *et al.*, Phys. Rev. Lett. **104**, 153202 (2010).]. Starting from a binary three-dimensional (3D) Gross-Pitaevskii equation (GPE) and using a Lagrangian variational approach we derive a binary effective nonlinear Schrödinger equation with components in different reduced dimensions, for example, the first component in one dimension and the second in two dimensions as appropriate to represent a cigar-shaped BEC coupled to a disk-shaped BEC. We demonstrate that the effective reduced binary equation, which depends on the geometry of the system, is quite reliable when compared with the binary 3D GPE and can be efficiently used to perform numerical simulation and analytical calculation for the investigation of static and dynamic properties of a binary BEC in mixed dimensions.

DOI: 10.1103/PhysRevA.82.053601 PACS number(s): 03.75.Mn, 03.75.Hh, 03.75.Kk

I. INTRODUCTION

It is now well established that, at ultralow temperature, dilute Bose-Einstein condensates (BECs) can be accurately described by the three-dimensional (3D) Gross-Pitaevskii equation (GPE) [1,2]. Some years ago it was found that, starting from the 3D GPE and using a Gaussian variational approach [3,4], it is possible to derive effective one-dimensional (1D) or two-dimensional (2D) wave equations which describe the dynamics of quasi-1D or quasi-2D BECs as appropriate for cigar or disk shapes [5]. For instance, in that derivation of the effective 1D equation the trapping potential is harmonic and isotropic in the transverse direction and generic in the axial one. The effective 1D equation, which is a time-dependent nonpolynomial Schrödinger equation (NPSE) [5], has been used to model a cigar-shaped condensate by many experimental and theoretical groups [6–10]. A similar reduction scheme also exists for a disk-shaped BEC leading to a 2D NPSE. (The lowest-order approximation of the NPSE leads to a GP-type nonlinear Schrödinger equation (NLSE) equation with cubic nonlinearity. Different variants of this reduction scheme have been suggested, which offer certain advantages in some cases [7,8].) Moreover, by using the 1D NPSE, analytical and numerical solutions have been found for solitons and vortices [11]. Recently, a discrete version of the 1D NPSE (1D DNPSE) has been obtained [12]. The 1D DNPSE has been used to model a BEC confined in a combination of a cigar-shaped trap and a deep optical lattice acting in the axial direction [12]. More recently the 2D NPSE, obtained for a disk-shaped BEC subject to strong confinement along the axial direction, has been used to predict the density profiles and dynamical stability of repulsive and attractive BECs with zero and finite topological charge in various planar trapping configurations, including the axisymmetric harmonic confinement and 1D periodic potential [13]. The reduction scheme has also successfully been applied [8,14] to the study of a density-functional formulation [15] for a Fermi superfluid at unitarity as well as to the study of Anderson localization in a BEC [16].

In a very recent experiment Lamporesi *et al.* [17] investigated the mixed-dimensional scattering occurring when the collisional atoms of two species of a binary BEC live in different space dimensions. This achievement opens the way to the experimental and theoretical studies of a binary BEC with the components belonging to mixed dimensions. In the present article we consider the dimensional reduction of a binary 3D GPE appropriate for the study of a binary BEC in mixed dimensions. Starting from a binary 3D GPE we derive a binary nonpolynomial Schrödinger equation (BNPSE) in reduced dimensions by using a Lagrangian variational approach. (The BNPSEs represent a set of coupled nonlinear differential equations with nonpolynomial non-power-law nonlinearities.) We also present a simplified version of the reduction scheme first, where the reduced equations in the form of a binary NLSE (BNLSE) have simpler power-law nonlinearities. The BNPSEs depend on the geometry of the system and also on the interspecies interaction. In fact, the main difference with respect to the case of a single BEC is the coupling between the two BECs, which gives rise, quite generally, to n integral term in the reduced wave equations. (In the past, a binary 1D NPSE has been derived and used [18] to study a binary cigar-shaped BEC, rather than a binary BEC in mixed dimensions as considered here.)

We use the BNLSE and BNPSE to study numerically the static and dynamic properties of a 1D-2D binary BEC where the first quasi-1D component lies along the z axis and the quasi-2D component lies in the (x, y) plane. For small nonlinearities both the BNLSE and BNPSE yielded results for density in good agreement with the full 3D result. At larger values of nonlinearities the BNPSE provided better approximation to the full 3D result. We also studied small oscillations of the 1D-2D binary BEC initiated by a sudden change of the

*lyoung@ift.unesp.br.
†luca.salasnich@cnr.it.
‡adhikari44@yahoo.com; [http://www.ift.unesp.br/users/adhikari/].

IOP PUBLISHING
IOP FTC
JOURNAL OF PHYSICS B: ATOMIC, MOLECULAR AND OPTICAL PHYSICS
J. Phys. B: At. Mol. Opt. Phys. **44** (2011) 101001 (6pp)
doi:10.1088/0953-4075/44/10/101001

FAST TRACK COMMUNICATION

Dynamics of quasi-one-dimensional bright and vortex solitons of a dipolar Bose–Einstein condensate with repulsive atomic interaction

Luis E Young-S[1], P Muruganandam[1,2] and S K Adhikari[1,3]

[1] Instituto de Física Teórica, UNESP—Universidade Estadual Paulista, 01.140-070 São Paulo, São Paulo, Brazil
[2] School of Physics, Bharathidasan University, Palkalaiperur Campus, Tiruchirapalli 620024, Tamilnadu, India

E-mail: anand@cnld.bdu.ac.in and adhikari@ift.unesp.br

Received 25 February 2011, in final form 3 April 2011
Published 27 April 2011
Online at stacks.iop.org/JPhysB/44/101001

Abstract
By numerical and variational analysis of the three-dimensional Gross–Pitaevskii equation, we study the formation and dynamics of bright and vortex-bright solitons in a cigar-shaped dipolar Bose–Einstein condensate for large *repulsive* atomic interactions. A phase diagram showing the region of stability of the solitons is obtained. We also study the dynamics of breathing oscillation of the solitons as well as the collision dynamics of two solitons. At large velocities the frontal collision is elastic and the two three-dimensional solitons pass through each other undeformed. Two solitons placed side by side at rest coalesce to form a stable bound soliton molecule due to dipolar attraction. Movie clips illustrating collision and molecule-formation dynamics of two bright and vortex-bright solitons are included.

S Online supplementary data available from stacks.iop.org/JPhysB/44/101001/mmedia

(Some figures in this article are in colour only in the electronic version)

A bright soliton is a self-reinforcing solitary wave that maintains its shape, while travelling at constant speed, due to a cancellation of nonlinear attraction and dispersive effects. Experimentally, bright matter-wave solitons and soliton trains were created in a Bose–Einstein condensate (BEC) of ^{7}Li [1, 2] and ^{85}Rb atoms [3] by turning the atomic interaction attractive from repulsive using a Feshbach resonance (FR) [4] and releasing the BEC in an axially free or an expulsive trap.

Lately, a BEC of ^{52}Cr atoms with a large long-range dipolar interaction has been made [5, 6]. This allows us to study the dipolar BEC (DBEC) with variable short-range interaction [5, 6] using a FR [4]. The DBEC has many distinct features [5, 7–9]. The stability of a DBEC depends not only on the scattering length, but also on the trap geometry [5, 7, 9]. A disc-shaped trap gives a repulsive dipolar interaction and the DBEC is more stable. In contrast, a cigar-shaped trap yields an attractive dipolar interaction and hence may favour a collapse [5, 9, 10]. Collapse instability of solitons in the nonpolynomial Schrödinger equation with dipole–dipole interactions was studied by Gligorić *et al* [11]. The controllable short-range interaction with the exotic dipolar interaction makes the DBEC an interesting system for soliton generation in the cigar configuration due to added *dipolar attraction* and a challenging system for theoretical investigation [12] to study the interplay between the dipolar and short-range interactions.

We suggest cigar-shaped bright and vortex solitons [13] for *repulsive* short-range interaction in a DBEC free to

[3] URL: http://www.ift.unesp.br/users/adhikari/

Journal of PhysCcs B: AtomCc, Molecular and OptCcal PhysCcs

SolCtons Cn dCpolar Bose-ECnsteCn condensates

Researchers from the InstCtute of TheoretCcal PhysCcs of São Paulo State UnCversCty Cn BrazCl have studCed the formatCo dynamCcs of brCght, vortex, and gap solCtons Cn dCpolar Bose-ECnsteCn condensates (BEC) through benchmark calculatCon three dCmensCons.

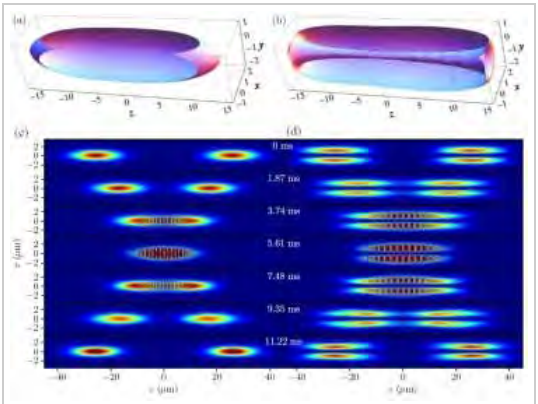

SolCton-BEC.

A bright soliton in an attractive BEC maintains its shape, while traveling at a constant speed. Vortex solitons of BECs are bright solitons of quantized angular momentum. In a repulsive BEC, on a periodic optical-lattice (OL), localized gap solitons in the band gap can also be made. An OL simulates the periodic electron-atom potential in a solid, and the study of gap solitons is also of interest in condensed-matter physics.

In a quasi-one-dimensional setting, realized by a strong confining trap in the radial direction, dynamics of axially free solitons of alkali metal atoms were studied in the laboratory. In the same setting, dynamically stable gap solitons were observed with a periodic OL in the axial direction.

Unlike alkali metal atoms, many bosonic atoms and molecules have large dipole moments and a chromium BEC, with a larger long-range anisotropic dipolar interaction, has been observed. The short-range atomic interaction can be modified in the laboratory by varying a background magnetic field near a Feshbach resonance. Thus the controllable isotropic short-range interaction together with the anisotropic dipolar interaction makes the dipolar BEC an attractive system for experimental soliton generation and a challenging one for theoretical investigation.

The research group have now demonstrated that bright and vortex solitons in a dipolar BEC can be formed, in a quasi-one-dimensional setting, even for a repulsive atomic interaction below a critical value (published in h011 *J. Phys. B: At. Mot. Opt. Phys.* **44 101001**). Additionally, gap solitons were predicted, in a three-dimensional setting with three OLs in orthogonal directions and with weak *attractive* atomic interaction (published in h011 *J. Phys. B: At. Mot. Opt. Phys.* **44 121001**). They performed a mean-field calculation in three dimensions to study the statics and dynamics of the solitons. Further, they showed that the solitons can undergo a head-on collision and come out undeformed at moderate velocities. While at very low velocities the two solitons of same phase never come out after interaction and form a soliton molecule. Gap solitons in dipolar BEC can be dragged with an OL without deformation. All solitons are found to be dynamically stable and can be observed in the laboratory.

Illustrative movies of the fascinating dynamics of bright, vortex, and gap solitons are available: **BrCght and vortex solCton collCsCon and molecule formatCon** and **DraggCng of the gap solCton**

More detaCls of the authors' work are published as a fast track communications in *Journat of Physics B: Atomic, Motecutar and Opticat Physics*.

About the author

L. E. Young-S

P. Muruganandam

S. K. AdhCkarC

LuCs Ever Young-S is a graduate student working in BEC at Institute of Theoretical Physics (IFT), São Paulo State University (UNESP). **Paulsamy Muruganandam**, an assistant professor at the School of Physics, Bharathidashan University, Tiruchirappalli, India, is visiting IFT. **Sadhan K. AdhCkarC**, Guggenheim Fellow, is a professor at IFT. This group is actively investigating the properties of Bose and Fermi superfluids. The research was supported by the CNPq and FAPESP (Brazil) and DST and CSIR (India).

PHYSICAL REVIEW A **85**, 033619 (2012)

Dipolar Bose-Einstein condensates with large scattering length

Luis E. Young-S,[1,*] S. K. Adhikari,[1,†] and P. Muruganandam[1,2,‡]

[1]*Instituto de Física Teórica, UNESP–Universidade Estadual Paulista, 01.140-070 São Paulo, São Paulo, Brazil*

[2]*School of Physics, Bharathidasan University, Palkalaiperur Campus, Tiruchirappalli 620024, Tamilnadu, India*

(Received 29 December 2011; revised manuscript received 30 January 2012; published 14 March 2012)

A uniform dilute Bose gas of known density has a universal behavior as the atomic scattering length tends to infinity at unitarity while most of its properties are determined by a universal parameter ξ relating the energies of the noninteracting and unitary gases. The usual mean-field equation is not valid in this limit, and beyond mean-field corrections become important. We use a dynamical model including such corrections to investigate a trapped disk-shaped dipolar Bose-Einstein condensate (BEC) and a dipolar BEC vortex for large scattering length. We study the sensitivity of our results on the parameter ξ and discuss the possibility of extracting the value of this parameter from experimental observables.

DOI: 10.1103/PhysRevA.85.033619 PACS number(s): 03.75.Hh, 03.75.Kk, 05.30.Jp

I. INTRODUCTION

The properties of a uniform dilute interacting (Bose or Fermi) atomic quantum gas interacting with an S-wave contact interaction at zero temperature is determined by two scales: the atomic scattering length a and density $\bar{n}$. As $a \to \infty$ at unitarity, the first scale is not of concern, and the observables of the gas are determined solely by density and the gas exhibits a universal behavior. Bulk chemical potential $\bar{\mu}$ of the unitary gas is proportional to the *only* available energy scale, the Fermi energy (or the chemical potential of the noninteracting gas) $E_F = \hbar^2(6\pi^2\bar{n})^{2/3}/2m$, so that $\bar{\mu} = \xi E_F$, where ξ is a universal parameter and m is the mass of an atom [1–16]. Similarly, the energy per particle $\bar{E}$ of the unitary gas is proportional to the energy per particle $E(\equiv 3E_F/5)$ of the noninteracting gas: $\bar{E} = \xi E$ [3,4]. The Fermi energy is a physically meaningful quantity for the Fermi gas, but the same can also be used as an energy scale for the Bose gas [2,12,14]. The Bose and Fermi gases behave similarly at unitarity because the Bose gas exhibits fermionization. If this fermionization of the Bose gas is absolute, then ξ should be the same for the Bose and Fermi gases.

The parameter ξ relating the energy of the noninteracting and unitary gases has been "measured" experimentally from a study at or near unitarity of the density [1,5–7], or of ground-state energy, or of sound velocity [8] of a trapped Fermi gas. But a similar experiment is more difficult for a Bose-Einstein condensate (BEC) due to a large probability of three-body loss by molecule formation at or near unitarity, which is the threshold for molecule formation [12]. In the weak-coupling limit ($an^{1/3} < 1$) the mean-field Gross-Pitaevskii (GP) equation gives a good description of a trapped BEC, where n is the density. In the strong-coupling regime ($an^{1/3} > 1$) the GP equation highly overestimates the atomic contact interaction and leads to unphysical results. Experimental activities to access the strong-coupling regime of a BEC, to test the beyond mean-field corrections [17,18], and to extract the parameter ξ from these studies have just began [12]. Although unitarity is also the threshold for molecule formation in a two-component (spin up and down) Fermi gas, the probability of formation of diatomic molecules is highly suppressed in this case due to Pauli repulsion among spin-parallel fermions in the three-fermion system and hence is not of concern [1].

Lately, BECs of ^{52}Cr [19,20] and ^{164}Dy [21,22] with large dipolar interaction have been observed and studied. The interatomic interaction now has two components: an S-wave contact interaction and an anisotropic long-range dipolar interaction. This allows one to study the dipolar BEC with a variable contact interaction [19,22] using a Feshbach resonance [23]. The intrinsically anisotropic dipolar BEC [24] has many distinct features [19,20,25–28]. The stability of a dipolar BEC depends not only on the scattering length, but also on the trap geometry [19,25,27]. A disk-shaped trap leads to a repulsive dipolar interaction and the dipolar BEC is more stable, whereas a cigar-shaped trap yields an attractive dipolar interaction and hence favors a collapse instability [19,27,29].

We study the static and dynamic properties of a disk-shaped dipolar BEC and dipolar BEC vortex, with the dipole moments aligned perpendicular to the plane of the disk, for large scattering length using a beyond-mean-field model [16,30] for the BEC-unitarity crossover. In this paper we consider the strong-coupling limit of the contact interaction only and *not* the same limit of dipolar interaction. In the weak-coupling limit, this crossover model reduces to the GP equation and the Lee-Huang-Yang (LHY) correction [31], whereas in the strong-coupling regime of large scattering length it reduces to the universal result at unitarity. We find that the radial densities are sensitive to the parameter ξ in the strong-coupling regime, and hence a study of density is expected to yield information about this parameter. However, the frequency of oscillation of the dipolar BEC is found to be insensitive to this parameter. From a study of vortices in a disk-shaped dipolar BEC we find that both density and radius of vortex core are sensitive to this parameter in the strong-coupling regime.

In the disk configuration, the dipolar interaction is highly repulsive, as parallel dipoles arranged in a plane with the dipole moment perpendicular to the plane repel each other [19,20]. The strongly repulsive dipolar interaction should reduce three-body loss by molecule formation in the strong-coupling regime, as the rate of the reaction $3A \to A_2 + A$ should be

*lyoung@ift.unesp.br
†adhikari44@yahoo.com
‡anand@cnld.bdu.ac.in

PHYSICAL REVIEW A **86**, 063611 (2012)

Mixing, demixing, and structure formation in a binary dipolar Bose-Einstein condensate

Luis E. Young-S.[*] and S. K. Adhikari[†]

Instituto de Física Teórica, UNESP, Universidade Estadual Paulista, 01.140-070 São Paulo, São Paulo, Brazil

(Received 14 August 2012; revised manuscript received 21 September 2012; published 11 December 2012)

We study the static properties of disk-shaped binary dipolar Bose-Einstein condensates of ^{168}Er-^{164}Dy and ^{52}Cr-^{164}Dy mixtures under the action of interspecies and intraspecies contact and dipolar interactions and demonstrate the effect of dipolar interaction using the mean-field approach. Throughout this study we use realistic values of interspecis and intraspecies dipolar interactions and the intraspecies scattering lengths and consider the interspecies scattering length as a parameter. The stability of the binary mixture is illustrated through phase plots involving a number of atoms of the species. The binary system always becomes unstable as the number of atoms increases beyond a certain limit. As the interspecies scattering length increases corresponding to more repulsion, an overlapping mixed state of the two species changes to a separated demixed configuration. During the transition from a mixed to a demixed configuration as the interspecies scattering length is increased for parameters near the stability line, the binary condensate shows special transient structures in density in the form of red-blood-cell-like biconcave and Saturn-ring-like shapes, which are direct manifestations of the dipolar interaction.

DOI: 10.1103/PhysRevA.86.063611 PACS number(s): 03.75.Hh, 03.75.Mn

I. INTRODUCTION

After the experimental realization [1–5] of a dipolar Bose-Einstein condensate (BEC) of ^{52}Cr atoms with magnetic moments, there has been renewed interest in the study of the static and dynamic properties of such a condensate in the pursuit of the novel and interesting properties and features emerging as a consequence of anisotropic long-range dipolar interaction. The atomic interaction in a dilute BEC of alkali-metal atoms is taken as an s-wave short-range (delta-function) potential. However, the anisotropic long-range dipolar interaction is nonlocal in nature acting in all partial waves. More recently, the BEC of ^{164}Dy [6,7] and ^{168}Er [8] atoms with larger dipole moments became available for experimental studies, and polar molecules with much larger (electric) dipole moments are being considered [9] for BEC experiments. Among the novel features of a BEC with anisotropic dipolar interaction, one can mention the peculiar shape and stability properties of a stationary state [10], a red-blood-cell-like biconcave shape in density due to radial and angular roton-like excitations [11]; anisotropic d-wave collapse [12]; the formation of an anisotropic soliton, vortex soliton [13], and vortex lattice [14]; anisotropic sound and shock wave propagation [15]; and anisotropic Landau critical velocity [16] among others. Distinct stable checkerboard, stripe, and star configurations in dipolar BECs have been identified in a two-dimensional (2D) optical lattice as a stable Mott insulator [17] as well as superfluid soliton [18] states. A new possibility of studying the universal properties of dipolar BECs for large scattering length has been suggested [19]. Many of these features have only been predicted theoretically, although some of them have already been experimentally confirmed. To enhance the effect of the anisotropic dipolar interaction in most of these theoretical studies, the contact interaction has been set equal to zero. In the ^{52}Cr atom, this could be necessary as the strength of the repulsive contact interaction is much stronger than that of the dipolar interaction. However, the dipolar BEC of atoms such as ^{164}Dy with much larger dipolar interaction can show the effects of an anisotropic nonlocal dipolar interaction without switching off the contact interaction.

Now with the available dipolar BECs of a different species of atoms, there is the possibility to investigate a binary mixture with two dipolar BECs of two types of dipolar interactions acting on each species (e.g., intraspecies and interspecies) superposed on intraspecis and interspecies contact interactions, thus creating a much richer platform to study the effect of dipolar interaction. Previously, there have been studies of nondipolar binary boson-boson [20,21], boson-fermion [22], and fermion-fermion [23], as well as dipolar-nondipolar binary boson-boson [24] mixtures. For a binary system without dipolar interactions it is possible to have either a mixed or demixed phase. In this paper, we consider binary dipolar BECs composed of ^{164}Dy and ^{52}Cr atoms as well as ^{164}Dy and ^{168}Er atoms. With all the dipole moments aligned along the z axis, the net dipolar interaction is attractive in the cigar shape along the z axis and repulsive in the disk shape confined in the x-y plane, as parallel dipoles in a chain along the z axis attract and those confined in the x-y plane repeal each other. Consequently, the binary dipolar BEC with dipoles polarized along the z axis is more stable in the disk shape confined in the x-y plane compared to the cigar shape along the z axis vulnerable to collapse. We shall consider only such a disk-shaped binary dipolar BEC in this study. Even such a disk-shaped binary dipolar BEC is found to be unstable due to the collapse instability for dipolar interaction above a critical value controlled by the number of atoms. This is consistent with a similar conclusion that a single-component dipolar BEC for any trap anisotropy collapses above a critical value of dipolar interaction [25,26].

We study the limits of the stability of binary dipolar disk-shaped BECs formed of ^{168}Er and ^{164}Dy atoms and of ^{52}Cr and ^{164}Dy atoms and present the results in terms of stability phase plots which should aid in the experimental

[*]lyoung@ift.unesp.br
[†]adhikari@ift.unesp.br; http://www.ift.unesp.br/users/adhikari

PHYSICAL REVIEW A **87**, 013618 (2013)

Dipolar droplet bound in a trapped Bose-Einstein condensate

Luis E. Young-S.[*] and S. K. Adhikari[†]

Instituto de Física Teórica, UNESP–Universidade Estadual Paulista, 01.140-070 São Paulo, São Paulo, Brazil

(Received 9 November 2012; published 17 January 2013)

We study the statics and dynamics of a dipolar Bose-Einstein condensate (BEC) droplet bound by interspecies contact interaction in a trapped nondipolar BEC. Our findings are demonstrated in terms of stability plots of a dipolar ^{164}Dy droplet bound in a trapped nondipolar ^{87}Rb BEC with a variable number of ^{164}Dy atoms and interspecies scattering length. A trapped nondipolar BEC of a fixed number of atoms can bind only a dipolar droplet containing fewer atoms than a critical number for the interspecies scattering length between two critical values. The shape and size (statics) as well as the small breathing oscillation (dynamics) of the dipolar BEC droplet are studied using numerical and variational solutions of a mean-field model. We also suggest an experimental procedure for achieving such a ^{164}Dy droplet by relaxing the trap on the ^{164}Dy BEC in a trapped binary ^{87}Rb-^{164}Dy mixture.

DOI: 10.1103/PhysRevA.87.013618 PACS number(s): 03.75.Hh, 03.75.Mn, 03.75.Kk

I. INTRODUCTION

The experimental observation of dipolar Bose-Einstein condensates (BECs) of ^{52}Cr [1–5], ^{164}Dy [6,7], and ^{168}Er [8] atoms with large magnetic dipole moments has opened new directions of research in cold atoms in the quest of novel and interesting features related to the anisotropic long-range dipolar interaction. Polar molecules, with much larger (electric) dipole moment, are also being considered [9] for BEC experiments. The atomic interaction in a dilute BEC of alkali metal and other types of atoms (with negligible dipole moment) is represented by an S-wave contact (δ-function) potential. However, the nonlocal anisotropic long-range dipolar interaction acts in all partial waves and is attractive in certain directions and repulsive in others.

An untrapped three-dimensional (3D) BEC with attractive interaction does not exist in nature due to collapse instability [10]. However, the collapse of an untrapped BEC can be avoided due to the interspecies contact interaction in a binary mixture with a trapped BEC. The shape of such a stable droplet bound in a trapped BEC is controlled by the interspecies interactions, whereas that of a trapped BEC is determined by the underlying trap. Here we consider such a dipolar droplet bound in a trapped nondipolar BEC. The effect of the underlying atomic interaction, especially that of the anisotropic dipolar interaction, will easily manifest itself in such a dipolar droplet. These droplets will be termed quasifree as they can easily move around inside the larger trapped BEC responsible for their binding. By taking the trapped BEC to be nondipolar, one can easily study the effect of intraspecies dipolar interaction on the quasifree droplet in the absence of any interspecies dipolar interaction.

Dipolar BECs are immediately distinguishable from those with purely contact interactions by their strong shape and stability dependence [11] on the trapping geometry. Here, we are proposing a different way to trap a dipolar BEC in the form of a quasifree dipolar droplet, using an attractive interspecies mean-field potential, which introduces a unique trapping geometry that results in further interesting shape and stability characteristics of dipolar BECs. We study the statics and dynamics of a quasifree dipolar droplet using numerical solution and variational approximation of a mean-field model [12,13]. For this purpose we consider a binary mixture of nondipolar ^{87}Rb and dipolar ^{164}Dy where the trapped nondipolar ^{87}Rb BEC could be in a cigar or disk shape. Among the available dipolar BECs [4,7,8], ^{164}Dy atoms have the largest (magnetic) dipolar interaction strength [1,6]. The existence of stable 3D ^{164}Dy droplets is illustrated by stability plots involving the number of atoms of the two species and the interspecies scattering length. For a fixed number N(Rb) of ^{87}Rb atoms the dipolar droplet could be bound below a critical number N(Dy) of ^{164}Dy atoms between two limiting values of interspecies attraction. If the interspecies attraction is too small, the ^{164}Dy atoms in the droplet cannot be bound and, for a very large interspecies attraction, the droplet is destroyed by collapse instability. Usually, the dipolar droplet has the same shape as the trap acting on the nondipolar BEC. However, for a large number of ^{164}Dy atoms, as the interspecies attraction approaches the collapse instability, the dipolar droplet always is of cigar shape even if the external trap is disk shaped, and eventually the dipolar droplet collapses on the axial z axis from the cylindrical configuration. For a small number of atoms, the dipolar droplet collapses to the center, maintaining its shape, rather than on the axial z axis.

The variational approximation to the sizes and chemical potentials of the stationary droplets is compared with the numerical solution of the mean-field model. The numerical study of breathing oscillation of the stable dipolar droplet is found to be in reasonable agreement with a time-dependent variational model calculation. We also demonstrate a viable experimental way of creating a ^{164}Dy droplet bound in a trapped ^{87}Rb BEC, e.g., by slowly removing the trap on a trapped binary ^{164}Dy-^{87}Rb mixture, while the trapped ^{164}Dy BEC evolves into a quasifree droplet.

In Sec. II the mean-field model for a dipolar BEC droplet bound in a trapped nondipolar BEC is developed. A time-dependent, analytic, Euler-Lagrange Gaussian variational approximation of the model is also presented. The results of numerical calculation are shown in Sec. III. Finally, in Sec. IV we present a brief summary of our findings.

[*]lyoung@ift.unesp.br
[†]adhikari@ift.unesp.br; URL: http://www.ift.unesp.br/users/adhikari

PHYSICAL REVIEW A **87**, 043603 (2013)

Self-trapping of Fermi and Bose gases under spatially modulated repulsive nonlinearity and transverse confinement

Luis E. Young-S.,[1] L. Salasnich,[2] and Boris A. Malomed[3]
[1]*Instituto de Física Teórica, UNESP-Universidade Estadual Paulista, 01.140-070 São Paulo, São Paulo, Brazil*
[2]*Dipartimento di Fisica e Astromia "Galileo Galilei" and CNISM, Università di Padova, Via Marzolo 8, 35131 Padova, Italy*
[3]*Department of Physical Electronics, School of Electrical Engineering, Faculty of Engineering, Tel Aviv University, Tel Aviv 69978, Israel*
(Received 5 December 2012; published 4 April 2013)

We show that self-localized ground states can be created in the spin-balanced gas of fermions with repulsion between the spin components, whose strength grows from the center to periphery, in combination with the harmonic-oscillator (HO) trapping potential acting in one or two transverse directions. We also consider the ground state in the noninteracting Fermi gas under the action of the spatially growing tightness of the one- or two-dimensional (1D or 2D) HO confinement. These settings are considered in the framework of the Thomas-Fermi–von Weizsäcker (TF–vW) density functional. It is found that the vW correction to the simple TF approximation (the gradient term) is nearly negligible in all situations. The properties of the ground state under the action of the 2D and 1D HO confinement with the tightness growing in the transverse directions are investigated too for the Bose-Einstein condensate with the self-repulsive nonlinearity.

DOI: 10.1103/PhysRevA.87.043603 PACS number(s): 03.75.Lm, 05.45.Yv, 42.65.Tg

I. INTRODUCTION

One of the fundamental conclusions produced by ongoing studies of the dynamics of matter waves in Bose-Einstein condensates (BECs) is that the effective local nonlinearity, induced by interatomic collisions, gives rise to robust bright solitons and soliton complexes [1–7]. In addition to their fundamental significance, the solitons may be employed in applications. In particular, the use of solitons in matter-wave interferometers should help to dramatically increase the accuracy of these devices (see Refs. [8–12] and a recent review [13]).

In the usual settings, the existence of bright solitons requires the presence of the self-focusing nonlinearity. They may also be supported by nonlinear lattices, which feature alternation of spatial domains of self-focusing and defocusing, which give rise to the corresponding periodic *pseudopotential* [7,14]. On the other hand, self-defocusing nonlinearities, acting in combination with periodic linear (lattice) potentials, support bright solitons of the band-gap type [2,3,5]. Nevertheless, a common belief was that the self-defocusing per se could not give rise to bright solitons. The situation had changed when it was demonstrated that the repulsive cubic nonlinearity with the local strength growing with the distance from the center r faster than r^D, where D is the spatial dimension, can readily support stable solitons and solitary vortices [15,16]. In the same works, it was proposed how the corresponding profiles of the nonlinearity modulation can be created in BEC and nonlinear optics. In particular, the spatial modulation of the scattering length of interatomic collisions, induced by spatially inhomogeneous magnetic or optical fields via the Feshbach-resonance mechanism, can give rise to the required profile in BEC. Similarly, robust solitons and vortices were predicted in a more exotic model, with the constant strength of the defocusing nonlinearity but the diffraction coefficient decaying faster than r^{-D} [17].

It may be interesting to implement this option for the creation of bright solitons by purely repulsive nonlinearity landscapes in other physical settings. For instance, it was recently demonstrated that the same mechanism works too in one- and two-dimensional (1D and 2D) media with the repulsive quintic nonlinearity [18].

This work aims to propose a way of creating bright solitons in Fermi gases, with balanced spin-up and -down components. The possibility is to combine the spatial growth of the s-wave scattering length, which accounts for the repulsion between the components, in one or two directions, and the harmonic-oscillator (HO) confining potential acting in the other directions. It should be noted that the dilute two-spin-component fermionic gases with the repulsive s-wave interaction do not feature phase coherence, as they are not superfluids [19]. Nevertheless, their ground states can be accurately described by means of the density-functional theory [20–22].

Here, we adopt the Thomas-Fermi–von Weizsäcker (TF–vW) form of the density functional to predict density profiles and chemical potentials of the Fermi droplets (i.e., bright solitons) in two different configurations, which are considered in Secs. II and III, respectively: the quadratic growth of the scattering length in one direction (z) and transverse HO confinement in the (x,y) plane; or the quadratic growth of the scattering length in the (x,y) plane and HO confinement acting along z. Then, in Secs. IV and V, following previous results obtained in the framework of the mean-field description of BEC [23–25], we consider Fermi gases without intrinsic interactions (in particular, it may be a spin-polarized, i.e., single-spin-component, gas) and demonstrate that they give rise to localized ground states under the action of the 2D or 1D HO confinement, if its tightness, i.e., the corresponding confinement frequency, grows in the transverse directions faster than $\sqrt{|z|}$ or r^4, respectively. In addition, we demonstrate that the same confinements with the spatially growing tightness support, in a similar way, localized ground states in BEC with the self-repulsive nonlinearity.

II. 1D NONLINEARITY MODULATION WITH THE 2D TRANSVERSE CONFINEMENT FOR THE SPIN-BALANCED INTERACTING FERMI GAS

In the presence of an external trapping potential $U_{\rm ext}(x,y,z)$, the Hohenberg-Kohn theorem [20] ensures that the

Preprint in preparation for publication in *Comput. Phys. Commun.*, **2013**.

Contribution submitted to INTERNATIONAL LASER PHYSICS WORKSHOP 2013.

Fortran and C programs for the time-dependent dipolar Gross-Pitaevskii equation in an anisotropic trap ☆

R. Kishor Kumar[a], Luis E. Young-S.[b], Dušan Vudragović[c], Antun Balaž[c], P. Muruganandam[a], S. K. Adhikari[b]

[a] *School of Physics, Bharathidasan University, Palkalaiperur Campus, Tiruchirappalli – 620024, Tamil Nadu, India*
[b] *Instituto de Física Teórica, UNESP – São Paulo State University, 01.140-70 São Paulo, São Paulo, Brazil*
[c] *Scientific Computing Laboratory, Institute of Physics Belgrade, University of Belgrade, Pregrevica 118, 11080 Belgrade, Serbia*

Abstract

Many of the static and dynamic properties of an atomic Bose-Einstein condensate (BEC) are usually studied by solving the mean-field Gross-Pitaevskii (GP) equation, which is a nonlinear partial differential equation for short-range atomic interaction. More recently, BEC of atoms with long-range dipolar atomic interactions are extensively used in theoretical and experimental studies. In the presence of dipolar atomic interactions, the corresponding GP equation becomes a partial integro-differential equation, requiring the implementation of a complex algorithm for calculation of its numerical solution. Here we present numerical algorithms for calculating both stationary and non-stationary solutions of the full three-dimensional GP equation for a single dipolar BEC as well as for a binary mixture of two types of dipolar BECs. We also consider the effective one- and two-dimensional GP equations satisfied by cigar- and disk-shaped dipolar BECs, respectively. We employ the split-step Crank-Nicolson semi-implicit method with real and imaginary time propagations, respectively, for the numerical solution of the GP equation for dynamic and static properties of a dipolar BEC, which is already used in codes for solving the GP equation for BECs with contact interaction [1, 2]. There are eight different cases that we consider, e.g., stationary and non-stationary solutions of the GP equation for dipolar BEC in one, two, and three dimensions, and of the binary GP equation in three dimensions and we provide working codes in Fortran 90/95 and C for these eight cases (sixteen programs in all). Using these codes, we also calculate and present numerical results for energy, chemical potential, root-mean-square sizes and density of the dipolar BECs and where available, compare them with results of other authors.

Keywords: Bose-Einstein condensate; Gross-Pitaevskii equation; Split-step Crank-Nicolson Scheme; Real- and imaginary-time propagation; Fortran and C programs; dipolar atoms.

[1] P. Muruganandam and S. K. Adhikari, Comput. Phys. Commun. **180**, 1888 (2009).
[2] D. Vudragović, I. Vidanović, A. Balaž, P. Muruganandam and S. K. Adhikari, Comput. Phys. Commun. **183**, 2021 (2012).

☆D.V. and A.B. acknowledge support by the Ministry of Education and Science of the Republic of Serbia under projects No. ON171017 and NAD-BEC, by DAAD - German Academic and Exchange Service under project NAD-BEC, and by the European Commission under EU FP7 projects PRACE-1IP, PRACE-2IP, HP-SEE, and EGI-InSPIRE.